ACKNOWLEDGEMENTS

I am deeply indebted to my research guide, **Prof. B. Viswanathan,** for his unlimited dedication in inspiring us, consistent thought provoking discussions and tireless guidance. I am grateful to him for introducing myself to different aspects of Science. It is my great privilege to being associated with him. I am also greatful to him for giving me enormous chances to understand and explore myself.

I am very much grateful to **Prof. T. K. Varadarajan,** my research co-guide, for his constant encouragement, support and invaluable suggestions.

I express my sincere gratitude to the former Heads of the Department, **Prof. M.S. Gopinathan, Prof. S. Vancheesan** (late), **Prof. M. N. Sudheendra Rao, Prof. G. Sundararajan** (late) and the present Head **Prof. R. Dhamodharan,** of the Department of Chemistry, IIT Madras for providing the necessary infrastructural facilities in carrying out my research work.

I sincerely thank all my doctoral committee members, **Prof. M.V. Sangaranarayanan**, **Dr. G. Ranga Rao**, **Prof. V.R.K. Murthy**, **Prof. D.V.S. Murthy** and **Prof. K. Krishnaiah, Dean, Academic**, for their constant encouragement and suggestions.

I wish to acknowledge **CSIR** for the research fellowship and **DST** for funding **NCCR,** for the necessary infrastructure.

I thank all the non-teaching staff members of the Department of Chemistry for their timely help.

My greatful thanks are due to **Mr. Narayanan**, for his technical support and suggestions throughout my research work.

My thanks are also due to **Mr. Ramkumar, Mr. Sivaramakrishnan** and **Mrs. Srividya** for their CHN and SEM analysis.

I would like to extend my thanks to present and former heads of SAIF, DST Nano Science Unit, Central Glass Blowing Section and Department of Metallurgy, IIT Madras for providing various facilities.

My sincere gratitudes are due to Mr. Ragavaiah, for his passionate SEM analyses, and Ms. Banupariya for her TEM analyses.

I would like to extend my sincere thanks to **Dr. Sreedhar**, IICT, Hyderabad, for his XPS analyses.

I express my sincere thanks to my seniors, **Dr. Rajesh**, **Dr. Aulice**, **Dr. Raghuveer**, **Dr. Ganesan, Dr. Ch. Subramanian, Dr. Shanmugam, Dr. Sathish, Dr. Chidambaram**, **Dr. Sankaran**, **Dr. Srimurugan, Dr. Suresh, Dr. Maiyalagan, Dr. Navaladian, Dr. Janet, Dr. Venkateshwara Rao, Dr. Hima Kumar, Dr. Kishore,** for their suggestions and support.

I thank my colleagues **Mr. Indraneel, Mr. Magesh, Mr. Kuppan, Mr. Vamsi Krishna, Mr. Ramana Murthy, Mr. Mahendran, Mr. Anil Kumar, Mr. Jude, Mr. Ganesh, Mr. Poli Raju, Mr. Sudhakar, Mr. Sankaranarayanan, Mr. Venkatesan, Ms. Banu, Ms. Sumathy, Ms. Indumathi, Mrs. Premlatha, Dr. Joseph Antony, Dr. Thirunavukarasu, Dr. Joyce, Dr. Sabiah, Dr. Sangeetha, Dr. Jancy, Dr. Anuradha** and **Dr. George** for their timely helps, support, suggestions and friendliness.

My grateful thanks are also due to **Mr. Murali** and **Mr. Koteswaraiah**, for their helps, suggestions and support.

I would like to express my deep sense of gratitude to my family members, especially my **Parents**, my **husband** and **my children**.

Above all, I thank the **Almighty** for having given me this chance.

S. Chandravathanam

ABSTRACT

Key words: Pt nanoparticles, carbon supported catalysts, methanol oxidation, functionalization of carbon support, fuel cell catalysts

Fuel cells are envisioned as the future energy conversion device for wide applications. Among the different types of fuel cells, the PEM (Polymer electrolyte membrane) fuel cells employing hydrogen as the fuel and the DMFC (Direct methanol fuel cell) employing methanol as the fuel are under development for successful commercialization. The commercialization of fuel cells is impeded mainly because of the high cost of the catalyst layer which needs expensive noble metal such as Pt and its alloys. The sluggish kinetics of oxygen reduction reaction in H_2 based PEMFC and both oxygen reduction and methanol oxidation reactions in DMFC, apart from other practicalities have also caused concern. Even a slight enhancement in the activity and durability of these catalysts can bring down the cost significantly. The typical catalyst mostly used in fuel cell electrodes is Pt dispersed on carbon black support, for both anode and cathode electrodes. Commonly carbon black is used as the support for various reasons such as, its good electrical conductivity, high surface area and porosity, light weight and cheap availability as compared to many other support materials like, transition metal oxides, organic polymers and other forms of carbon materials like carbon nanotubes and carbon nanofibers.

Carbon black has many kinds of functional groups like hydroxyl, carboxyl, lactone, quinone and hydroquinone. Using carbon black support the catalysts are mostly prepared through the impregnation step, where the metal ions are adsorbed on to the support functional groups especially carboxylic groups. In order to increase the metal particle site density on the carbon black support, the support needs to have more of

the carboxyl functional groups. Treatment with mineral acids, especially nitric acid, has been employed to convert other functional groups like quinones on carbon to carboxyl groups. The studies relating to this aspect have clearly shown enhancement in the activity of the electrocatalyst for methanol oxidation. Even though the treatment with mineral acid increases the hydrophilicity of the catalyst, the presence of the surface oxygen groups also induces strong metal support interaction with the precursor species and lead to aggregation of the Pt nanoparticles on the surface. The presence of surface oxygen functional groups also causes the support surface to be acidic, and affects the anchoring of the anionic precursor species such as chloroplatinic acid. Nitrogen functionalization of the carbon black support renders the surface basic and expected to anchor the anionic precursor molecules. Apart from the surface functional groups, another important aspect of fuel cell catalysts is the three phase boundary (the coexistence of the electron conducting support particles, proton conducting polymer ionomer and the catalyst particle). In fuel cell catalysts, only those catalyst particles which exist in the three phase boundary are utilized. But the smaller Pt nanoparticles existing with in the inner pores of the carbon black support are not accessible for the bulky proton conducting polymer, and are not utilized for the electrocatalytic reaction. There are a few studies aimed at to extend the three phase boundary to the inner pores of the support material. These are focused on the introduction of sulfonic acid groups on the carbon black support, as sulfonic acid groups are strong protonic acids compared to carboxylic acids. Another factor which has more influence on the performance of the metal nanoparticles is the particle size. Nanoparticles are thermodynamically unstable and their apparent stability comes from an acquired kinetic hindrance to agglomeration. Hence, in order to produce desired sizes of Pt nanoparticles with uniform dispersion on the carbon support, some kind of

stabilizing agents, such as surfactants, ligands or polymers, are usually employed during the preparative process. The removal of these bulky stabilizer molecules by thermal treatment induces particle sintering, thereby undoing the effort in nanoparticle synthesis. Therefore, electrostatic stabilization by carboxylic anions is preferred to the steric stabilization by polymers, as these carboxylic anions can be easily washed off with distilled water.

The present work therefore is focusing upon the different kinds of functionalization of the carbon black support, which can lead to smaller particle size of the supported Pt and hence enhanced electroactive surface area, and finally better utilization of the expensive, less abundant noble metal catalyst, so that the fuel cell performance could be commercially viable. The different kinds of functionalization like carboxylic, sulfonic and aminopyridine has been carried out on the carbon black support. Effect of carboxylic acid functionalization of the carbon black support CDX975 has been studied with nitric acid treatment under two different concentrations of nitric acid and two different reaction times. Effect of sulfonic acid functionalization of the carbon black support CDX975 has been studied with three different sulfonating agents, namely, 2-aminoethanesulfonic acid, ammonium sulfate and sodium sulfite with formaldehyde. Effect of aminopyridine functionalization of the carbon black support CDX975 has been studied with 2-amino-5-chloropyridine. Effect of the capping agent on the dispersion and activity of the Pt nanoparticles on the carbon black support was studied by using citrate as the stabilizing agent. All the prepared catalysts were characterized with appropriate techniques like, XRD, FT-IR, TGA, TEM and XPS. The prepared catalysts were evaluated for their catalytic activity for methanol electro-oxidation reaction.

TABLE OF CONTENTS

Table of Contents (Contd.) **Page No.**

Table of Contents (Contd.) **Page No.**

Table of Contents (Contd.) **Page No.**

LIST OF TABLES

List of Tables (Contd.) **Page No.**

LIST OF FIGURES

List of Figures (Contd.) **Page No.**

List of Figures (Contd.) **Page No.**

List of Figures (Contd.) **Page No.**

LIST OF SCHEMES

CHAPTER 1

INTRODUCTION

1.1 Introduction

Fuel cells, the energy conversion devices with a high efficiency and low/zero emission, have been attracting more attention in recent decades due to high energy demands, fast depletion of fossil fuels, and concern for environmental pollution throughout the world (Liu *et al*., 2006). Apart from the Green house gas emissions, the chemical energy of the fossil fuels are only very feebly utilized by the internal combustion engines, as they are limited by Carnot condition. In addition energy conversion involves too many steps from chemical energy of the fossil fuel to the usable electrical energy as shown in Scheme 1. The high efficiency of fuel cells stems from the direct conversion of the chemical energy to the usable electrical energy in a single process at the electrode/electrolyte interface, which makes the process free from Carnot limitation.

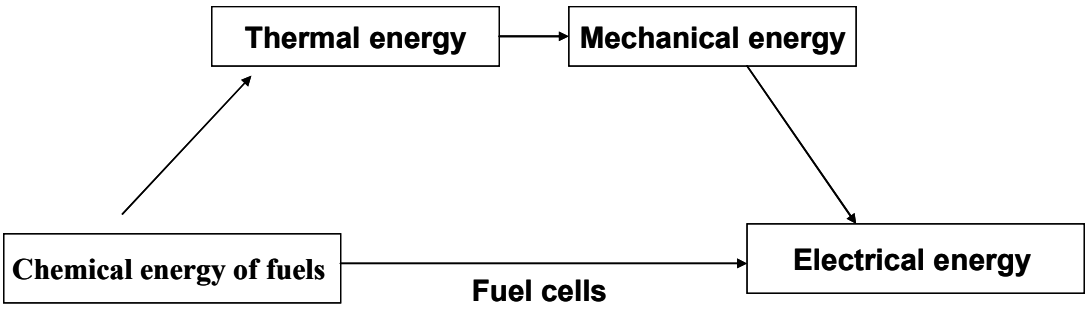

Scheme 1.1 The schematic of the energy conversion in fuel cells in comparison to internal combustion engines

The raising concern over the increasing emissions of harmful pollutants like, NOx, SOx, CO_2 and particulate matter from fossil fuel combustion is the driving force for

the commercial feasibility of fuel cells. A comparison of the obvious alternative electrochemical technologies reveals that although batteries offer the prospect of a true zero emission vehicle, all available batteries have considerable environmental and engineering draw backs which will be difficult to overcome (Hamnett, 1997). Unlike batteries, fuel cells do not need longer time for recharging. It operates at the convenience of the internal combustion engine and gives energy as long as the fuel is supplied. In fuel cells, the fuel is oxidized at the anode with the release of electron to the external circute, producing current. The generated protons pass through the electrolyte to the cathode where the oxygen reduction takes place together with the formation of water. The simple schematic of fuel cell is shown in Scheme 1.2.

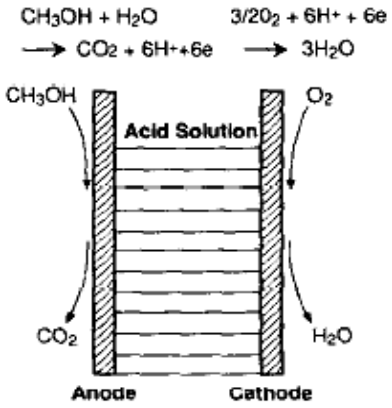

Scheme 1.2 Simple schematic of the fuel cell using methanol as the fuel

1.2 Performance of fuel cells

The performance of any fuel cell is judged from its polarization plot, which is a plot of the potential vs current density. The polarization plot for hydrogen-air fuel cell is shown in Fig. 1.1 (Gasteiger *et al*., 2005). In Fig.1.1, E_{eq} is the theoretical maximum realizable equilibrium potential. It is expected that in any fuel cell system, this potential remains to be the same even after drawing current for as long as the fuel cell

is operating. But as the Fig.1.1 shows, it starts decreasing as soon as drawing current from the fuel cell. This decrease of potential is due to the presence of various overvoltages, such as, the activation, ohmic and mass transport overvoltages. Lower value of open circuit potential at zero current density is due to the poor activity of the electrocatalyst and is expressed as activation overvoltage. If the catalyst is active enough, then the open circuit potential must have remained close to E_{eq}. As the hydrogen oxidation on platinum electrodes is a very facile reaction, this overvoltage is caused by the slow kinetics of the oxygen reduction reaction or the high voltage required to push the oxygen reduction reaction (η_{ORR}). By the start of drawing current from the fuel cell, the decrease of the potential is more, and the another factor contributing more to the already existing η_{ORR} is, the ohmic losses, ΔE_{ohmic}, due to both electronic contact resistances between the flow-fields and the diffusion media as well as the ohmic resistance due to proton conduction through the membrane. The still decrease of the cell potential at the high current density region is contributed mainly by the mass transport of the reactive molecules to the active sites (i.e., mass transport overvoltage η_{tx}). It has been shown that with the elimination of 50% of $\eta_{tx,}$ (Diamond symbols in Fig. 1.1) it could be seen from Fig. 1.1 that, the slope of the polarization curve was reduced. By adding the measured ohmic losses, ΔE_{ohmic}, to the purely kinetically controlled conceptual polarization curve (square symbols in Fig. 1.1), yields the mass-transport free (i.e., η_{tx} =0) cell voltage (triangular symbols in Fig. 1.1). Therefore Figure 1.1 explains in detail, the role played by different overvoltages on the decrease of cell voltage and the increase of cell voltage by curbing each particular overvoltage. Also from Fig. 1.1, it could be concluded that the major part of overvoltage (~30%) is contributed by the slow kinetics of the oxygen reduction

reaction. In order to curb the overvoltage caused by this part, innovative catalysts, with catalytic activity many times more than the existing ones are required.

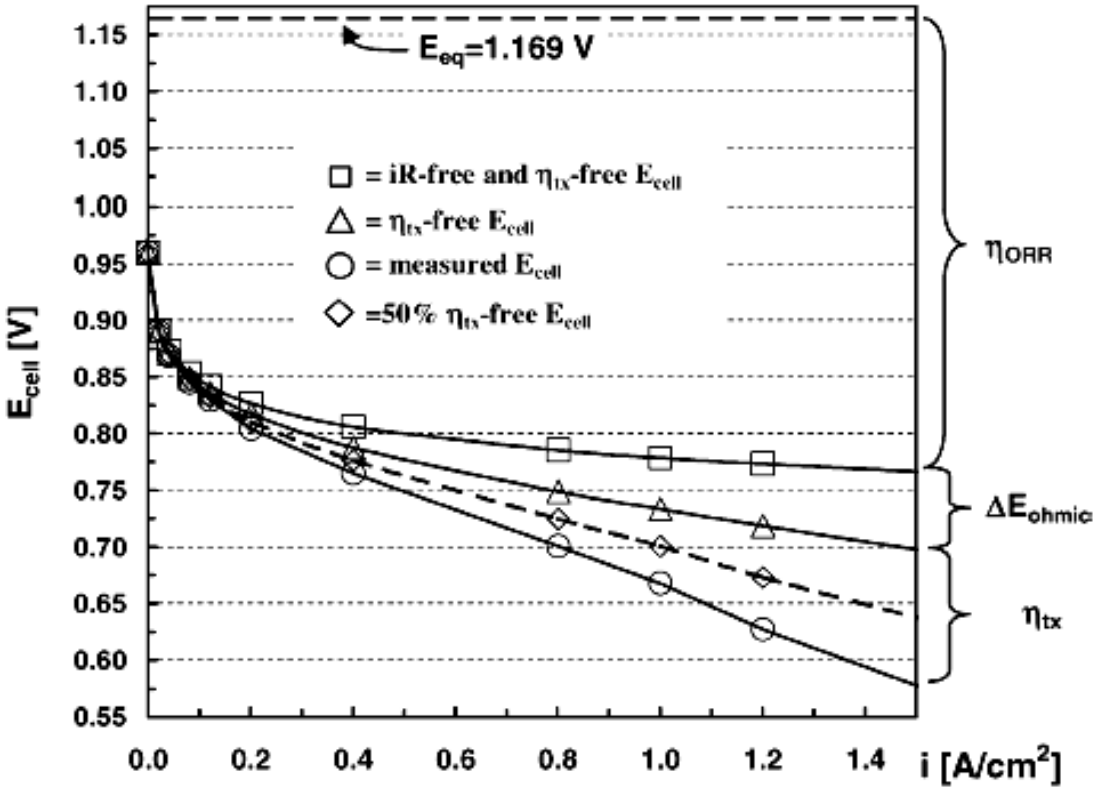

Fig. 1.1 Current-Potential curve for H_2 - Air fuel cell at 80 °C (Gasteiger *et al*., 2005)

1.3 Types of fuel cells

Fuel cells can be classified into different types depending upon the type of the fuel or the electrolyte used or their working temperature. Scheme 1.3 gives the details of the fuels, electrolyte and operating temperatures of the different fuel cells along with the main applications.

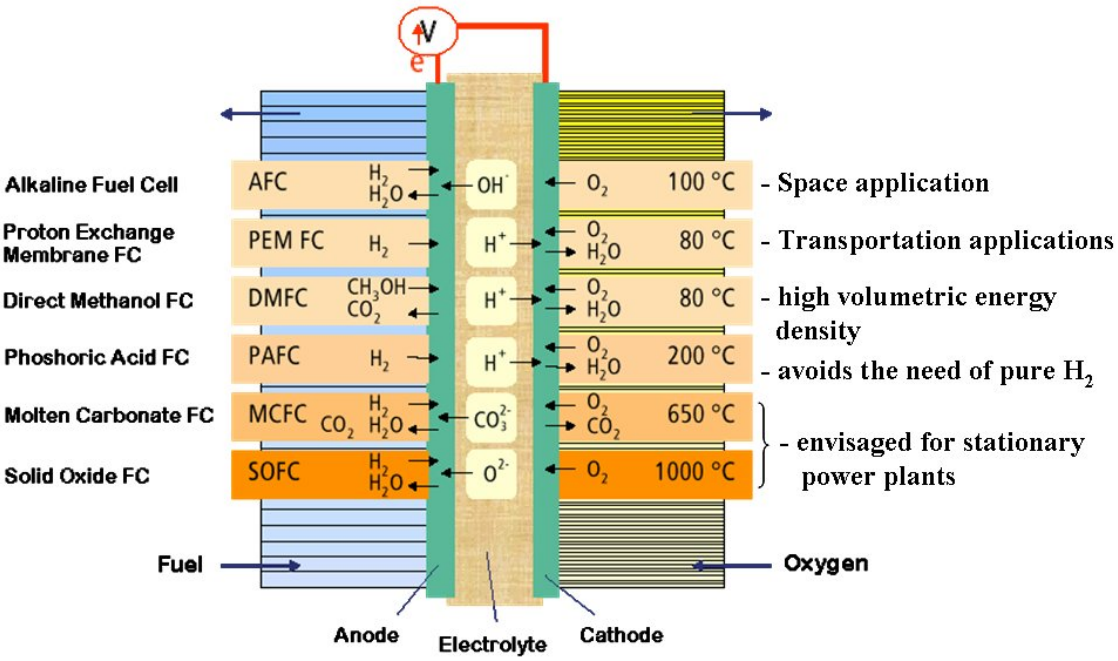

Scheme 1.3. Types of fuel cells

Polymer electrolyte membrane fuel cells (PEMFCs) are studied extensively, because of the versatile hydrogen oxidation reaction on Pt electrode. This versatility of hydrogen oxidation causes less over potential for this reaction. For hydrogen gas fed fuel cells at their current technological stage, hydrogen production, storage, and transportation are the major challenges in addition to cost, reliability and durability issues (Liu *et al*., 2006). The limitations on these issues of hydrogen as a fuel led to another technology, the reforming of different fuels like methane or methanol to hydrogen, on-site of the fuel cell (for example, Indirect methanol fuel cell). But the presence of reformers on-site make the vehicles bulky, with the reformers as the mini refinery (McNicol *et al*., 2001), and adds more problems to the fuel cell. Also the reformed hydrogen is contaminated with significant quantity of CO, which is a well known poison for Pt catalyst. Therefore, the use of fuels other than hydrogen is favoured. Compared to other hydrocarbon fuels, methanol is having next highest

energy density (Table 1.1, Aulice and Viswanathan, 2007). Methanol is advantageous in many more aspects such as highest volumetric energy density than hydrogen; the liquid nature, so that the ease of storage and transport; as well as the existing gasoline infrastructure can be used for methanol also; and its ease of availability. However, the commercialization of direct methanol fuel cells (DMFC) is still hindered by some technical challenges. The two major ones are (i) sluggish methanol oxidation kinetics even on some state-of-the-art anode catalysts and (ii) methanol crossover through the membrane, which not only depresses cathode performance, but also reduces fuel efficiency.

Table 1.1 Electrochemical energy data of different fuels

S.No.	Fuel	E^0_{theor} (V)	E^0_{max} (V)	Energy density (KWh/Kg)
1	Hydrogen	1.23	1.15	32.67
2	Methanol	1.21	0.98	6.13
3	Ammonia	1.17	0.62	5.52
4	Hydrazine	1.56	1.28	5.22
5	Formaldehyde	1.35	1.15	4.82
6	Formic acid	1.48	1.14	1.72
7	Methane	1.06	0.58	-
8	Propane	1.08	0.65	-

E^0_{theor} - theoretical electrochemical energy of the fuel

E^0_{max} - Maximum attainable electrochemical energy (Theoretical – overvoltage)

1.4 Electrode materials for methanol oxidation

Pt is the only element found to give atleast appreciable methanol oxidation current density and also could sustain the acidic condition of the fuel cell. It is due to its good

adsorption capacity for methanol and its stability under oxidative conditions. The direct methanol fuel cell (DMFC) shown in Scheme 1.2, consists of an anode at which methanol is electro-oxidised to CO_2 through the reaction (Hamnett, 1997).

$$CH_3OH + H_2O \rightarrow CO_2 + 6\,H^+ + 6\,e^- \quad E^0 = 0.016 \text{ V vs SHE} \qquad (1)$$

And a cathode at which oxygen (usually as air) is reduced to water or steam.

$$3/2\,O_2 + 6\,H^+ + 6\,e^- \rightarrow 3\,H_2O \qquad E^0 = 1.229 \text{ V vs SHE} \qquad (2)$$

With the over all reaction of,

$$CH_3OH + 3/2\,O_2 \rightarrow CO_2 + 2\,H_2O \qquad E^0 = 1.213 \text{ V vs SHE} \qquad (3)$$

The basic mechanism for methanol oxidation was reviewed by Parsons and VanderNoot, 1988, and can be summarized in terms of two basic functionalities: (a) Electrosorption of methanol onto the substrate. (b) Addition of oxygen to adsorbed carbon containing intermediates to generate CO_2. Very few electrode materials are capable of adsorption of methanol; only platinum and platinum based catalysts have been found to show both sensible activity and stability in acidic condition of fuel cells.

The mechanism of oxidation of methanol is supposed to follow the sequence of steps as follows;

$$CH_3OH + Pt(s) \rightarrow Pt\text{-}CH_2OH + H^+ + e^- \qquad (4)$$

$$Pt\text{-}CH_2OH + Pt(s) \rightarrow Pt_2\text{-}CHOH + H^+ + e^- \qquad (5)$$

$$Pt_2CHOH + Pt(s) \rightarrow Pt_3\text{-}COH + H^+ + e^- \qquad (6)$$

$$Pt_3\text{-}COH \rightarrow Pt\text{-}CO + 2\,Pt(s) + H^+ + e^- \quad (7)$$

$$Pt(s) + H_2O \rightarrow Pt\text{-}OH + H^+ + e^- \quad (8a)$$

$$Pt\text{-}OH + Pt\text{-}CO \rightarrow 2\,Pt + CO_2 + H^+ + e^- \quad \ldots\ldots\ldots (9)$$

The formation of OH by water activation on the Pt surface (8a), which is a necessary step for the oxidative removal of adsorbed CO, requires a high potential. In terms of methanol oxidation at anode, such a high potential will limit the fuel cell application of a pure platinum catalyst. Therefore a second metal that can provide oxygenated species at lower potentials for oxidative removal of adsorbed CO is envisaged. Binary Pt-based alloys, such as PtRu, PtOs, PtSn, PtW and PtMo have been investigated in order to improve the electro-oxidation activities of methanol. Among them, the Pt–Ru alloy has been found to be the most active binary catalyst. The enhanced activity of the Pt–Ru catalyst when compared with Pt for methanol oxidation has been attributed to both a bi-functional mechanism and a ligand (electronic) effect. The bi-functional mechanism involves the adsorption of oxygen containing species on Ru atoms (10) at lower potentials thereby promoting the oxidation of CO to CO_2, which can be summarized as follows:

$$Pt + CH_3OH \rightarrow Pt\text{-}CO_{ads} + 4H^+ + 4e^- \quad (10)$$

$$Ru + H_2O \rightarrow Ru(OH)_{ads} + H^+ + e^- \quad (11)$$

$$Pt\text{-}CO_{ads} + Ru(OH)_{ads} \rightarrow CO_2 + Pt + Ru + H^+ + e^- \quad (8b)$$

Understanding of this bifunctional nature of the methanol electro-oxidation mechanism, combination of different metals has been studied. For example ternary catalysts like PtRuOs, PtRuSn, PtRuMoOx and quarternary catalysts such as

PtRuRhNi have been studied with an emphasis to include one sacrificial element (Ni), so that the leaching of the active component is avoided (Park *et al*., 2004). But still the state-of-the-art catalyst remains to be Pt-Ru/C. It is worthwhile to point out that the criteria for Pt–Ru catalyst evaluation in terms of composition, structure and particle size are still controversial. It is generally recognized that Pt–Ru catalysts with a Pt:Ru atomic ratio of 1:1 may be the best DMFC catalysts in terms of activity and stability. However, Dubau *et al*., 2003 reported that the best composition of Pt–Ru/C catalysts for methanol oxidation largely depends on working potentials of the electrode. A ruthenium-rich catalyst showed higher performance at lower potentials, while a platinum-rich catalyst was better at higher potentials. Contrary to the current understanding of Pt–Ru electrocatalyzed oxidation of methanol, Long *et al*., 2000 argued that the Pt–Ru alloy is not the most desirable form of the catalyst and argued that a mixed-phase Pt–RuO_xH_y catalyst shows better electrocatalytic activity than alloyed Pt–Ru catalyst. The catalytic activity of the Pt–Ru catalyst is strongly dependent on the composition, structure, morphology, particle size and degree of alloying. The current consensus is that the optimal Pt/Ru ratio is 1:1, and the particle sizes are better brought down to the nanoscale in order to improve the catalyst utilization.

However, from the practical standpoint in a real fuel cell environment, a high catalyst loading (2–8 mg cm^{-2}) is required, even when using a 1:1 Pt–Ru alloy catalyst, in order to achieve acceptable fuel cell performance, especially when considering the lifetime of the fuel cell. This high loading of noble metal catalyst contributes to the high cost and hinders the commercialization of DMFCs. Reduction in loading through increasing Pt utilization is one of the R & D directions. Exploring new catalysts such as non-noble catalysts (Zhang *et al*., 2005) and optimization of catalyst activity

through supporting strategy (Lee *et al*., 2006) are two important approaches. Even though few studies on oxide materials are showing activity for methanol oxidation (Raghuveer and Viswanathan, 2002), the commercial viability is still far to reach. However, at this current stage, non-noble DMFC anode catalysts are not yet feasible. Alloying and nanoparticle supporting strategies could dramatically reduce the Pt content in the catalysts without performance compromise. The other strategy is support modification. Rapid development of nanotechnology, especially in the area of the synthesis of carbon nano-materials, expected to create more stable and active supported catalysts.

1.5 Catalyst preparation methods

In recent years, methodological development for Pt–Ru catalyst preparation has been one of the major topics in DMFC anode catalyst exploration. The Pt–Ru catalyst has been supported on some high surface area materials, such as carbon particles, in order to achieve high dispersion and maximum utilization, as well as to avoid catalyst agglomeration during the fuel cell operation. Although unsupported Pt–Ru catalysts have also drawn some attention in recent years, the latest reports have focused primarily on supported Pt–Ru/C catalysts. The common criteria for high performance catalysts are: (1) a narrow nanoscale size distribution; (2) a uniform composition throughout the nanoparticles; (3) a fully alloying degree; (4) high dispersion on carbon support. According to these criteria, some innovative and cost effective preparation methods have been developed and show promise for reaching performance optimization by controlling synthetic procedures and conditions. Typical methods used to prepare carbon supported Pt–Ru catalyst are the impregnation method, the colloidal method and the microemulsion method. All of these include a

chemical step for forming nanoparticles, and a deposition step for dispersing the catalyst onto the carbon particles, as summarized schematically in Scheme 1.4 (Liu *et al*., 2006).

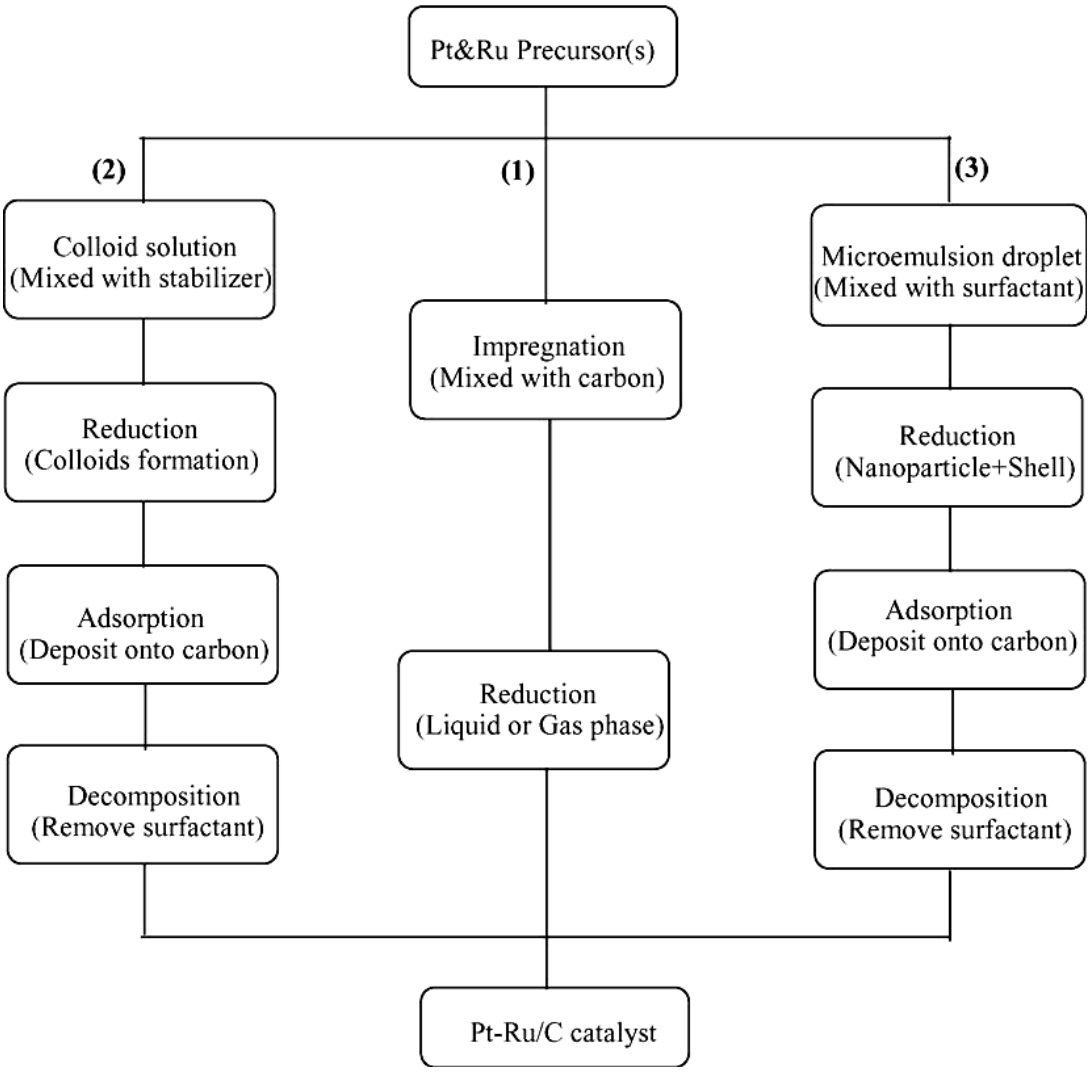

Scheme 1.4 **Synthesis methods for Pt–Ru/C catalysts: (1) The impregnation method, (2) the colloidal method and (3) the microemulsion method** (Liu *et al*., 2006)

1.5.1 The impregnation method

The impregnation method is the most widely used, and is a simple and straightforward technique for Pt–Ru catalyst preparation. This method includes an impregnation step, followed by a reduction step. During the impregnation step, Pt and Ru precursors are mixed with high surface area carbon black in aqueous solution to form a homogeneous mixture. As a catalyst support, carbon black plays a major role in terms of penetrating and wetting the precursors, and it also limits nanoparticle growth by strong metal support interaction. The chemical reduction step can be carried out by liquid phase reduction using $Na_2S_2O_3$, $NaBH_4$, $Na_4S_2O_5$, N_2H_4 or formic acid as a reducing agent, or gas phase reduction using a flowing hydrogen stream under elevated temperature.

During the impregnation process, many factors can affect the composition, morphology and dispersion of Pt–Ru/C catalyst, resulting in the variation of catalytic activity. The porosity of carbon black support can effectively control the catalyst nanoparticle size and dispersion. Many studies have indicated that synthetic conditions, such as the nature of the metal precursors used, the reduction method and the heating temperature, are also crucial in the impregnation process. Metal chloride salts (e.g., H_2PtCl_6 and $RuCl_3$) are commonly used as precursors due to their easy availability. However, it was argued that the metal chloride salts might lead to chloride poisoning, reducing the dispersion degree, catalytic activity and stability of the Pt–Ru/C catalyst. Pt–Ru/C catalysts by direct thermal decomposition of Pt and Ru carbonyl complexes (i.e., $[Pt(CO)_2]_x$ and $[Ru_3(CO)_{12}]$, Dickinson *et al*., 2002) onto carbon support was also studied. The results showed that the catalytic activity is favourably comparable with those commercially available. A drawback of this route is

that Ru carbonyl decomposition is more favourable than Pt carbonyl decomposition, resulting in a Ru-rich catalyst. In order to improve that, another modified impregnation route using single source metal precursor was recently developed, where single source precursors were used for the thermal decomposition to produce Pt–Ru nanoparticles on carbon black support under a reductive H_2 atmosphere. These single source precursors include molecular clusters, such as $PtRu_5C(CO)_{16}$, $Pt_2Ru_4(CO)_{16}$ (Nashner *et al*., 1997 and 1998) and organometallic complexes. To reduce the effect of thermal treatment on particle size, microwave dielectric loss heating also was introduced into this route (Boxall *et al*., 2001). Because the metal composition is predetermined, this route is advantageous for preparing stoichiometric and homogeneous Pt–Ru catalysts with a narrow size distribution. However, the synthesis of these single source precursors is too complicated and uses too many organic compounds, which may limit its application.

The major drawback of the impregnation method is the difficulty in controlling nanoparticle size and distribution. However, a highly dispersed Pt–Ru/C catalyst can still be obtained by carefully controlling appropriate preparation conditions. More recently, Guo *et al*., 2005 reported a modified impregnation method using citric acid as stabilizer of metal ions to prepare well dispersed Pt–Ru/C catalysts. Their in-house Pt–Ru/C catalyst gave a power density of 44 mW cm^{-2} in a single DMFC testing at 70 °C, which was comparable to the power density of 42 mW cm^{-2} for a commercially available E-TEK catalyst with the same composition at the similar testing conditions.

1.5.2 The colloidal method

The colloidal method is another extensively explored preparation route for the Pt–Ru/C catalyst (Watanabe *et al*., 1987; Radmilovic *et al*., 1995; Luna *et al*., 2000; Bonnemann *et al*., 1994; Schmidt *et al*., 1997; Paulus *et al*., 2000). Usually, the colloidal method includes the following common steps: (1) preparation of Pt–Ru containing colloids; (2) deposition of the colloids onto the carbon support; (3) chemical reduction of the mixture as shown in Scheme 1.4. It is also schematically shown in Fig. 1.2. Using this method a Pt–Ru catalyst with much higher specific surface area compared to that of a conventional impregnation method was reported. However, the particle growth and agglomeration control in this route seem to be problematic. Bonnemann *et al*. developed an organometallic colloid route by stabilizing the Pt/Ru metal particles with organic molecules, resulting in easy control of particle size and distribution. Bonnemann's route mainly consists of three steps, i.e. pre-forming surfactant-stabilized Pt–Ru colloids (e.g., PtRu-$N(oct)_4Cl$ colloids), adsorbing the colloids on high-surfacearea carbon, and removing the organic stabilizer shell by thermal treatment in an O_2 atmosphere and H_2 atmosphere, respectively. By this route, Pt–Ru catalysts with well defined, completely alloyed particles and a very narrow particle size distribution (<3 nm) were obtained, and showed comparable activity (~ 70 mA mg^{-1} (PtRu) at 500 mV (versus RHE) in 0.5 M CH_3OH and 0.5 M H_2SO_4 at 60 °C) with that of state-of-the-art commercially available catalyst (~ 80 mA mg^{-1} (PtRu). The organometallic colloid route is still not favourable in practical applications due to the complexity of the preparation steps and the relatively high cost.

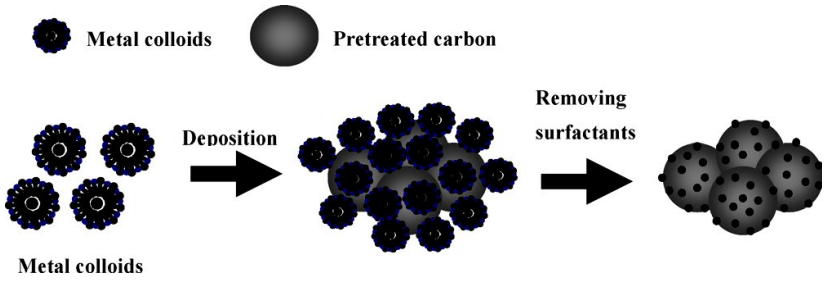

Fig. 1.2 Schematic illustration to prepare Pt/C catalysts by colloidal method (Lima *et al*., 2008)

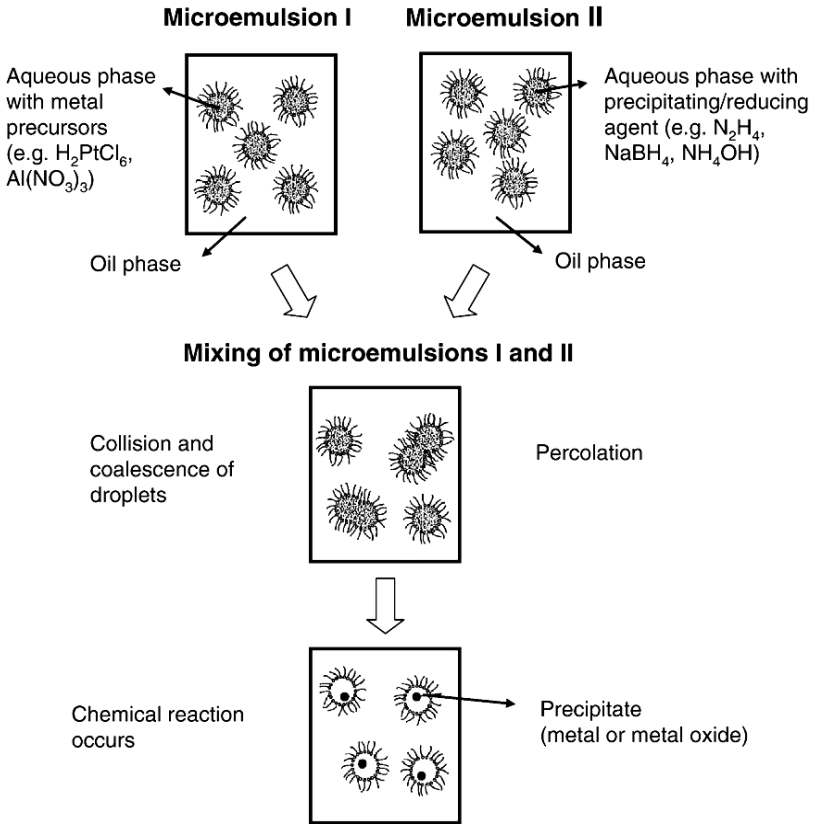

Fig. 1.3 Schematic illustration of formation of metal particles by reverse (w/o) microemulsion method (Boutonnet *et al*., 2008)

1.5.3 The microemulsion method

In this method, the first step is the formation of Pt–Ru nanoparticles through a water-in-oil microemulsion reaction, followed by a reduction step (Scheme 1.4). Fig. 1.3

explains schematically the formation of metal particles by reverse microemulsion method (i.e., water in oil phase, w/o). The microemulsion serves as a nanoscaled reactor in which the chemical reaction takes place. The microemulsion is a nanoscaled aqueous liquid droplet containing a noble metal precursor. The droplets are engulfed by surfactant molecules and uniformly dispersed in an immiscibly continuous organic phase. The reduction step is carried out either by adding a reducing agent (e.g., N_2H_4, HCHO, and $NaBH_4$) into the microemulsion system, or by mixing it with another microemulsion system containing reducing agent. As a result, the reduction reaction is confined to the inside of the nanoscaled microemulsion, and the formed metal particle sizes can be easily controlled by the magnitude of the microemulsion size. The surfactant molecules function as protective agents to prevent the Pt–Ru nanoparticles from agglomeration. The removal of surfactant molecules are carried out by heat treating high surface area carbon supported nanoparticles. Pt–Ru/C catalysts prepared by this method were found to exhibit higher activity than those commercially available for methanol oxidation in both electrochemical half cell containing sulphuric acid and methanol and in a DMFC. The main advantage of the microemulsion method is its ease in controlling metallic composition and particle size within a narrow distribution by varying the synthetic conditions. Liu *et al*., 2002 studied the formation conditions of microemulsion in a (H_2PtCl_6 + $RuCl_3$ + NaOH)–(NP_5 +NP_9)–cyclohexane system. A limited region in the phase diagram was identified to be suitable for microemulsion formation. The microemulsion produced Pt–Ru/C catalyst was found to give smaller particle sizes, with higher anodic peak current density (0.24 mA cm^{-2} (metal)) towards methanol oxidation in CV measurement, compared with the catalyst produced by a conventional emulsion method (0.05 mA $cm^{-2}_{(metal)}$). However, like the organometallic colloid method, the microemulsion method also

uses expensive surfactant molecules and requires a substantial number of separation and washing steps, which may not be suitable for large scale production.

1.6 Catalyst supports

In order to achieve fine dispersion, high utilization and stable nanoscale metallic particles, catalyst supporting strategies have been explored. Compared to bulk metal catalysts, supported catalysts show higher activity and stability. Support plays an important role in controlling the dispersion, particle size and activity through the different nature and degree of metal-support interaction. From the understanding of methanol oxidation mechanism, which needs the oxygen functional group for the oxidation of the adsorbed CO intermediate, different transition oxide support materials (WO_6, MoO_x, TiO_2 etc.) were also exploited for noble metal catalysts for methanol oxidation. Different kind of support materials, like organic polymers (Rajesh *et al*., 2004) were exploited as the noble metal supports. But the highly acidic conditions of the fuel cell cause these materials less stability. Carbon particles are frequently used as catalyst supports because of their relative stability in both acidic and basic media, good electric conductivity and high specific surface area. In recent years numerous studies have concentrated on understanding the effects of carbon supports and exploring new carbon supports.

1.6.1 Carbon black

Carbon blacks are commonly used as supports for DMFC anode catalysts. There are many types of carbon blacks, such as acetylene black, furnace black, etc., and these are usually manufactured by pyrolyzing hydrocarbons such as natural gas or oil fractions taken from petroleum processing. These carbon blacks show different physical and chemical properties, such as specific surface area, porosity, electrical

conductivity and surface functionality. Among these factors, specific surface area has a significant effect on the preparation and performance of supported catalysts. Generally, highly dispersed, supported catalysts cannot be prepared from low surface area carbon blacks (e.g., acetylene black). High surface area carbon blacks (e.g., Ketjen Black) could support highly dispersed catalyst nanoparticles. However, Ketjen Black supported catalysts showed high ohmic resistance and mass transport limitation during fuel cell operation. Vulcan XC-72 with a surface area of ~ 250 m^2 g^{-1} has been widely used as a catalyst support, especially in DMFC anode catalyst preparation. An accessible and sufficiently large surface for maximum catalyst dispersion has been argued to be a necessary but insufficient condition for obtaining optimized carbon supported catalysts. Other factors, such as pore size and distribution, and surface functional groups of carbon blacks, also affect the preparation and performance of carbon black supported catalysts. For example, in a conventional impregnation process, a portion of the metal nanoparticles may be sunk into the micropores of Vulcan XC-72. This portion inside the micropores has less or no electrochemical activity due to the difficulty in reactant accessibility. This is the major reason why some catalysts prepared by the impregnation method have not shown high activity even when the metal loading is very high. By keeping Pt nanoparticle size larger than the micropore size, Anderson *et al*., 2002 found that the saturated weight loading of Pt onto Vulcan carbon by the colloid method was 9–10 wt.% versus 10–40 wt.% by the impregnation method. Their results indicated that micropores, which are smaller than the Pt nanoparticle size, could effectively block the sinking of the metal nanoparticles.

1.6.2 Nanostructured carbon

In recent decades, a series of new nanostructured carbon materials were explored as catalyst supports. The family of carbon nanotubes (CNTs) is the most well-known nanostructured carbon, which has shown very promising results in catalyst support for fuel cell applications due to their unique electrical and structural properties. The reported studies have shown that CNTs were superior to carbon blacks as catalyst supports for proton exchange membrane fuel cells (PEMFCs). A CNT supported Pt catalyst with 12 wt.% Pt loading could give a 10% higher fuel cell voltage, and twice the power density than that of carbon black supported catalyst with 29 wt.% Pt loading (Matsumoto *et al*., 2004; Tang *et al*., 2004). On the other hand, many studies have explored CNTs as supports for DMFC catalysts in recent years. Li *et al*., 2002 reported that multi-wall carbon nanotube (MWNT) supported catalysts exhibited better performance in DMFCs compared to those supported by carbon black (XC-72) under identical conditions both in half-cell characterization and in a fuel cell performance test. Che *et al*., 1999 found that the current density of methanol oxidation on a Pt/MWNT catalyzed membrane electrode was 20 times higher than that of a bulk Pt electrode. Rajesh *et al*., (2002 and 2003) investigated methanol oxidation catalyzed by various metal catalysts that could be supported on CNTs and commercially available Vulcan carbon. The activity and stability of these electrodes were ranked from highest to lowest as: Pt–WO_3/CNT > Pt–Ru/Vulcan > Pt/CNT > Pt/Vulcan > bulk Pt. Single wall carbon nanotube (SWNT) supported Pt electrodes were also reported to exhibit higher catalytic activity both for methanol oxidation and oxygen reduction than that seen in an unsupported Pt electrode. The higher catalytic activity was thereby attributed to the larger surface area of carbon nanotube

architecture and the lower overpotential for methanol oxidation. Therefore, CNTs appear to have promising potential as catalyst supports for DMFCs.

However, the CNT synthesis, metal loading and electrode preparation based on CNT supports still face some challenges, especially when applied to fuel cells. CNTs are usually synthesized by carbon-arc discharge, laser ablation of carbon, or chemical vapor deposition. These synthetic methods have their limitations in terms of large scale production and cost effectiveness. Their harsh synthetic conditions and low production yields are major disadvantages. Additionally, it was found that the surface modification of CNTs before metal deposition is important for achieving optimal interaction between the support and the catalyst precursor (Serp *et al*., 2003; Han *et al*., 2004). Because the pristine surface of CNT is inert, it is difficult to attach metal nanoparticles to the substrate surface. Through surface modification or pre-treatments, some anchoring sites were introduced onto the surface so that the metal nanoparticles be easily attached onto the CNTs surface. The most widely used pre-treatment is refluxing CNTs in nitric acid to create an acid site on the surface, which can act as a nucleation center for metal ions. In addition to CNTs, other nanostructured carbons, such as carbon nanofibers, carbon nanocoils and fullerenes, were also explored as catalyst supports for DMFCs.

1.6.3 Mesoporous carbon

A high performance DMFC anode requires the provision of an efficient transport passage for liquid-phase reactants (CH_3OH, H_2O) and the gas-phase product (CO_2). Too many small micropores (<2 nm) in carbon supports (e.g., Vulcan XC 72) decreases catalyst utilization because the mass transport of reactants and product is poor in these micropores. When macroporous size is larger than 50 nm, the surface

area becomes small and leads to increased electrical resistance (Chan *et al*., 2004). Mesoporous carbons with tuneable pore sizes in the range 2–50 nm are, thus, attractive for use as catalyst supports and have the potential to enhance both the dispersion and utilization of metal catalysts. The ordered mesoporous carbon is usually synthesized by a template method starting with either highly ordered mesoporous silica or nanosized silica spheres. With mesoporous silica or nanosized silica as a template, organic materials were diffused into the pores followed by carbonization. Uniform mesoporous carbon can be formed after removing the silica template by etching with hydrofluoric acid (Chan *et al*., 2004; Yu *et al*., 2002) synthesized a series of porous carbons with pore sizes in the range 10 –1000 nm by this procedure and investigated the performance of these porous carbon supported Pt–Ru catalysts under DMFC conditions. They found that the porous carbon with a mesopore size (25 nm) showed the highest performance, which corresponds to a 43% increase in activity as compared to that of a commercially available Pt–Ru/C catalyst (E-TEK). This higher performance was considered to be not only due to the higher surface areas and larger pore volumes, which allowed a higher degree of catalyst dispersion, but also due to highly integrated interconnected pore systems with periodic order, which allowed efficient transport of reactants and products. Raghuveer and Manthiram (2004 and 2005) used a modified colloidal template route to control the pore size of porous carbon. The obtained mesoporous carbon produced larger surface area and pore volume than the Vulcan XC 72R. The electrochemical measurements using catalyst-coated glassy carbon electrodes with a catalyst loading of 0.28 mg cm^{-2}, has shown that the mesoporous carbon loaded with 5% Pt exhibited three times higher mass activity (mA mg^{-1} Pt) than the commercially available 20% Pt/C catalyst for methanol oxidation Therefore, mesoporous carbons appear to have

great potential for catalyst supports in DMFC anode catalysis by offering significant cost reduction through improved catalyst utilization and lowered the catalyst loading.

Carbon material has a strong influence on the properties of the supported noble metal catalysts, such as metal particle size, morphology, size distribution, degree of alloying, stability and dispersion. Carbon supports also affect the performance of supported catalysts in fuel cells, such as mass transport, catalyst layer electronic conductivity, electrochemical active surface area, and metal nanoparticle stability during the operation. Hence, the optimization of carbon supports is very important in DMFC development.

1.7 Motivation and objectives of the present investigation

The present work, therefore is focusing on the different kinds of functionalization of the carbon black support, which can lead to smaller Pt particle size and hence enhanced dispersion, higher active surface area, better utilization of the expensive, less abundant noble metal catalyst, so that the fuel cell performance could be commercially viable. This thesis work focuses on the following aspects of the carbon black support towards enhancement in the supported noble metal catalysts for methanol electro-oxidation.

- Effect of carboxylic acid functionalization of the carbon black support CDX975
- Effect of sulfonic acid functionalization of the carbon black support CDX975
- Effect of aminopyridine functionalization of the carbon black support CDX975

- Effect of the capping agent on the dispersion and activity of the Pt nanoparticles on the carbon black support

As this study is focusing on the effect of different functionalization of the carbon support, the study has been restricted to mainly on Pt/C catalyst rather than Pt-Ru/C to keep the system simple with out any complication for understanding.

CHAPTER 2

EXPERIMENTAL METHODS

2.1 CHEMICALS AND MATERIALS

Hexachloroplatinic acid was procured from Arora Matthey, Kolkatta, India. 5 wt.% Nafion solution was purchased from Sigma Aldrich. CDX975 carbon black was provided by Columbian Chemicals Company, USA. Analytical grades of nitric acid and sulphuric acid were purchased from Merck. Ananlytical grades of solvents like acetone, ethanol, methanol and sodium sulphite were purchased from Sisco Research Laboratories Pvt. Ltd. High pure N_2 and H_2 gases were obtained from M/S Indian Oxygen Ltd.

2.2 CHARACTERIZATION TECHNIQUES

2.2.1 X-ray diffraction studies

X-ray diffraction studies of the samples were carried out on Rigaku miniflex(II) Desktop X-ray diffractometer using Cu Kα(λ = 1.5405 Å), with Ni filter. The crystallite size was calculated by X-ray line broadening method using Debye-Schrrer equation (Patterson, 1939),

$$d\ (nm) = K\ \lambda / (\beta \cos\theta) \qquad (2.1)$$

where, d is the crystallite size in nm, K is the numerical constant, 0.9, λ is the wave length of radiation used, β is full width at half maximum in radians and θ is the Bragg diffraction angle in degrees, at the peak maximum. The X-ray diffraction patterns

were recorded at the scan rate of 3 deg./min, sampling width of 0.020 deg. for the 2θ range of 10 – 90°.

2.2.2 FT-IR analysis

FT-IR spectra were recorded with BRUKER FT-IR Spectrometer by KBr pellet method at the resolution of 2 or 4 cm^{-1}.

2.2.3 Thermogravimetric analysis (TGA)

TGA was performed with Perkin Elmer Diamond TG/DTA analyzer under nitrogen or air for the temperature range of 313-1073 K at a heating rate of 10 K/min.

2.2.4 BET surface area measurements

Nitrogen adsorption/desorption studies were done with Micromeritics ASAP2020. Surface area of the sample was calculated using BET equation. Degassing of the sample was done at 373 K for 2 h and at 423 K for 3 h.

2.2.5 Scanning electron microscopic (SEM) analysis

Scanning electron micrographs were recorded using FEI, Quanta 200. The samples in the powder form were taken on the carbon tape and mounted on the SEM sample holder.

2.2.6 Transmission electron microscopic (TEM) analysis

Transmission electron micrographs and high resolution transmission electron micrographs were recorded on a JEOL 3010 model. Few milligrams of the samples (1-2 mg) were dispersed in few mL (1-2 mL) of acetyl alcohol by ultrasonication for 5

min and a drop of the dispersion was placed on a carbon coated copper grid and allowed to dry in air at room temperature.

2.2.7 X-ray photoelectron spectroscopic (XPS) analysis

The X-ray photoelectron spectroscopic studies were performed using KRATOS-AXIS 165 instrument equipped with dual aluminum–magnesium anodes using Mg Kα radiation. The X-ray power supply was run at 15 kV and 5 mA. The pressure of the analysis chamber during the scan was 10^9 Torr. The peak positions were based on calibration with respect to the C 1s peak at 284.6 eV. The obtained XPS spectra were fitted using a non-linear square method with the convolution of Lorentzian and Gaussian functions after polynomial background subtraction from the raw data.

2.2.8 pH determination

pH measurements were done with Elico pH meter, using aqueous slurry of the samples. The aqueous slurry of the sample was prepared by taking 30 mg of the sample in 7 mL of distilled water and ultrasonicating for 5 min.

2.2.9 Estimation of platinum metal loading

Platinum was extracted from Pt/C catalyst by burning off carbon at 1073 K in air for 5 h; then extracting Pt with aqua regia (3 mL) thrice and with conc. HCl (2 mL) twice. The extraction was made upto 25 ml with 2M HCl. The extraction was estimated for Pt with inductively coupled plasma optical emission spectroscopy (ICP-OES).

2.2.10 Elemental Analysis

The C, H and N analysis were done with Perkin Elmer CHN analyzer.

2.2.11 Electrochemical measurements

BAS Epsilon Potentiostat was used for the electrochemical studies. All the electrochemical measurements were performed with three electrode cell assembly, consists of glassy carbon disk (dia. = 0.3 cm, geometrical surface area = 0.07 cm^2) as the working electrode, Pt foil (1.5 cm^2) as the counter electrode and Ag/AgCl as the reference electrode. Cyclic voltammetric studies for hydrogen adsorption/desorption charge determinations were conducted in 1M H_2SO_4. Methanol oxidation and chronopotentiometric studies were carried out in 1M methanol and 1M sulphuric acid.

The working electrode was fabricated by dispersing 5 mg of the catalyst in 0.25 mL of distilled water by ultrasonication for 20 min. 10 μL of the dispersion was placed on 0.07 cm^2 of the glassy carbon electrode, and dried in an air oven at 363 K for a few minutes. Then, the resulting catalyst coating was covered with 5 μL of 5 wt% Nafion solution followed by drying in air for a few minutes.

2.2.11.1 Determination of Electrochemical Active Surface Area (EAS)

The electrochemical active surface area of the Pt/C catalyst was determined from the charge for hydrogen adsorption/desorption using equation 2.2. A model calculation for EAS is given in the subsequent section.

Electrochemical active surface area (EAS) (m^2/g) = Q_H/([Pt]x0.21) …… (2.2)

Q_H – Average charge for hydrogen adsorption/desorption in mC/cm^2

[Pt] – loading of platinum in mg/cm^2

0.21 – charge (in mC) required to oxidize one monolayer of hydrogen from 1 cm^2 of platinum black (Ralph *et al.*, 1997; Pozio *et al.*, 2002).

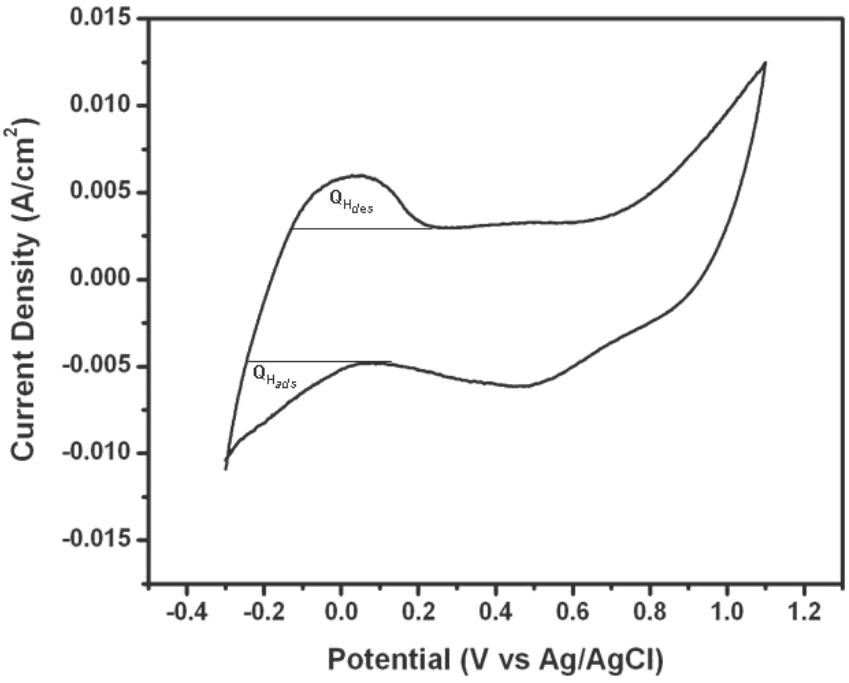

Fig. 2.1 A model Cyclic voltammogram of Pt/C catalyst in 1M H_2SO_4 at 25 mV/s

Calculation of [Pt] - Pt Loading

100 mg catalyst contains 10 mg Pt

$\therefore$ 5 mg catalyst contains = (10/100) × 5 = 0.5 mg of Pt

0.5 mg of Pt is dispersed in 0.25 ml (250 μL) of dist. H_2O, and 10 μL of the dispersion is dispensed on 0.07 cm^2 area of glassy carbon electrode.

$\therefore$ 10 μL contains = (0.5 mg/250 μL) × 10 μL = 0.02 mg Pt = 20 μg Pt

Pt loading (mg /cm^2) = (0.02/0.07) = **0.286**

Charge calculation for hydrogen desorption

No. of square units during hydrogen desorption = 122

Area of each square unit = 122 x8.33 x 0.123 (mA/cm^2)x mV

= 125 (mA/cm^2)x mV

Charge during hydrogen desorption = [125 (mA/cm^2)x mV] / 25 mVs^{-1}

= 4.99 (mA/cm^2)s

= [4.99 (mA/cm^2)s]/3600

= 1.39 x 10^{-3} mA.h/cm^2

26.8 Ah = 96500 C

$\therefore$ Charge (mC/cm^2) = [(1.39 x 10^{-3} mA.h/cm^2) x 96500]/ 26.8

= 5.00 mC/cm^2

Charge calculation for hydrogen adsorption

No. of square units during hydrogen adsorption = 302

Area of each square unit = 302 x8.33 x 0.123 (mA/cm^2)x mV

= 309.4 (mA/cm^2)x mV

Charge during during hydrogen adsorption = [309.4 (mA/cm^2)x mV] / 25 mVs^{-1}

= 12.38 (mA/cm^2)s

= [12.38 (mA/cm^2)s]/3600

= 3.438 x 10^{-3} mA.h/cm^2

26.8 Ah = 96500 C

$\therefore$ Charge (mC/cm^2) = [(3.438 x 10-3 mA.h/cm2) x 96500]/ 26.8

= 12.38 mC/cm^2

Average Q_H = [5 + 12.38]/2 = 8.689 mC/cm^2

[Pt] = 0.286 mg/cm^2

EAS = 8.689/[0.286 x 0.21] = 144.67 (mC/cm^2)/[mg/cm^2 x mC/cm^2]

= 144.7 cm^2/mg = 144.7 x 10^{-4} $m^2/10^{-3}g$

EAS = 14.5 m^2/g

2.2.11.2 Determination of Mass Specific Activity

Mass Specific Activity of the Pt/C catalyst was determined using equation 2.3. The current density (forward peak current density) for methanol oxidation is obtained from the cyclic voltammogram of the catalyst in 1M methanol and 1M H_2SO_4.

Mass Specific Activity (mA/ mg) = current density (mA/cm^2)/ Pt loading (mg/cm^2) (2.3)

2.2.11.3 Determination of Specific Activity

Specific activity was determined using equation 2.4.

Specific Activity (A/m^2 of Pt) = Mass Specific Activity (A/g)/EAS (m^2/g) (2.4)

CHAPTER 3

EFFECT OF CARBOXYLIC ACID FUNCTIONALIZATION OF CDX975 CARBON BLACK SUPPORT OF Pt/CDX975 CATALYST FOR METHANOL ELECTRO-OXIDATION STUDIES

3.1 Introduction

Carbon materials are finding an increasing number of applications in catalysis, either as supports for active phases or as catalysts on their own (Figueiredo *et al*., 1999). Carbon supported Pt and Pd catalysts have been extensively used not only for fuel cell electrodes but also for hydrogenation, dehydrogenation and oxidation reactions in the area of fine chemicals (Du *et al.*, 2008; Harada *et al.*, 2007). Loading of the same metal particles on different carbon supports could exhibit different catalytic activities. The main reason is that the activity of these catalysts strongly depends on the physicochemical properties of the carbon supports such as their texture and surface chemistry, and these properties largely affect the size and dispersion of the supported metal particles (Molina-Sabio and Rodrıguez-Reinoso, 2004 and Job *et al*., 2006). Carbon is supposed to contain various functional groups like hydroxyl, phenolic, carbonyl, carboxylic, lactone etc. as shown in Fig. 3.1.

It is well known that the physical and chemical properties of carbon materials have the possibility of being tailored and the performance of catalysts can be optimized by modifying the surface functional groups on the carbon supports (Figueiredo *et al*., 1999; Li, J. *et al*., 2005;, Li, Z. *et al*., 2005). Generally, studies on surface functionalization of carbon including activated carbon, carbon black and carbon nanotubes carried out by treating them with concentrated acids like nitric acid and

sulphuric acid had shown high reactivity and the Pt loaded on these modified support catalysts exhibited excellent catalytic activities (Yeung and Wolf, 1992; Li, Z. *et al*., 2005; Suh *et al*., 1993; Rosca *et al*., 2005; Peng *et al*. 2003; Fraga *et al*., 2002; Yu *et al*., 1998).

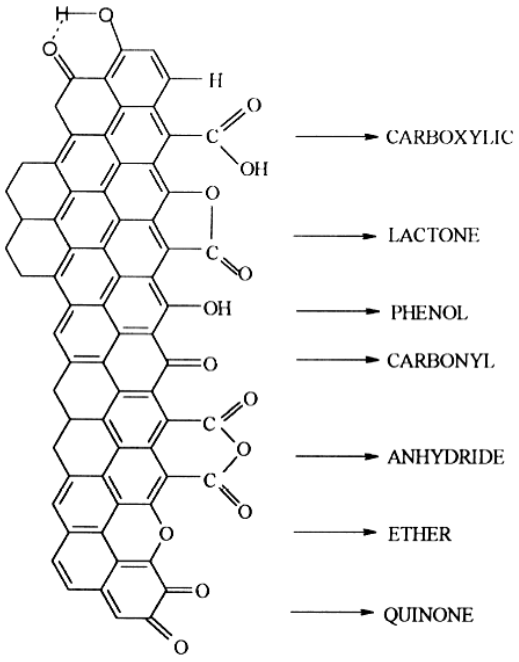

Fig. 3.1 Schematic of the surface groups on the carbon black support

One of the key parameters of the catalyst in this respect is its hydrophilicity. Wetting of the catalyst particles would be expected to be important for their effective utilization, although a catalyst layer that was too hydrophilic might become flooded and therefore restrict gas access. Increasing the hydrophilicity of the catalyst might therefore increase the performance, and/or decrease the amount of proton exchange polymer needed in the catalyst layer for optimum performance (Jia *et al*., 2001). The 'activation' of the carbons commonly used as catalyst supports, under oxidizing conditions, is well known (Kinoshita, 1988). Treatment of carbon black with concentrated nitric acid is known to increase its hydrophilicity by forming surface

carboxylic acid functionality. One such example is the treatment of acetylene black with boiling nitric acid, prior to the deposition of platinum in the preparation of supported catalysts for use in phosphoric acid fuel cells (Watanabe *et al*., 1985).

However, some controversies exist with the nitric acid treatment of the carbon black support and the Pt nanoparticles dispersed on it. The measurement of electro active surface area (measure of Pt dispersion), from hydrogen adsorption current density by cyclic voltammetry had shown decreased electrochemical active surface area with the increase of surface oxygen functional groups (Antonucci *et al*., 1994). Measurement of platinum dispersion by hydrogen chemisorption studies (Roman-Martinez *et al*., 1995) had shown a decrease of Pt dispersion with an increase of surface oxygen functional groups. This was attributed to the aggregation of the Pt nanoparticles on the surface of the carbon black support itself due to the high concentration of the surface oxygen groups and resulted into a lesser diffusion of Pt nanoparticles to the inner pores of the carbon black support. The existence of these controversies has encouraged to study further on these oxidative treatment of carbon black support with nitric acid.

3.2 Nitric acid treatment scheme

CDX975 carbon black support was treated with two different concentrations of nitric acid (1N and concentrated) at two different reaction times (60 and 95 min) by taking the required quantities of 1N or conc. HNO_3 (20 or 40 mL for the reaction times of 60 and 95 min respectively) with 500 mg of CDX975 and stirring at 333-343 K. After cooling to room temperature it has been filtered and washed with copious quantity of distilled water to remove the nitrate impurities. Then it was dried at 353-363 K in an air oven.

3.3 Loading of Pt on the nitric acid treated CDX975

100 mg of the nitric acid treated CDX975 was impregnated with the required quantity (to obtain 10 wt% Pt/C) of aqueous slurry of hexachloroplatinic acid (5 wt% of H_2PtCl_6) and evaporated to dryness at 333-343 K. The impregnated catalyst was reduced in hydrogen atmosphere at 623 K for 4 h. For comparison, Pt loaded on untreated CDX975 was also prepared.

3.4 Characterization of the carbon black samples and the Pt loaded catalysts

3.4.1 pH determination

The pH of aqueous slurry of 30 mg of the untreated and oxidized CDX975 carbon black samples in 7 mL of dist. H_2O was determined after ultrasonication for 5 min. As shown in Table 3.1, decrease in pH was observed with the increase of oxidative conditions (i.e., concentration of nitric acid and reaction time). This decrease of pH is indicative of the formation of carboxylic functional groups on the carbon black support on treatment with nitric acid (Boehm, 1994; Roman-Martinez *et al*., 1995).

Table 3.1 pH values of the untreated and the different nitric acid treated CDX975 carbon black support

S. no.	Sample	pH
1	untreated CDX	6.1
2	1N HNO_3 treated CDX-60 min	5.0
3	conc. HNO_3 treated CDX-60 min	4.5
4	1N HNO_3 treated CDX-95 min	4.1
5	conc. HNO_3 treated CDX-95 min	3.7

3.4.2 FT-IR studies

Fig. 3.2 shows the FT-IR spectra of untreated and nitric acid treated CDX975 carbon black support. Nitric acid treatment for 60 min with both 1N and conc. HNO_3 has shown a slight increase in absorbance for the carboxylic –OH group vibration in the range of 3000-3600 cm^{-1} and a decrease in absorbance for the carbonyl vibration at 1642 cm^{-1}. But the treatment for 95 min with both 1N and conc. HNO_3, shows clearly the vibrations for carboxylic carbonyl group (1725 cm^{-1}) and broad strong bands due to vibrations for carboxylic -OH groups (3000-3600 cm^{-1}). These observations show the oxidation of the carbonyl groups of the carbon black support to the carboxylic groups, upon nitric acid treatment. However the pH (Table 3.1) determination has shown a decrease in pH with the treatment of nitric acid for both 60 and 95 min. This might be due to the less concentration of the produced carboxylic groups in case of 60 min reaction time. This also might be due to the formation of less acidic phenolic or carbonyl groups during the mild oxidative conditions as stated by Antonucci *et al*., 1994.

3.4.3 NH_3-TPD studies

Fig. 3.3 shows the NH_3-TPD profiles of the untreated CDX975 and 1N and conc. HNO_3 treated CDX975 for 60 min. As observed with the results of FT-IR, NH_3-TPD also does not show much difference in acidity for the carbon black samples, untreated and the 1N nitric acid treated for 60 min. But with increased oxidative conditions such as with concentrated nitric acid, the resulting carbon has shown significant increase in the NH_3 signal, which is a direct measure of the carboxylic acidity.

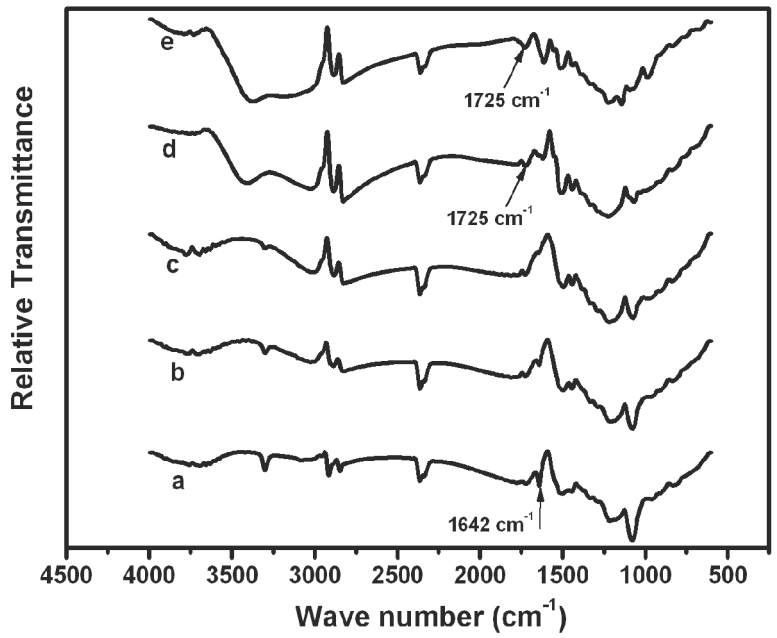

Fig 3.2 FT-IR spectra of the CDX975 carbon black support (a) unmodified (b) 1N HNO_3 treated CDX975-60 min (c) conc. HNO_3 treated CDX975-60 min (d) 1N HNO_3 treated CDX975-95 min and (e) conc. HNO_3 treated CDX975-95 min

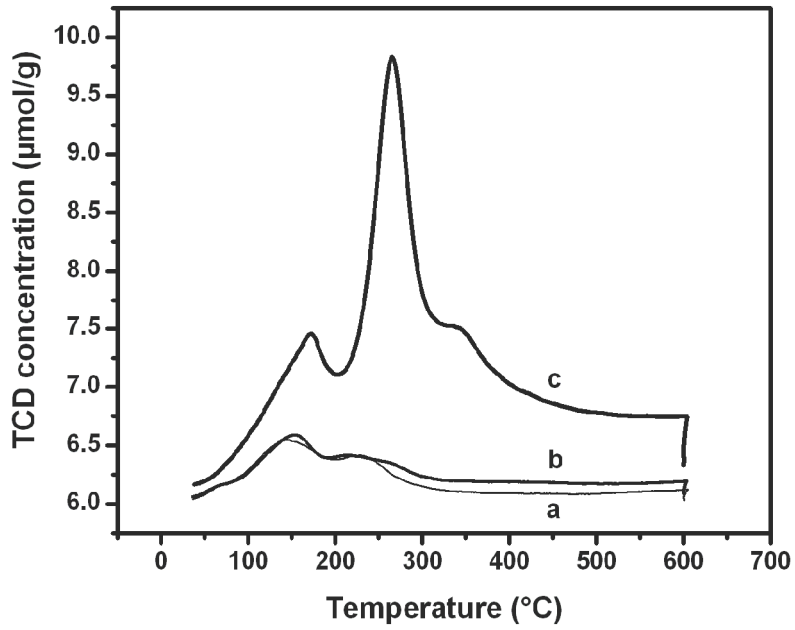

Fig 3.3 NH_3-TPD profiles of CDX975 carbon black support (a) unmodified (b) 1N HNO_3 treated CDX975-60 min and (c) conc. HNO_3 treated CDX975-60 min

3.4.4 Thermogravimetric analysis

Fig. 3.4 shows the TGA profiles of the different nitric acid treated CDX975 and that of the untreated CDX975 in nitrogen atmosphere. As the oxidative condition of nitric acid was increased (increase in concentration of nitric acid or increase in oxidative reaction time), the thermal stability of the CDX975 carbon black founds to decrease. This is complementary to the observations made from FT-IR and TPD results. The increase of oxidative conditions produced more of carboxylic groups, which resulted in lesser thermal stability, as the carboxylic group decomposes at low temperatures (423-473 K) compared to other functional groups on the carbon black (Olga Baturin *et al*., 2006).

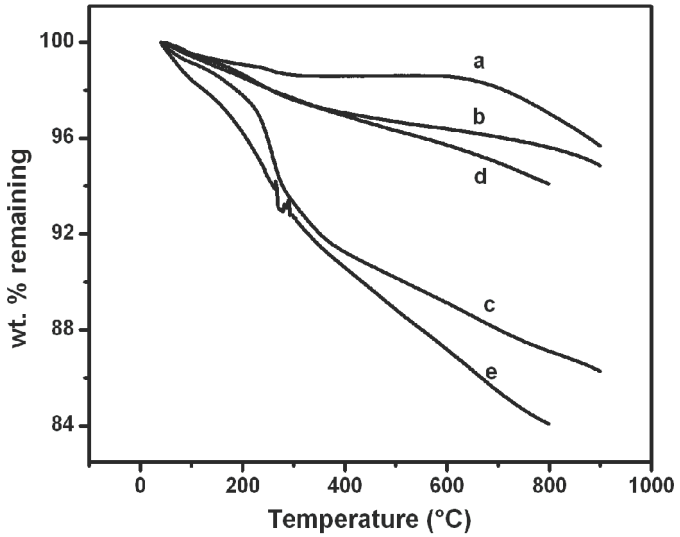

Fig. 3.4 TGA profiles of CDX975 carbon black support (a) unmodified (b) 1N HNO_3 treated CDX975-60 min (c) conc. HNO_3 treated CDX975-60 min (d) 1N HNO_3 treated CDX975-95 min and (e) conc. HNO_3 treated CDX975-95 min in N_2 at 10°C/min

3.4.5 Studies on textural properties

Nitrogen adsorption/desorption isotherms of the untreated and nitric acid treated CDX975 are shown in Fig. 3.5. Surface area and pore volume are given in Table 3.2. A decrease in BET surface area and pore volume was observed with an increase in oxidative condition of nitric acid treatment. Similar results are reported for studies of oxidative treatment of carbon black support with nitric acid (Moreno-Castilla *et al*., 1995; Moreno-Castilla *et al*., 1998; Figueiredo *et al*., 1999). It is reported that the higher the degree of activation of the carbon sample, the higher is the decrease in surface area and pore volume, as increase in the degree of activation makes the pore walls thinner and thus are easily destroyed.

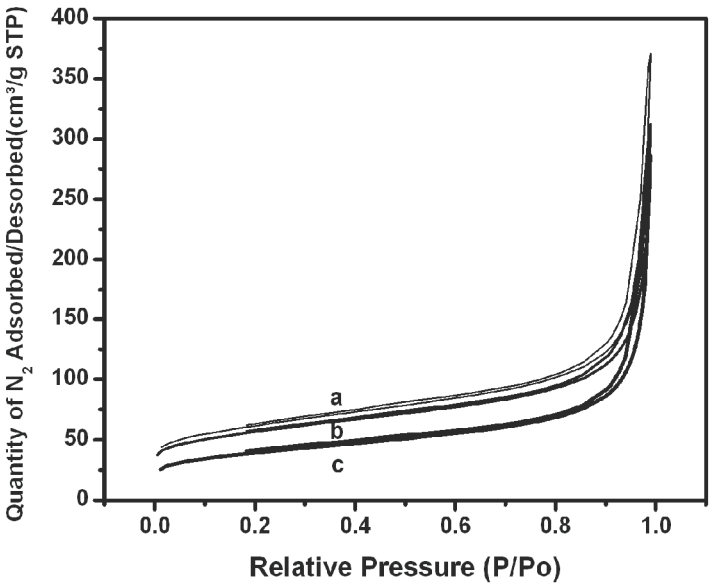

Fig. 3.5 N_2 Adsorption/ Desorption isotherms of (a) unmodified CDX975 (b) 1N HNO_3 treated CDX975-60 min and (c) conc. HNO_3 treated CDX975-60 min

Table 3.2 Textural properties of untreated and the different nitric acid treated CDX975 carbon black support

S. no.	Sample	BET surface area (m^2/g)	Pore volume (cm^3/g)
1	untreated CDX	211	0.54
2	1N HNO_3 treated CDX-60 min	194	0.44
3	conc. HNO_3 treated CDX-60 min	136	0.42
4	1N HNO_3 treated CDX-95 min	-	-
5	conc. HNO_3 treated CDX-95 min	139	0.4

3.4.6 X-ray diffraction studies

XRD patterns of the carbon black samples with and without nitric acid treatment are shown in Fig. 3.6 (A). The diffraction peak at the 2θ value around 25°, corresponds to the (002) diffraction peak of the hexagonal structure of the CDX975 carbon black support. It shows the detainment of carbon structure even after the oxidative conditions used in this study.

Fig. 3.6 (B) shows the XRD patterns of the 10% Pt catalysts loaded on the different oxidatively treated CDX975. It shows the characteristics Pt peaks at 2θ values around 40°, 46°, 68°, 81° and 86° corresponding to the (111), (200), (220), (311) and (222) planes of face centered cubic (*fcc*) structure of Pt (JCPDS file 4-802). The average crystallite sizes determined with Debye-Scherrer equation are given in Table 3.3. The explanation for XRD profiles can be described well by considering the treatment with 1N HNO_3 and conc. HNO_3 separately.

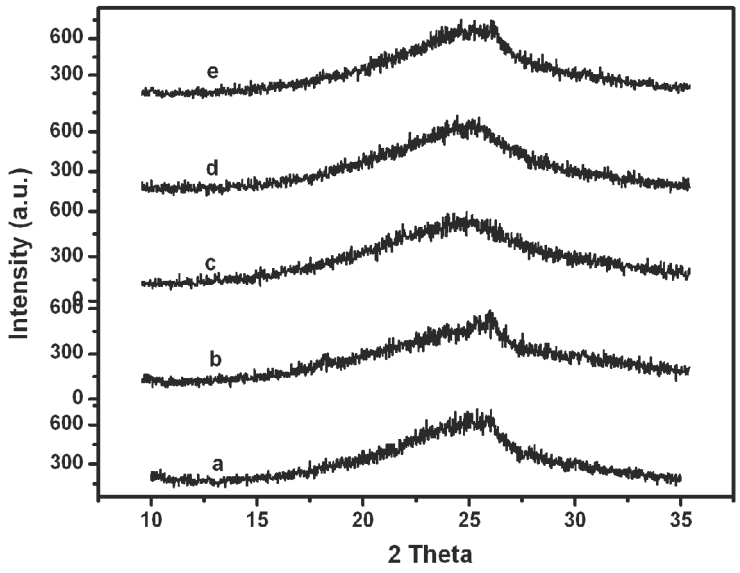

(A)

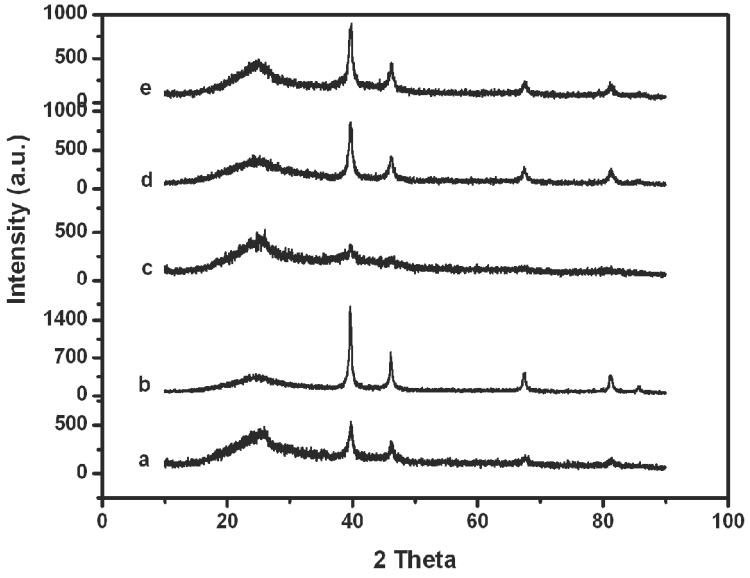

(B)

Fig. 3.6 (A) XRD patterns of the carbon blacks (a) unmodified (b) 1N HNO_3 treated CDX975-60 min (c) conc. HNO_3 treated CDX975-60 min (d) 1N HNO_3 treated CDX975-95 min and (e) conc. HNO_3 treated CDX975-95 min and (B) XRD patterns of 10% Pt loaded on the different nitric acid treated carbon blacks

In case of the treatment with 1N HNO_3 for 60 min the particle size increases. Further increase of the oxidative treatment condition to 95 min the particle size decreases. This can be explained as follows. The treatment at very mild oxidative condition is supposed to produce phenolic or carbonyl groups, which are not anchoring Pt nanoparticles, on the carbon black support as evidenced from FT-IR and NH_3-TPD studies but resulted in mere heat treatment of the support. But the increase of treatment time to 95 min, the appearance of carboxyl carbonyl group at 1725 cm^{-1} and broadening of carboxyl –OH stretching at 3000-3600 cm^{-1} shows the occurrence of the oxidation of the carbon black support. The introduction of these carboxyl groups cause better dispersion of the Pt nanoparticles and resulted in the decrease of the crystallite size.

But the treatment with conc. HNO_3 for 60 min itself has produced sufficient carboxylic functional groups as supported by NH_3-TPD studies. This causes better dispersion of the Pt nanoparticles and resulted in the decrease of the crystallite size. Further increase of oxidative condition to 95 min, is supposed to produce more carboxylic groups on the surface of the carbon black support and hence results in the aggregation of the nanoparticles as reported by earlier studies (Roman-Martinez *et al*., 1995).

Table 3.3 Average Pt crystallite size from XRD studies for the 10% Pt loaded on untreated and the different nitric acid treated CDX975 carbon black support

S. no.	Sample	Crystallite size (nm)
1	10% Pt/untreated CDX	13.5
2	10% Pt/1N HNO_3 treated CDX-60 min	21.2
3	10% Pt/1N HNO_3 treated CDX-95 min	12.9
4	10% Pt/conc. HNO_3 treated CDX-60 min	6.6
5	10% Pt/conc. HNO_3 treated CDX-95 min	13.4

3.5 Electrochemical measurements

Cyclic voltammograms of 10% Pt loaded on different nitric acid treated and untreated CDX975 in 1M sulfuric acid are shown in Fig. 3.7 (A). At mild oxidative conditions (60 min treatment time) the current density for hydrogen adsorption/desorption increased with an increase in oxidative conditions (from 1N to conc. HNO_3). But on further increase of oxidative condition (for 95 min treatment), the current density decreased. One of the reasons might be due to the smaller particle size of Pt at lesser oxidative conditions (conc. HNO_3 for 60 min) and increase of Pt particle size at strong oxidative conditions. The values of electrochemical active surface area of the Pt/CDX975 catalysts are presented in Table 3.4. It shows an increase at first when treated with 1N HNO_3 for 60 min. For the oxidation with conc. HNO_3, even though the actual current density is the maximum for hydrogen adsorption/desorption, the calculation of electrochemical active surface area values show lesser. This might be due to the increased double layer current density (measure of capacitance) in the double layer region as expected for the nitric acid treated carbon blacks (Kinoshita, 1988; Jia *et al*., 2001). This capacitive behaviour of the carbon black suppresses the determination of charge for hydrogen adsorption/desorption and cause lesser electrochemical active surface area. With further increase of oxidative condition, the electrochemical active surface area decreases as reported by Antonucci *et al*., 1994 and Roman-Martinez *et al*., 1995. This decrease of EAS is attributed to the presence of more surface oxygen functional groups, which causes the surface aggregation of the Pt nanoparticles rather than diffusion to the inner pores of the carbon black support.

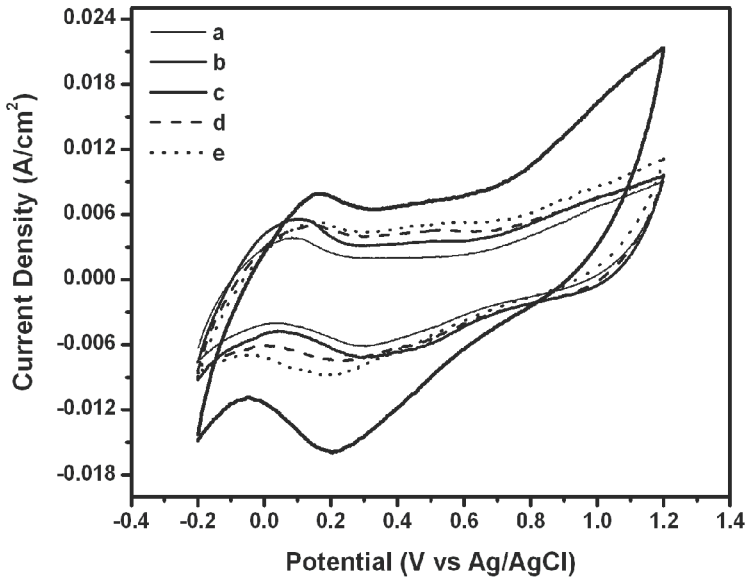

(A)

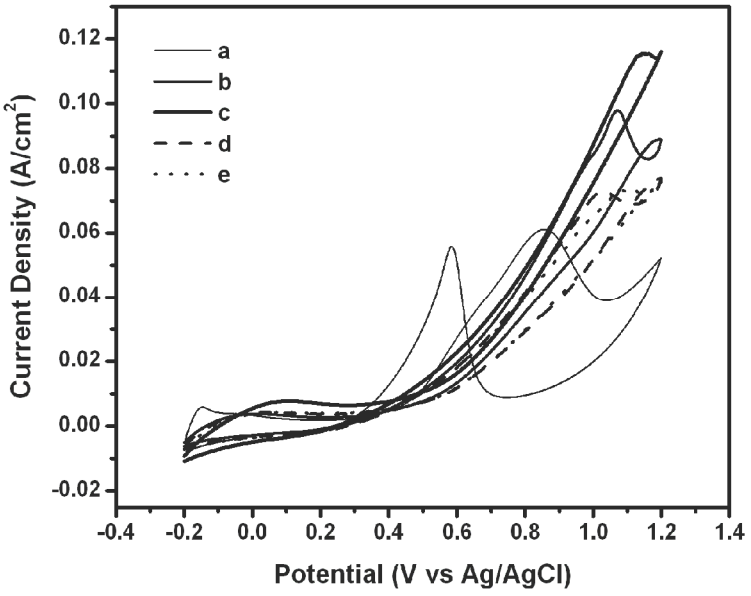

(B)

Fig. 3.7 Cyclic voltammogram of 10% Pt loaded on carbon blacks of (a) unmodified (b) 1N HNO_3 treated CDX975-60 min (c) conc. HNO_3 treated CDX975-60 min (d) 1N HNO_3 treated CDX975-95 min and (e) conc. HNO_3 treated CDX975-95 in (A) 1M H_2SO_4 and (B) 1M H_2SO_4 and 1M methanol at the scan rate of 25 mV/s

Fig. 3.7 (B) shows the methanol oxidation current density in 1M sulfuric acid and 1M methanol. The methanol oxidation activity measured in terms of the forward peak current density is presented in Table 3.4. It shows an increase of methanol oxidation activity with an increase in oxidative condition (from 1N HNO_3 to conc. HNO_3 for 60 min treatment time). The maximum methanol oxidation activity is observed for the catalyst for which the carbon black support is treated with conc. HNO_3 for 60 min. The increase in activity can be attributed to better dispersion of the Pt nanoparticles, which resulted in smaller Pt crystallite size as observed with XRD. Further increase of oxidative treatment time to 95 min, the activity is found to decrease. The increased oxidative treatment time might have produced more of surface oxygen functional groups on the treated support, which is also evidenced from the pH determination and FT-IR studies. The decrease in activity with increasing oxidative conditions may in part also be attributed to the loss of textural properties upon increasing oxidative conditions.

Table 3.4 Electrochemical active surface area of 10% Pt loaded on untreated and the different nitric acid treated CDX975 carbon black support

S. no.	Sample	% Pt (ICP)	EAS (m^2/g)	Mass specific methanol oxidation activity (A/g)
1	10% Pt/untreated CDX	9.1	18.1	214
2	10% Pt/1N HNO_3 treated CDX-60 min	-	24.8	311
3	10% Pt/conc. HNO_3 treated CDX-60 min	-	9.0	406
4	10% Pt/1N HNO_3 treated CDX-95 min	9.5	10.2	269
5	10% Pt/conc. HNO_3 treated CDX-95 min	8.1	5.2	265

Fig. 3.8 shows the chronoamperometry of the 10% Pt loaded on the untreated and the different nitric acid treated CDX975 catalyst. It shows a similar loss of activity trend for the treated catalysts to that of the untreated catalyst, but the higher current density could be observed for the study time of 30 minutes for the catalyst, whose support is treated with conc. HNO_3 for 60 minutes. The lesser performance in terms of stability of the other catalysts can be attributed to the loss of textural properties, especially pore volume and aggregation of the Pt nanoparticles on the support surface itself rather than the uniform dispersion in the inner pores of the carbon black support.

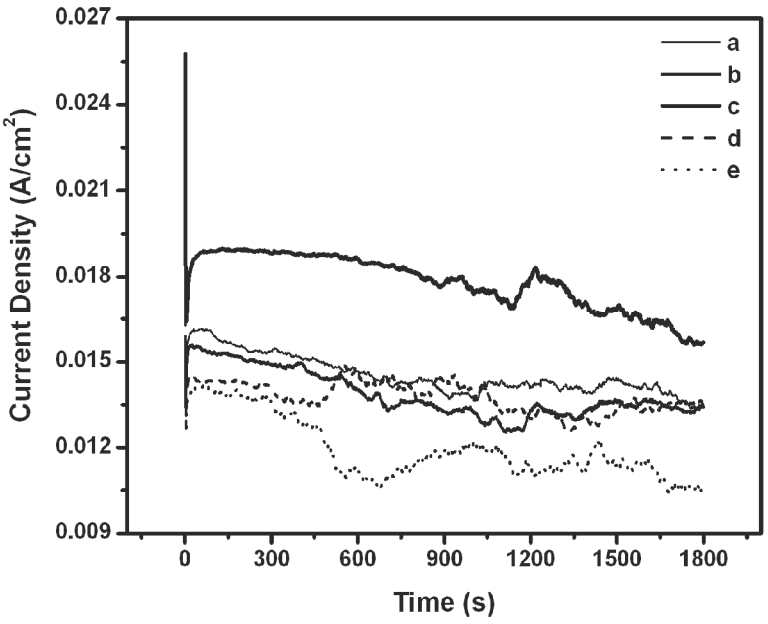

Fig. 3.8 Chronoamperometry of 10% Pt loaded on carbon blacks of (a) unmodified (b) 1N HNO_3 treated CDX975-60 min (c) conc. HNO_3 treated CDX975-60 min (d) 1N HNO_3 treated CDX975-95 min and (e) conc. HNO_3 treated CDX975-95 min in 1M H_2SO_4 and 1M methanol at 0.6 V

3.6 Summary

- The increase of oxidative treatment conditions with nitric acid of the carbon black support showed an increase in the concentration of carboxylic acid functional groups on the support, as confirmed by different characterization techniques.

- XRD studies showed smaller particle size for Pt for the catalyst prepared with conc. HNO_3 treated CDX975-60 min, which can be attributed to the optimum concentration of the carboxyl functional groups on the surface of the carbon black support. Further increase of oxidative condition leads to the aggregation of the Pt nanoparticles due to the lesser diffusion of Pt in to the inner pores of the carbon black support.

- The methanol oxidation studies showed the maximum activity for the catalyst which has been treated with conc. HNO_3 for 60 min, which has also been found to have smaller particle size. Hence, the enhanced methanol oxidation activity can be attributed to the increased dispersion of the Pt nanoparticles. The decrease of activity with further increase of oxidative treatment conditions can be attributed to the aggregation of Pt nanoparticles on the surface of the support. The is expected to be caused by the high concentration of carboxyl functional groups generated on the surface which reduces the diffusion of Pt into the inner pores of the support.

CHAPTER 4

EFFECT OF SULFONIC ACID FUNCTIONALIZATION OF CDX975 CARBON BLACK SUPPORT OF Pt/CDX975 CATALYST FOR METHANOL ELECTRO-OXIDATION STUDIES

4.1 Introduction

In the carbon supported Pt catalysts, the three phases, namely, the electron conducting carbon support, the proton conducting ionomer and the catalyst nanoparticle need to co-exist at the, for the electrooxidation to occur as shown in Fig. 4.1 (Kuroki and Yamaguchi, 2006). Several efforts have been made to extend this three phase boundary to the inner pores of the catalyst support, to enhance the catalyst utilization. First, a major breakthrough was accomplished by the method based on impregnation of the traditional gas diffusion electrode with a solubilized Nafion ionomer (Ticianelli *et al.*, 1988). Further improvements on the electrode were made by Willson and Gottesfeld 1992, by mixing solubilized ionomer with a carbon supported catalyst to form a catalyst layer. Although several efforts have been made to optimize this three phase boundary structure, still substantial mass of the platinum catalyst may not be utilized (Shimazu *et al.*, 1987). One feasible explanation for low platinum utilization was presented by Uchida *et al.* 1996, by investigating the microstructure of the catalyst layer. In the general process of catalyst fabrication, nanometer-sized platinum catalysts are dispersed on the surface of 30–40 nm sized carbon substrates to increase the platinum catalyst surface area as shown in Fig. 4.2 (Mizuhata *et al.*, 2004). However, these small carbon particles tend to agglomerate via intermolecular interaction between their surfaces; thus the platinum inside the agglomerated carbon structure cannot be utilized in electrochemical reactions, as the perfluorosulfonate

ionomer (ca. 0.04 μm), which is generally added to the catalyst layer as a proton conducting agent during the electrode fabrication process, cannot penetrate into the smaller pores (< ca. 0.04 μm of the agglomerated carbon structure) (Mizuhata *et al.*, 2004). Therefore, it is obvious that the Pt particles access to the three phase boundary is very limited. Studies were also conducted to understand, if the carbon support itself can be made to conduct protons as well. Some studies in this direction using conducting polymer-polyanion composites as supports for catalyst have been reported (Qi and Pickup, 1998). But these composites lose their electronic conductivity soon in the acidic fuel cell working conditions. Studies on linking sulfonated silane on to a carbon supported catalyst (Easton *et al.*, 2001) were showing better performance at lower Nafion content. However with higher Nafion content, the modified catalyst has shown lower performance than the unmodified one. This was explained due to the covering of the catalyst particles by the silane groups.

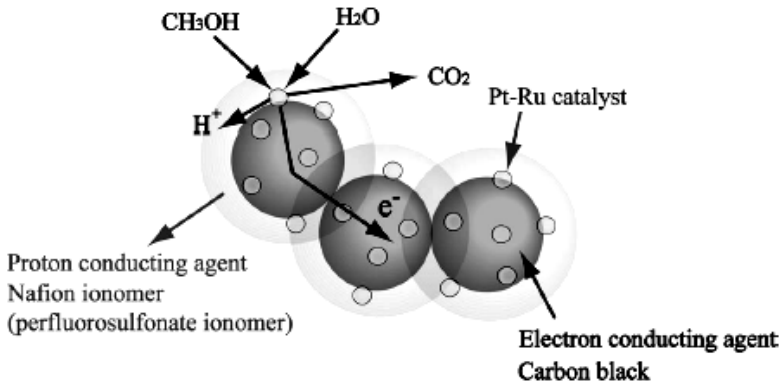

Fig. 4.1 Schematic illustration of the three phase boundary structure of the carbon black supported Pt-Ru catalyst

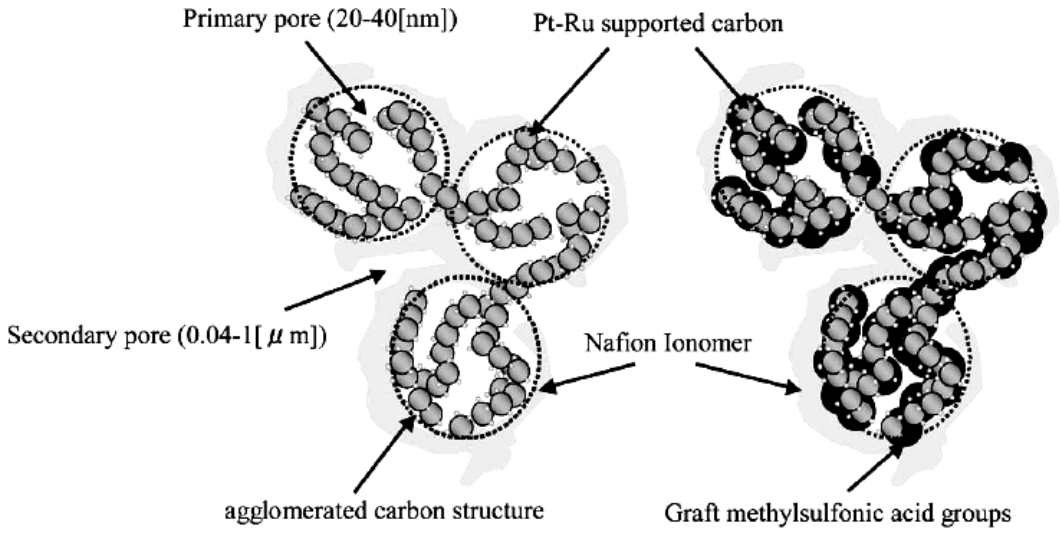

Fig. 4.2 Schematic illustration of the internal structure of the (a) existing and (b) anticipated carbon black supported Pt-Ru catalyst

Creation of acidic carboxyl groups on the carbon support with nitric acid oxidation was also studied (Jia *et al.*, 2001). However, because carboxylic acid is a weak acid and a poor proton conductor, the increased performance was limited. Studies on grafting of polyacrylamide tertiary butyl sulfonic acid (PATBS) on Vulcan carbon support had shown a decrease of performance. However, this decrease in performance was attributed to the bulkiness of the ATBS molecule (Mizuhata *et al.*, 2004). Therefore linking of shorter chain sulfonic acid groups was envisaged and study of grafting of methylsulfonic acid groups on to the catalyst supported carbon particles was carried out by the same group and an increase in performance was observed (Kuroki and Yamaguchi, 2006). Due to its small molecular size, the grafted sulfonic acid groups are able to penetrate into the small pores of the agglomerated carbon structure and so ensure the three phase boundary structure to the interior of the carbon particles. Chemically linked shorter chain sulfonic or phosphonic acid groups onto the

carbon support of the supported catalysts through diazonium salts formed by reacting 2-aminoethanesulfonic acid or 2-aminoethanephosphonic acid with isobutyl nitrite was studied, and the resulting sulfonated catalysts showed better performance than the untreated counterparts (Xu *et al.*, 2003). Another simple method to link sulfonic acid groups onto the surface of carbon particles functioning as catalyst supports was studied by Xu *et al.* 2005, with ammonium sulfate as the sulfonating agent. But these studies by Xu *et al.* (2003 and 2005) are lacking complete characterization of the prepared catalysts with respect to FT-IR and XRD analysis, but are mainly studied for electrochemical activities at different Nafion contents. Linking of phenylsulfonic acid on the Pt loaded carbon particles also has shown enhanced performance as seen from the studies of Selvarani *et al.*, 2007. Therefore, we were encouraged to carry out studies on linking of sulfonic acid groups on to the Pt loaded CDX975 carbon particles.

4.2 Different schemes of sulfonation

Part A: Grafting of ethylsulfonic acid group using 2-aminoethanesulfonic acid

Part B: Grafting of sulfonic acid group using ammonium sulphate

Part C: Grafting of methylsulfonic acid group using sodium sulphite and formaldehyde

4.3 Part A: Grafting of ethylsulfonic acid group using 2-aminoethanesulfonic acid

The sulfonation or grafting of ethylsulfonic acid group to the 10% Pt loaded on CDX975 carbon black was carried out with 2-aminoethanesulfonic acid as the sulfonating agent, following the procedures of Xu *et al.*, 2003, but with sodium nitrite as the nitrite source rather than isobutyl nitrite. It was carried out through diazotization step. It is expected that the azo compound formed with the sulfonating

agent 2-aminoethanesulfonic acid and sodium nitrite in the presence of mineral acid reacts with the CDX975 carbon black support and incorporates the alkyl sulfonic acid group on the carbon black support.

4.3.1 Loading of Pt on CDX975 carbon black support

The Pt loading of the CDX975 carbon black support was done with ethylene glycol reduction method, by taking 2.25 g of CDX975 and 13 mL of 5 wt% hexachloroplatinic acid with 150 mL of ethylene glycol and stirring at 393-403 K for 4 h. After cooling to room temperature, it was filtered, washed with acetone and distilled water and then dried in vacuum oven at 343 K for 36 h.

4.3.2 Sulfonation scheme

In a typical procedure, 10% Pt/CDX975 catalyst was stirred with an aqueous solution of 10% as well as 20 % of 2-aminoethanesulfonic acid and heated to 353 K. To this, 2 mL of conc. HNO_3 was added and treated at 353 K for 10 min. Then, it was cooled to room temperature and then to less than 283 K. To this, an ice cold solution of sodium nitrite was added and the reaction was carried out for 30 min. After bringing to room temperature, it was filtered, washed with warm distilled water and then dried in a vacuum oven at 343 K for 20 h. The prepared catalysts were characterized by different techniques and their catalytic activity is evaluated for methanol electro-oxidation reaction.

4.3.3 Textural properties

The BET surface area values of the sulfonated samples have not shown any significant difference from that of the unsulfonated one. The BET surface area values

for the unsulfonated and the 10 and 20% 2-aminoethanesulfonic acid modified samples were 170, 168 and 168 m^2/g respectively.

4.3.4 FT-IR studies

FT-IR spectra of unsulfonated and 10 and 20% 2-aminoethanesulfonic acid modified samples are shown in Fig. 4.3. The presence of S-O stretching vibration at 1100 cm^{-1} for the sulfonated catalysts show the incorporation of the sulfonic acid group on the carbon black support of the catalysts.

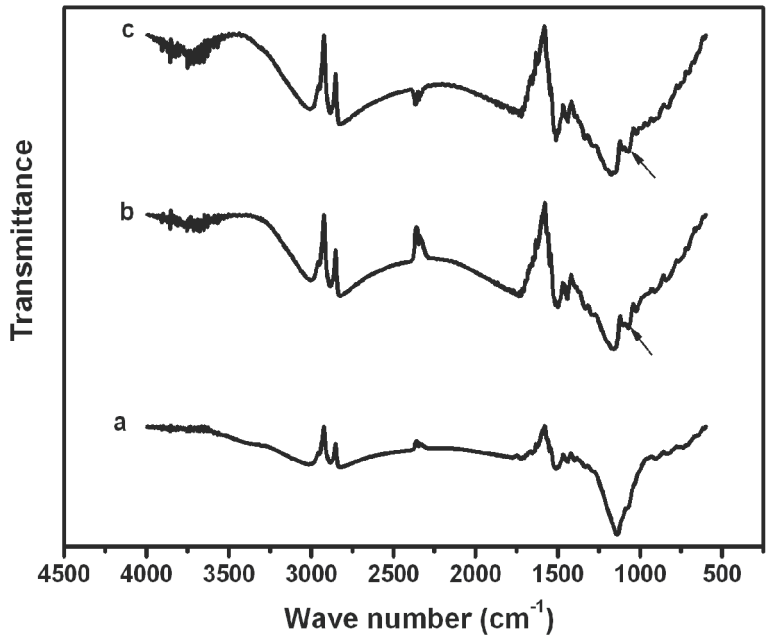

Fig. 4.3 FT-IR spectra of (a) unmodified (b) 10% and (c) 20% of 2-aminoethanesulfonic acid modified 10% Pt/CDX975 catalysts (arrow mark in b) and c) indicate the stretching vibration for S-O)

4.3.5 pH determination

A decrease in pH is observed (Table 4.1) with sulfonation and further with the increase of the quantity of the sulfonating agent, which is indicative of the incorporation of alkylsulfonic acid group on the carbon black support of the catalysts.

Table 4.1 pH values of unsulfonated and catalysts sulfonated with 2-aminoethanesulfonic acid

S.No	Catalyst	pH
1	0% 2-aesa/10% Pt/CDX	6.0
2	10% 2-aesa/ 10% Pt/CDX	4.4
3	20% 2-aesa/ 10% Pt/CDX	4.2

4.3.6 Thermogravimetric analysis

Fig. 4.4 shows TGA profiles in nitrogen atmosphere of the unsulfonated and the sulfonated catalysts. It shows a weight loss of the sulfonic acid group around 523 K for the sulfonic acid modified catalyst and not for the unsulfonated catalyst. These results are similar to the studies reported by Xu *et al.* (2003 and 2005). This also supports the incorporation of sulfonic acid group by the sulfonation step followed.

4.3.7 X-ray diffraction studies

Fig. 4.5 shows the XRD patterns of the unsulfonated and sulfonated 10% Pt loaded CDX975 catalysts. It shows the characteristic Pt peaks at 2θ values around 40°, 46°, 68°, 81° and 86° corresponding to the (111), (200), (220), (311) and (222) planes of face centered cubic (*fcc*) structure of Pt (JCPDS card: 4-802). The diffraction peak at the 2θ value around 25° corresponds to the (002) diffraction peak of the hexagonal structure of the CDX975 carbon black support. The average Pt crystallite size determined using Debye-Scherrer equation is given in Table 4.1. It shows a slight decrease in particle size with sulfonation. This can be attributed to the redistribution of Pt nanoparticles with better dispersion upon sulfonation.

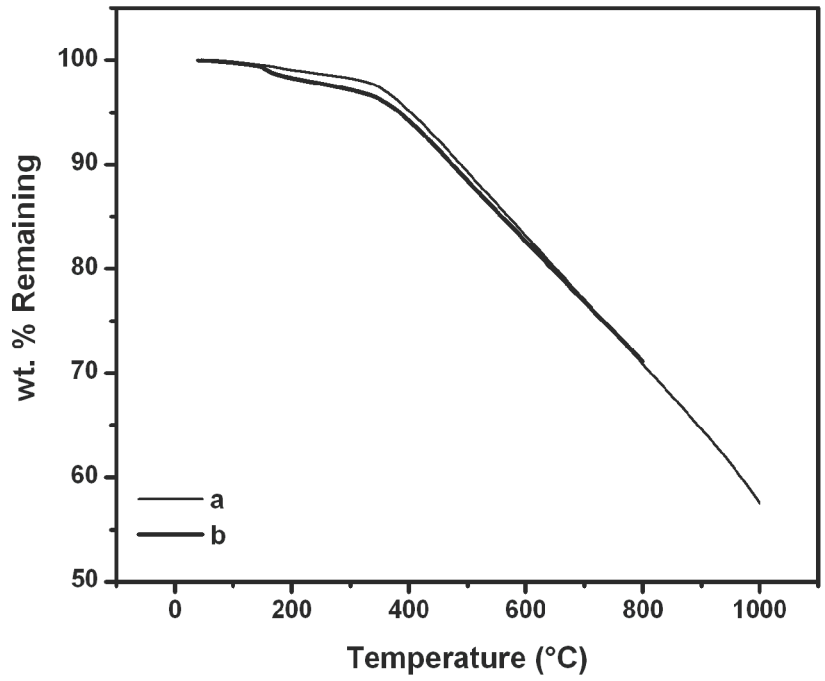

Fig. 4.4 TGA profiles of (a) unmodified and (b) 5% of 2-aminoethanesulfonic acid modified 10% Pt/CDX975 catalyst

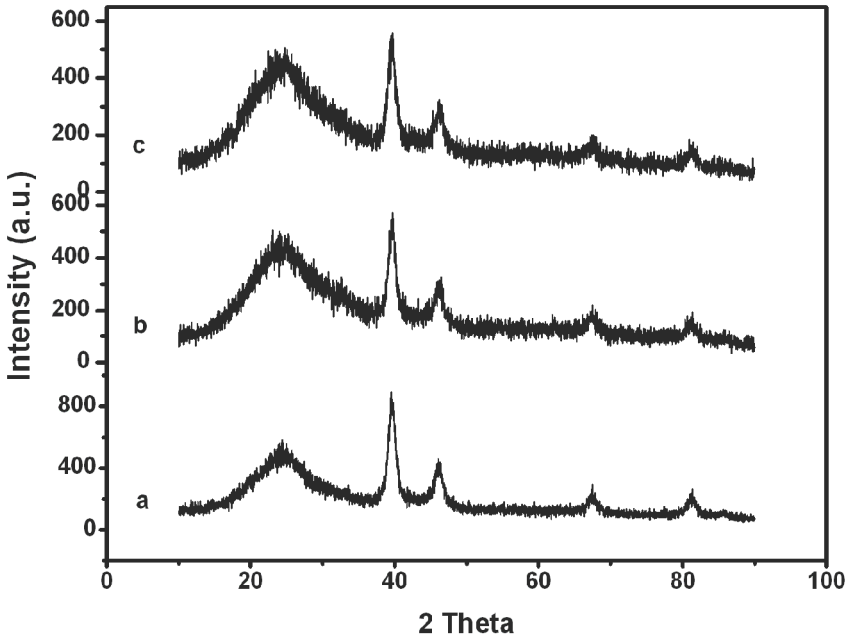

Fig. 4.5 XRD patterns of (a) unmodified (b) 10% and (c) 20% of 2-aminoethanesulfonic acid modified 10% Pt/CDX975 catalyst

Table 4.2 Average crystallite size and methanol oxidation activity for unsulfonated and the catalysts sulfonated with 2-aminoethanesulfonic acid

Catalyst	Crystallite size XRD (nm)	Wt% of Pt from ICP	Peak Current Density (mA/ cm^2)	Mass specific methanol oxidation activity (A/g)
0% 2-aesa/10% Pt/CDX	8.6	6.1	35.7	125
10% 2-aesa/ 10% Pt/CDX	8.0	7.0	78.6	275
20% 2-aesa/ 10% Pt/CDX	7.9	-	82.9	290

4.3.8 Electrochemical measurements

Fig. 4.6 (A) shows the cyclic voltammograms in 1M sulphuric acid of the unsulfonated and sulfonic acid modified catalysts. Upon sulfonic acid modification, the current density for hydrogen adsorption/desorption shows an increase (Table 4.2), which supports the increase of electrochemical active surface area of the catalyst, which can be attributed to the better dispersion of the Pt nanoparticles upon sulfonic acid modification. These results are in agreement with that of the deductions based on XRD studies.

Fig. 4.6 (B) shows the methanol oxidation current density in 1M methanol and 1M H_2SO_4 of the unsulfonated and the sulfonated catalysts. As given in Table 4.2, the sulfonic acid modification with 2-aminoethanesulfonic acid shows a significant increase in activity. This is similar to the results reported by Xu *et al.* 2003. The increase in activity can be attributed to two factors; (i) better dispersion / redistribution of the Pt nanopartilces and (ii) the increased proton conductivity of the catalyst to the interior of the support.

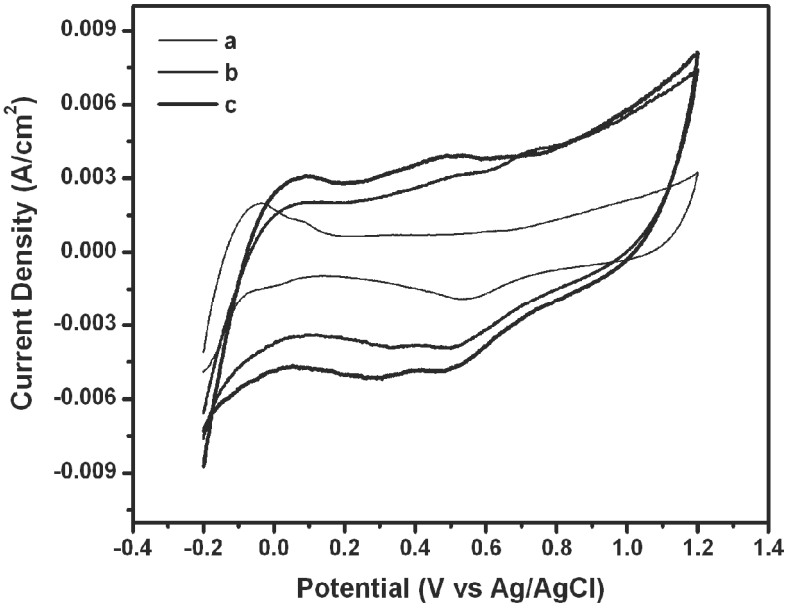

(A)

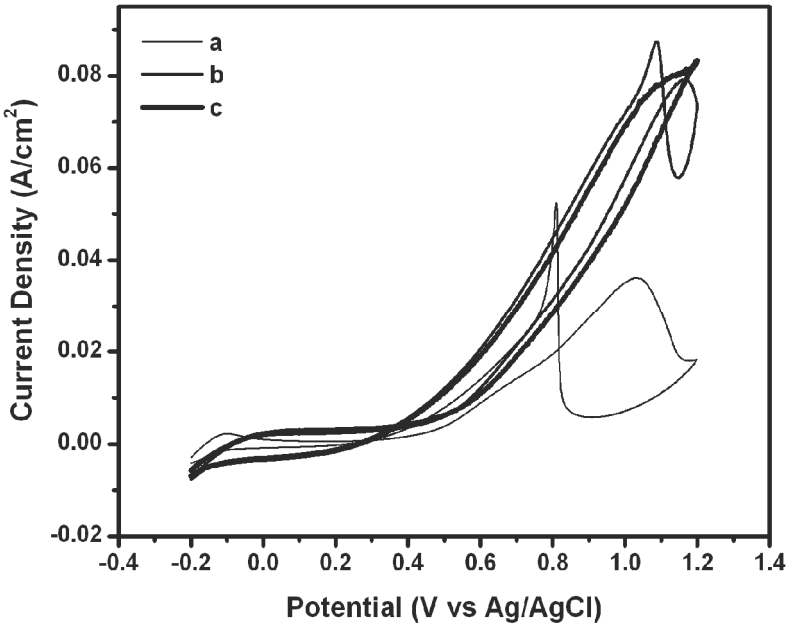

(B)

Fig. 4.6 Cyclic voltammograms of (a) unmodified (b) 10% and (c) 20% of 2-aminoethanesulfonic acid modified 10% Pt/CDX975 catalyst in (A) 1M H_2SO_4 and (B) 1M H_2SO_4 and 1M methanol at the scan rate of 25 mV/s

4.4 Part B: Grafting of sulfonic acid group using ammonium sulphate

The grafting of the sulfonic acid group on the carbon black support CDX975 is carried out with ammonium sulphate by following the procedures of Xu *et al.*, 2005. It is expected that ammonium sulphate decomposes at 508 K to ammonia and sulfur trioxide (equation 4.1). The formed sulfur trioxide incorporates between the C-H terminal bond of the carbon black support and grafts the sulfonic acid group on the support.

$$(NH_4)_2SO_4 \xrightarrow{508\ K} 2NH_3 + H_2O + SO_3 \quad (4.1)$$

$$\text{Carbon-H} + SO_3 \longrightarrow \text{Carbon-}SO_3H \quad (4.2)$$

4.4.1 Loading of Pt on the carbon black support

The Pt loading of the CDX975 carbon black support was done with ethylene glycol reduction method, by taking 2.25 g of CDX975 and 13 mL of 5 wt% hexachloroplatinic acid with 150 mL of ethylene glycol and stirring at 393-403 K for 4 h. After cooling to room temperature, it was filtered, washed with acetone and distilled water and then dried in a vacuum oven at 343 K for 36 h.

4.4.2 Sulfonation scheme with ammonium sulfate

The sulfonation of 10% Pt/CDX975 catalyst has been carried out by mixing the catalyst with an aqueous solution of ammonium sulfate and heat treating for 30 min. After cooling to room temperature, it has been filtered, washed with distilled water and dried in a vacuum oven at 343 K for 20 h. The prepared catalysts were characterized by different techniques and their catalytic activity is evaluated for methanol electro-oxidation reaction.

4.4.3 pH determination

A decrease in pH was observed with sulfonation and further with the increase of the quantity of the sulfonating agent, ammonium sulfate, which is indicative of the incorporation of sulfonic acid group on the carbon black support of the catalyst, as reported by Xu *et al.*, 2005 (Table 4.3).

Table 4.3 pH values of unsulfonated and the catalysts sulfonated with ammonium sulfate

Catalyst	pH
0% $(NH_4)_2SO_4$/10% Pt/CDX	6.0
10% $(NH_4)_2SO_4$/ 10% Pt/CDX	5.1
20% $(NH_4)_2SO_4$/ 10% Pt/CDX	4.9

4.4.4 FT-IR studies

Fig. 4.7 shows the FT-IR spectra of unsulfonated and 10 and 20% sulfonic acid modified samples. The stretching vibration for S-O at 1100 cm^{-1} shows the incorporation of the sulfonic acid group on the carbon black support of the catalyst. FT-IR spectrum also shows an increased absorbance of the hydroxyl vibration at 3000-3600 cm^{-1} due to the increase of protonic acidity.

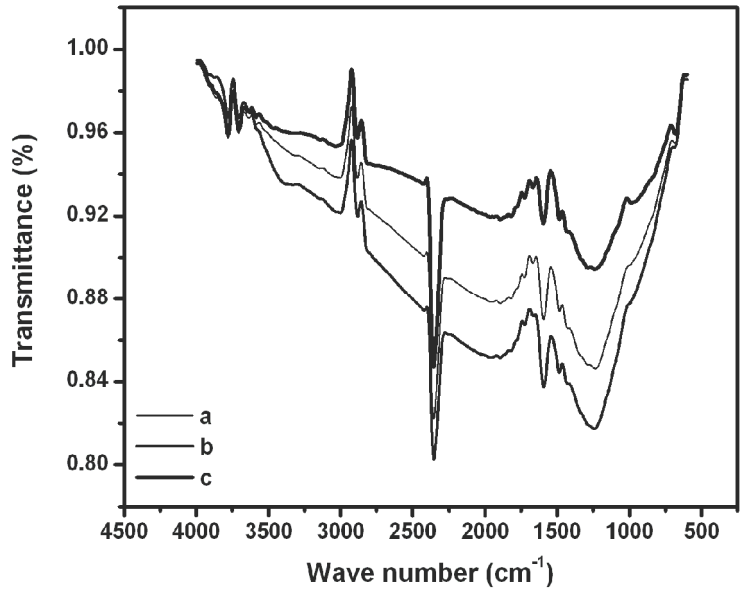

(A)

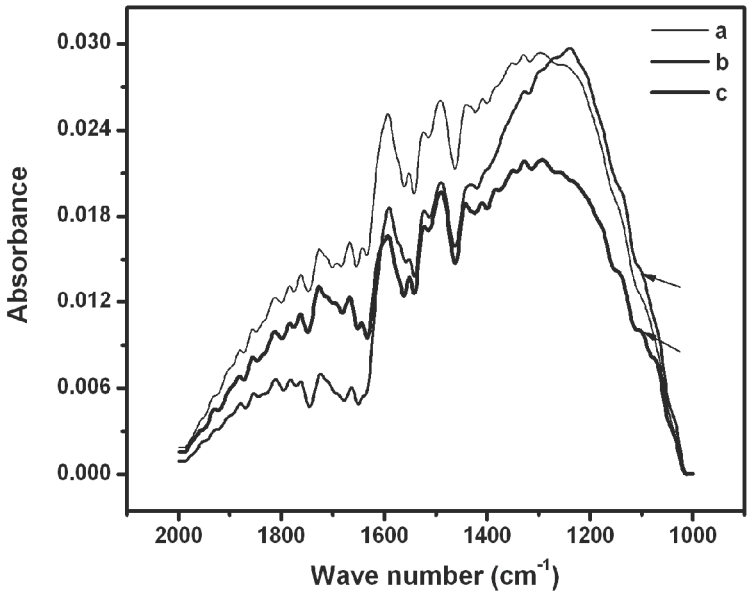

(B)

Fig. 4.7 FT-IR spectra of the (a) unmodified (b) 10% and (c) 20% ammonium sulfate modified 10% Pt/CDX975 catalyst at the resolution of (A) 4 cm^{-1} and (B) 2 cm^{-1}(arrow mark in b) and c) indicate the stretching vibration for S-O)

4.4.5 Thermogravimetric analysis

TGA profiles recorded in nitrogen atmosphere are shown in Fig. 4.8. It shows a weight loss of the sulfonic acid group around 150 °C for the sulfonic acid modified catalyst. This supports the incorporation of sulfonic acid group in the sulfonation step as observed by Xu *et al.*, 2003.

4.4.6 X-ray diffraction studies

The XRD patterns of the 10% Pt loaded CDX975 catalysts, unsulfonated and sulfonated with ammonium sulfate are given in Fig. 4.9. It shows the characteristic Pt peaks at 2θ values around 40°, 46°, 68°, 81° and 86° corresponding to the (111), (200), (220), (311) and (222) planes of face centered cubic (*fcc*) structure of Pt (JCPDS card: 4-802). The diffraction peak at the 2θ value around 25° corresponds to the (002) diffraction peak of the hexagonal structure of the CDX975 carbon black support. The crystallite size shown in Table 4.4, determined with Debye-Scherrer equation has not shown significant difference in size, showing no significant change in the redistribution of Pt nanoparticles by means of the sulfonation step.

Table 4.4 Average crystallite size and methanol oxidation activity of unsulfonated and the catalysts sulfonated with ammonium sulfate

Catalyst	Crystallite size XRD (nm)	Wt% of Pt from ICP	Peak Current Density (mA/ cm^2)	Mass specific methanol oxidation activity (A/g)
0% $(NH_4)_2SO_4$/10% Pt/CDX	9.9	-	35.7	125
10% $(NH_4)_2SO_4$/ 10% Pt/CDX	9.9	-	64.3	225
20% $(NH_4)_2SO_4$/ 10% Pt/CDX	10.2	6.9	48.6	170

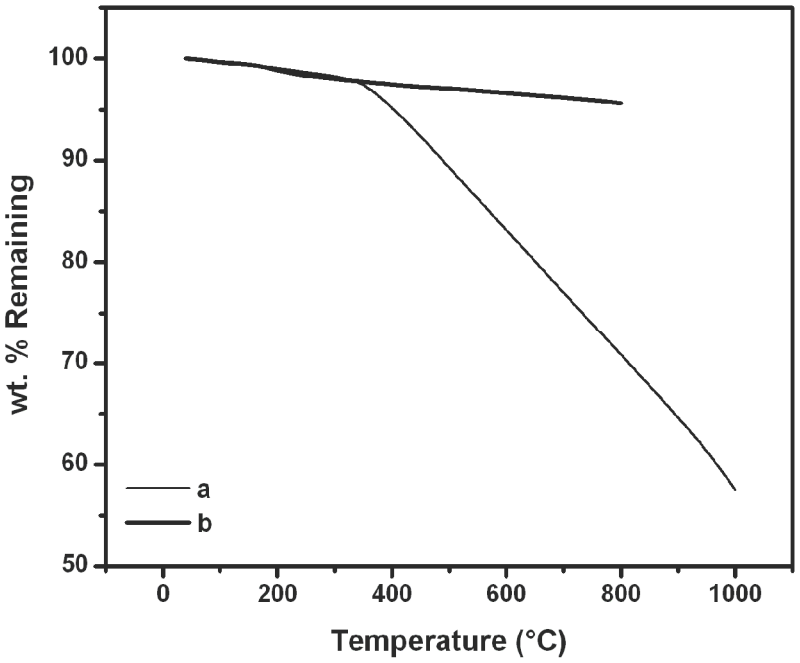

Fig. 4.8 TGA profile of (a) unmodified and (b) 10% ammonium sulfate modified 10% Pt/CDX975 catalyst in nitrogen atmosphere at a ramp rate of 10 °C/min

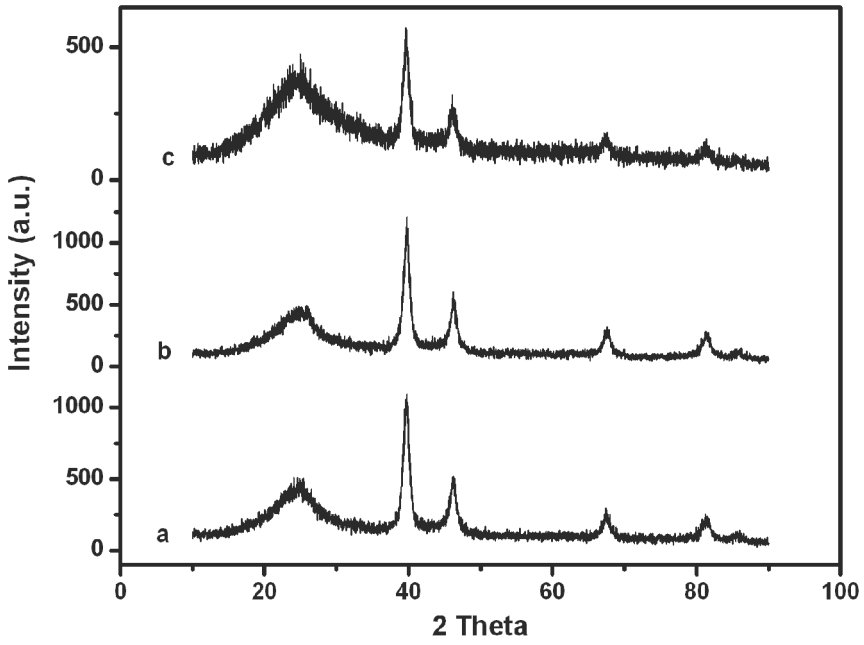

Fig. 4.9 XRD patterns of (a) unmodified (b) 10% and (c) 20% ammonium sulfate modified 10% Pt/CDX975 catalyst

4.4.7 Electrochemical measurements

The cyclic voltammograms in 1M sulphuric acid of the unsulfonated and the catalysts with sulfonic acid modification with ammonium sulfate are given in Fig. 4.10 (A). Upon sulfonic acid modification, the current density for hydrogen adsorption/desorption shows an increase, implying the increase of electrochemical active surface area of the catalyst. This can be attributed to the enhanced access to the Pt nanoparticles due to the increased proton conductivity to the interior of the carbon support upon sulfonic acid modification.

Fig. 4.10 (B) shows the current density for methanol oxidation in 1M methanol in 1M H_2SO_4 of the unsulfonated and the sulfonated catalysts. As given in Table 4.4, the sulfonic acid modification shows an increase in methanol oxidation activity for the 10% sulfonated catalyst. Further increase of sulfonating agent to 20%, it could be observed that the activity decreases. Similar results of maximum activity for 5-10% of ammonium sulfate and decrease of activity upon further increase in the quantity of the sulfonating agent was observed by Xu *et al.*, 2005. The increase in the activity can be attributed to the increased proton conductivity of the catalyst with the incorporation of sulfonic acid group to the inner pores of the carbon black support. The decrease of methanol oxidation activity with further increase of the quantity of ammonium sulfate, may be attributed to the blocking of the active sites with the increased sulfonic acid groups.

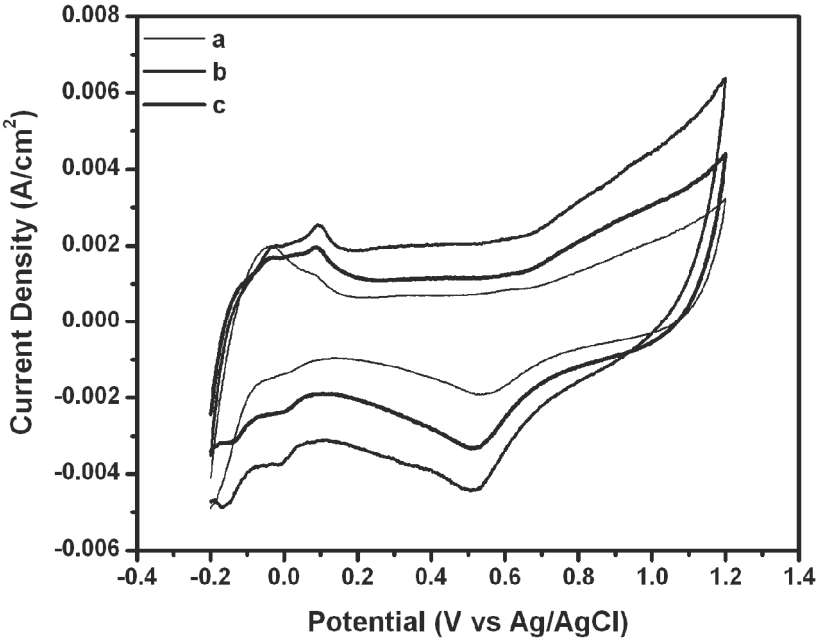

(A)

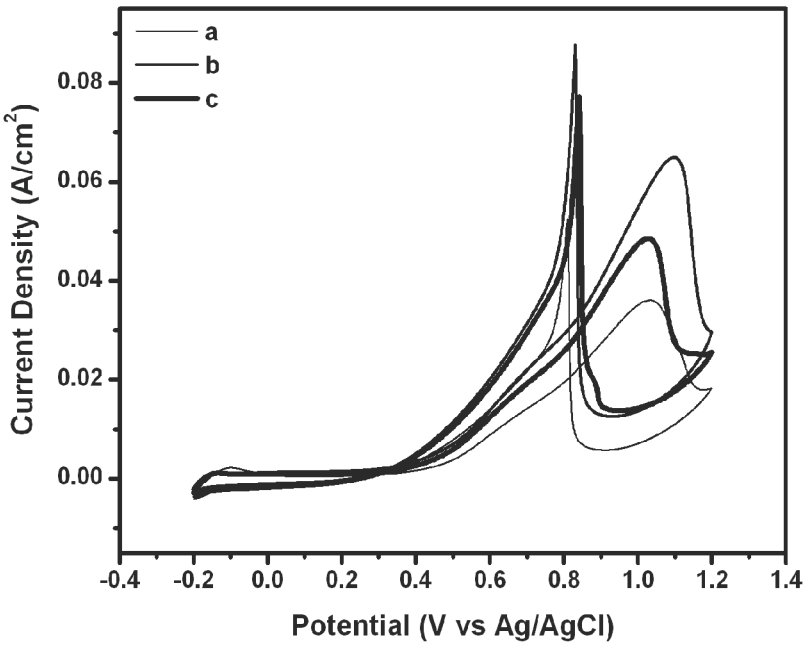

(B)

Fig. 4.10 Cyclic voltammogram of (a) unmodified, (b) 10% and (c) 20% of ammonium sulfate modified 10% Pt/CDX975 catalyst in (A) 1M H_2SO_4 and (B) 1M H_2SO_4 and 1M methanol at 25 mV/s

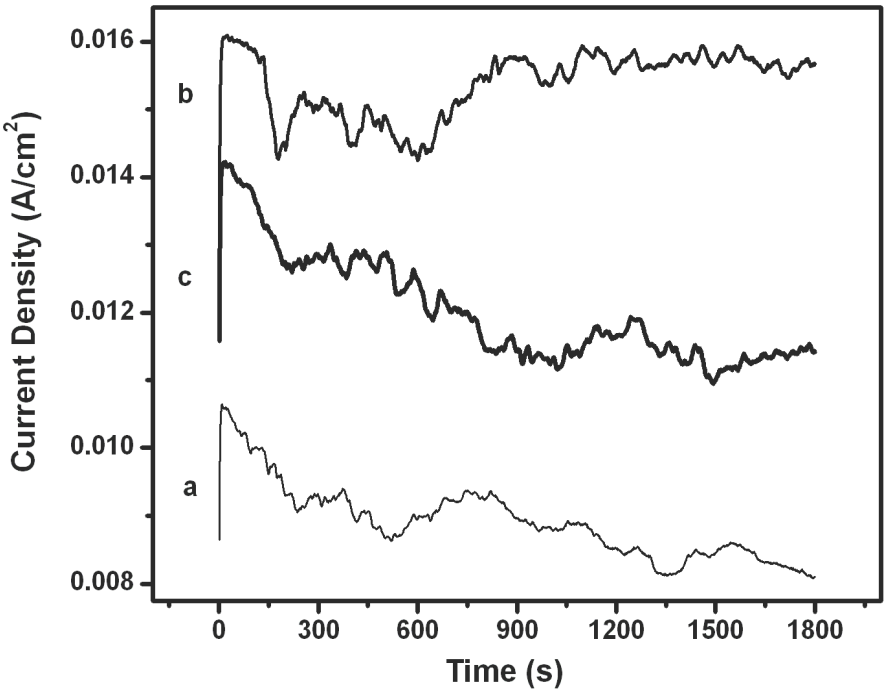

Fig. 4.11 Chronoamperometry of (a) unmodified, (b) 10% and (c) 20% of ammonium sulfate modified 10% Pt/CDX975 catalyst at 0.6 V

Fig. 4.11 shows the chronoamperometry at 0.6 V of 10% Pt/CDX catalyst with and without modification with ammonium sulfate. The sulfonic acid modified catalysts show restoration of activity for the studied time of 30 min, compared to the unmodified one.

4.5 Part C: Grafting of methylsulfonic acid group using sodium sulphite and formaldehyde

The grafting of methylsulfonic acid group with sodium sulfite and formaldehyde was carried out in two steps. In the first step, the hydroxymethyl group was grafted on the carbon black support by the reaction of formaldehyde at the ortho position to the phenolic hydroxyl group, as per the scheme 4.1. Then further reaction with sodium sulfite produces the sodium salt of the sulfonic acid, which is grafted to the methylene

group of the hydroxymethyl group. Then sulfonic acid is obtained by protonation with mineral acid.

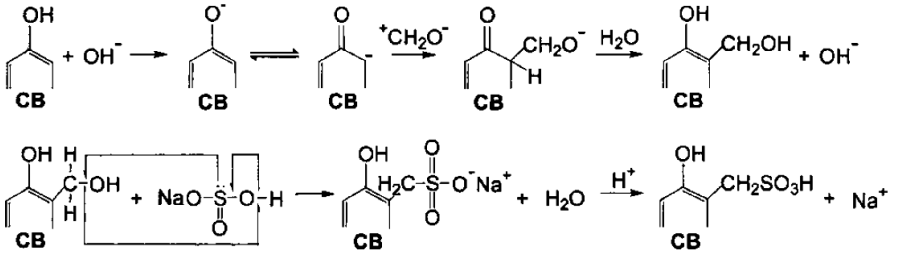

Scheme 4.1 Reaction scheme for grafting of methylsulfonic acid group onto the carbon supported catalyst

4.5.1 Loading of Pt on the carbon black support

In this part of the work, the Pt loading of the CDX975 carbon black support was done with hydrogen reduction method. At first the CDX975 carbon black is impregnated with the required quantity (for 10% Pt/CDX975) of the aqueous solution of 5 wt% hexachloroplatinic acid and stirred at 333-343 K, for evaporation to dryness. Then the reduction of platinum is done under the flow of hydrogen at 623 K for 4 h.

4.5.2 Schematic of grafting of methylsulfonic acid

To the slurry of the Pt loaded carbon black catalyst in distilled water, formaldehyde and sodium sulfite were added and refluxed at 383 K for 12 h. After cooling to room temperature, it was washed with distilled water and protonated with 1N HCl. It was further washed with distilled water and extracted with rotaevaporator to remove any sulfide by-products. Finally it was dried at 338 K in a vacuum oven for 24 h. The prepared catalysts were characterized by different techniques and their catalytic activity is evaluated for methanol electro-oxidation reaction.

4.5.3 FT-IR studies

FT-IR spectra of unsulfonated and methylsulfonic acid grafted samples are shown in Fig. 4.12. It shows the stretching vibrations for S-O at 1100 cm^{-1}, which evidences the incorporation of the sulfonic acid group on the carbon black support of the catalyst. FT-IR spectrum also shows an increased absorbance of the -OH vibration in the range of 3000-3600 cm^{-1} due to the increase of protonic acidity.

4.5.4 pH determination

The pH values have not shown any significant change between the unmodified and the methylsulfonic acid modified (3.3 for both) catalysts, may be due to the very small concentration of the sulfonic acid group grafted.

Table 4.5 pH values of unmodified and methylsulfonic acid modified catalysts

Catalyst	pH
unmodified 10% Pt/CDX975	3.3
methylsulfonic acid modified 10% Pt/CDX975	3.3

4.5.5 TGA analysis

TGA profiles recorded in nitrogen atmosphere are shown in Fig. 4.13. It shows the weight loss of the sulfonic acid group around 423 K for the sulfonic acid modified catalyst as expected (Xu *et al.*, 2003, Du *et al.*, 2008). This again supports the incorporation of methylsulfonic acid group on the carbon black support.

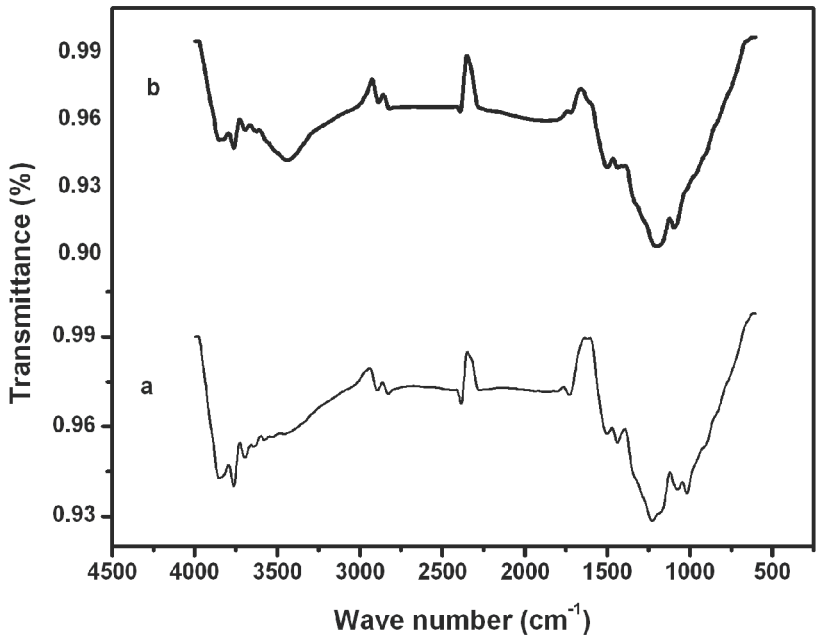

(A)

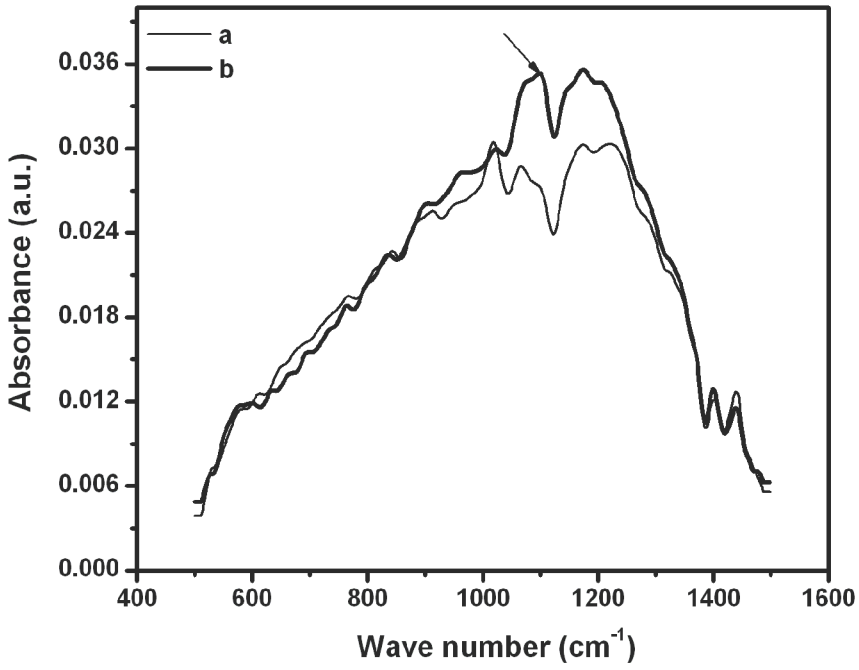

(B)

Fig. 4.12 FT-IR spectra of (a) unmodified and (b) methylsulfonic acid modified 10% Pt/CDX975 catalyst at the resolution of (A) 4 cm^{-1} and (B) 2 cm^{-1} (arrow mark in b) indicate the stretching vibration for S-O)

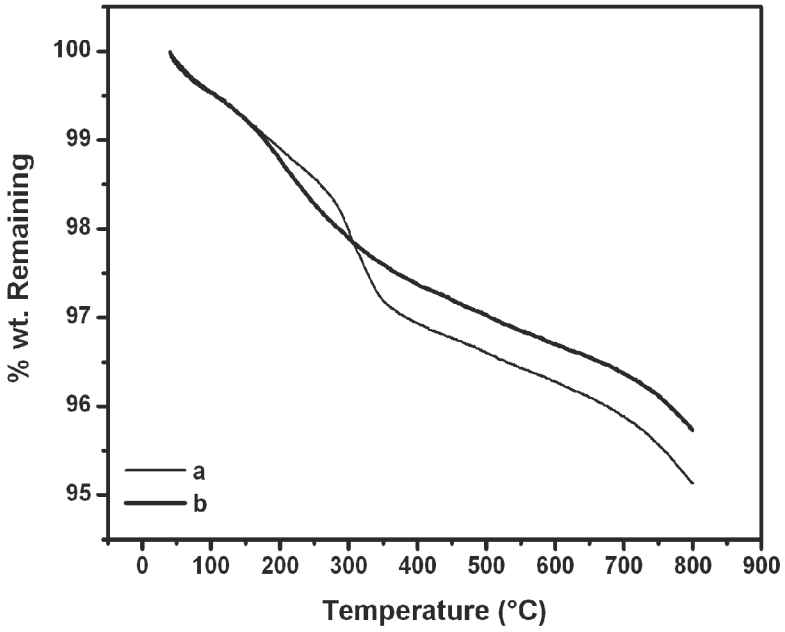

Fig. 4.13 TGA profiles of (a) unmodified and (b) methylsulfonic acid modified 10% Pt/CDX975 catalyst in N_2 at 10 °C/min

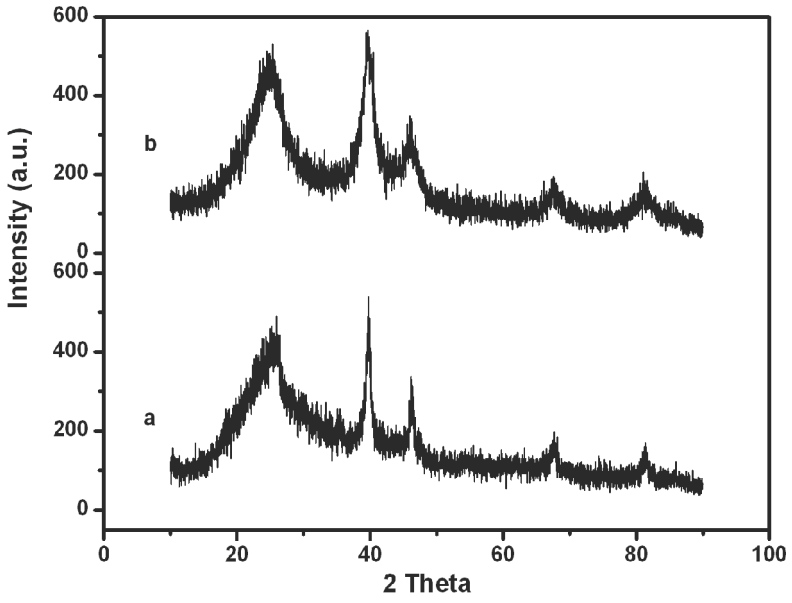

Fig. 4.14 XRD patterns of (a) unmodified and (b) methylsulfonic acid modified 10% Pt/CDX975 catalysts

4.5.6 X-ray diffraction studies

X-ray diffraction patterns of the 10% Pt/CDX975 catalysts, unsulfonated and the methylsulfonic acid grafted are shown in Fig. 4.14. It shows the characteristic Pt peaks at 2θ values around 40°, 46°, 68°, 81° and 86° corresponding to the (111), (200), (220), (311) and (222) planes of face centered cubic (fcc) structure of Pt (JCPDS card: 4-802). The diffraction peak at the 2θ value around 25°, corresponds to the (002) diffraction peak of the hexagonal structure of the CDX975 carbon black support. Fig. 4.14 shows broadening of the XRD peaks for the sulfonic acid modified catalyst. The crystallite size determined with Debye-Scherrer equation is given in Table 4.6. It shows a significant decrease in size upon sulfonation (from 13.5 nm of the unsulfonated to 4.4 nm of the sulfonated catalyst). This fact strongly evidences that the Pt nanoparticles are redistributed with better dispersion upon sulfonation.

Table 4.6 Average crystallite size and methanol oxidation activity for unsulfonated and methylsulfonic acid modified catalysts

Catalyst	Crystallite size XRD (nm)	Wt% of Pt from ICP	EAS (m^2/g)	Peak Current Density (mA/ cm^2)	Mass specific methanol oxidation activity (A/g)
unmodified 10% Pt/CDX	13.5	9.1	17.9	61.1	213
methylsulfonic acid modified 10% Pt/CDX	4.4	10.0	41.5	138.4	484

4.5.7 Electrochemical measurements

Fig. 4.15 (A) shows the cyclic voltammograms in 1M sulphuric acid of the unmodified and the methylsulfonic acid modified catalysts. Upon sulfonic acid modification, the current density for hydrogen adsorption/desorption shows a

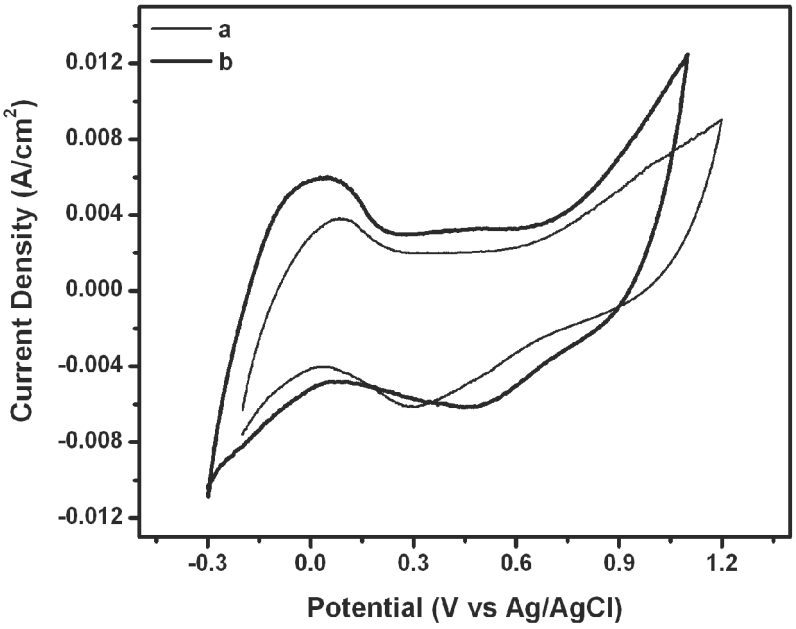

(A)

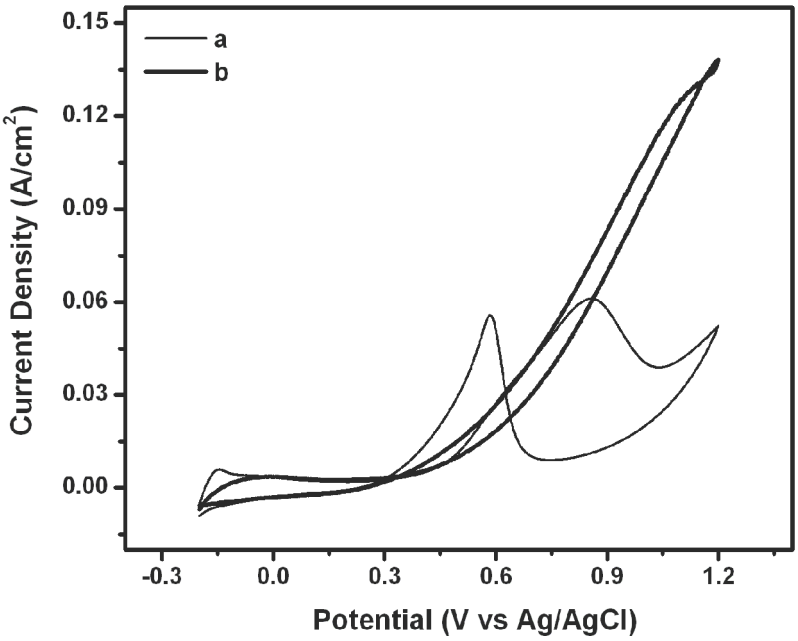

(B)

Fig. 4.15 Cyclic voltammograms of (a) unmodified and (b) methylsulfonic acid modified 10% Pt/CDX975 catalysts in (A) 1M H_2SO_4 and (B) 1M H_2SO_4 and 1M methanol at 25 mV/s

significant increase, implying the increase of electrochemical active surface area of the catalyst as shown in Table 4.6. This can be attributed to the better dispersion of the Pt nanoparticles upon sulfonic acid modification. This result supports the deductions based on the XRD studies.

Fig. 4.15 (B) shows the methanol oxidation current density in 1M methanol and 1M H_2SO_4 of the unsulfonated and the sulfonated catalysts. As given in Table 4.6 the sulfonic acid modification shows an increase in the activity for methanol oxidation compared to the unsulfonated one (Kuroki and Yamaguchi, 2006). As stated earlier, the increase in activity can be attributed to two factors; (i) the better dispersion / redistribution of the Pt nanopartilces and (ii) the increased proton conductivity of the catalyst with the incorporation of sulfonic acid groups to the inner pores of the carbon black support.

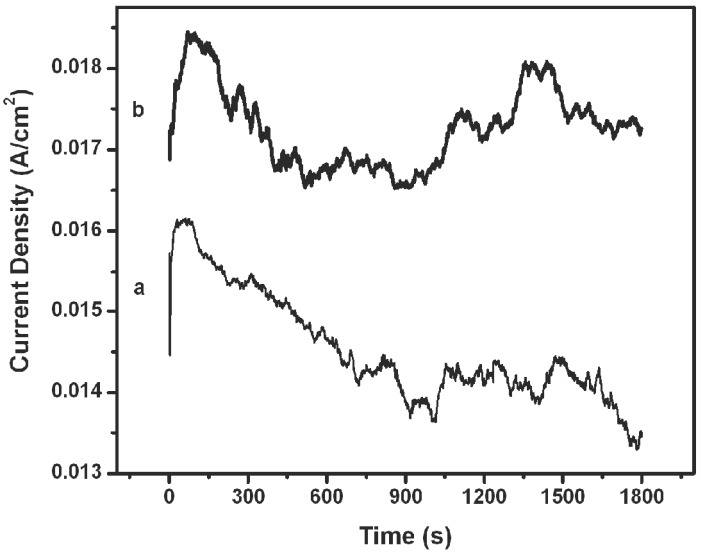

Fig. 4.16 Chronoamperometry of (a) unmodified and (b) methylsulfonic acid modified 10% Pt/CDX975 catalysts at 0.6 V

Fig. 4.16 shows the chronoamperometry of the unmodified and the methylsulfonic acid modified 10% Pt/CDX975 catalyst at 0.6 V. The sulfonic acid modified catalyst shows the restoration of activity for the studied time of 30 min as compared to the unmodified one.

4.6 Summary

- The grafting of sulfonic acid group on the CDX975 carbon black support has been carried out with three different sulfonating agents.
- Studies by FT-IR and pH measurements supported the successful grafting of the sulfonic acid group on the carbon black support.
- XRD studies show the Pt redistribution upon sulfonic acid grafting.
- The methanol oxidation activity studies have shown enhanced activity for the sulfonated catalysts, in case of all the three sulfonating agents. The increase in activity can be attributed to two factors: (i) Pt nanoparticle redistribution to smaller particles, thereby increasing the electrochemical active surface area of Pt and (ii) increased protonic conductivity inside the catalyst support.

CHAPTER 5

EFFECT OF AMINOPYRIDINE FUNCTIONALIZATION OF CDX975 CARBON BLACK SUPPORT OF Pt/CDX975 CATALYST FOR METHANOL ELECTRO-OXIDATION STUDIES

5.1 Introduction

The expensive nature of the fuel cell catalysts gears up the research activities to achieve enhanced utilization of the noble metal catalysts through different ways. The efficient utilization of any supported catalyst is better achieved only when the nearly atomic distribution of the active component on the support is attainable. The typical fuel cell catalysts are the noble metal particles supported on carbon black. Carbon is supposed to contain various surface oxygen functional groups like hydroxyl, phenolic, carbonyl, carboxylic, lactone, etc. Among the various factors which influence the dispersion of the noble metal particles, the surface properties and the surface functional groups of the carbon support plays an important role. But the different studies by Antonucci *et al*. and Roman-Martinez *et al*., on the carbon blacks enriched with oxygen functionalities through oxidative treatment with mineral acids, especially nitric acid, had shown aggregation of the Pt nanoparticles. This was attributed to the strong metal support interaction of the Pt-O bond, which inhibits the diffusion of the Pt nanoparticles to the inner pores of the support material, and leads to aggregation on the surface of the support itself (Antonucci *et al*., 1994 and Roman-Martinez *et al*., 1995). Therefore functionalization of the carbon support with different heteroatoms was studied by Roy *et al*., 1996 and 1997. They studied the effect of nitrogen, sulfur and phosphorous functionalization of the carbon black support, and found smaller Pt

particle size along with enhanced performance for oxygen reduction reaction, with the catalysts prepared with nitrogen and sulfur functionalized carbon support. The XANES studies on the nitrogen functionalized catalysts had shown the existence of nitrogen as pyridinic and pyrrolic groups (Roy *et al*., 1997). These nitrogen functionalization studies on the carbon black support were mostly carried out by heat treating at 1073 K under the flow of NH_3 gas (Roy *et al*., 1996 and 1997); Biniak *et al*., 1997); also by carbonizing the nitrogen containing polymer (Puziy and Poddubnaya, 1998), or through the conversion of carboxylic to acyl chloride with thionyl chloride, and then condensation of acyl chloride with di- or triamines (Silva *et al*., 2004 and Jarrais *et al*, 2005); or by exposing the carbon black to NH_3 plasma (Loh *et al*., 1987); One of the recent study involves a simple single step reaction of chloramine with the hydroxyl functional group of the mesoporous carbon material, which was synthesized by hydrothermal method (Titirici *et al*., 2007). So it was considered interesting to study the effect of grafting aminopyridine functional group on the carbon support material, for the methanol electro-oxidation reaction.

5.2 Aminopyridine modification of CDX975 carbon black support

CDX975 carbon support was modified with aminopyridine with two different weight percentages of 1 and 5 wt% of the aminopyridine agent, 2-amino-5-chloro-pyridine (acp). The required quantity of the aminating agent (5 and 25 mg) was dissolved in THF (15 ml) and then added to the CDX975 support. Then it was refluxed at 353-363 K for 3 h. After cooling to room temperature, it was extracted with THF (3mL) twice to remove the unreacted aminating agent and the reaction intermediates in a rotavapour. Then extracted with methanol (3 mL) twice, filtered, washed with dist. H_2O and dried in an air oven at 353 K for 15 h.

5.2.1 Loading of Pt on the aminopyridine modified CDX975 carbon black support

100 mg of the amino pyridine modified CDX975 was impregnated with the required amount (in order to get 10 wt% Pt/CDX975) of aqueous hexachloroplatinic acid (5 wt% of H_2PtCl_6) and evaporated to dry at 333-343 K. The impregnated catalyst was reduced in hydrogen atmosphere at 623 K for 4 h.

5.3 Characterization of the catalysts

5.3.1 pH determination

The determination of pH has not shown any change upon the aminopyridine modification. Both unmodified and the aminopyridine modified samples show the same pH of 6.4. But the aminopyridine modification of the nitric acid treated CDX975 carbon black support has shown an increase of pH from 4.5 to 6.0.

5.3.2 FT-IR studies

FT-IR spectra of the unmodified and aminopyridine modified samples are shown in Fig. 5.1. It shows the characteristic stretching vibrations of C=C and C=N of pyridine at 1480 cm^{-1} to 1648 cm^{-1} and N-H stretching of primary amine at 1619 cm^{-1}, indicative of the incorporation of the aminopyridine group on the CDX975 carbon black support.

5.3.3 Elemental Analysis

Table 5.1 shows the elemental analysis for the unmodified and the aminopyridine modified CDX975 carbon black samples. It shows a higher percentage of nitrogen for the modified samples compared to the unmodified one and therefore, confirming the incorporation of the aminopyridine group on the CDX975 carbon black.

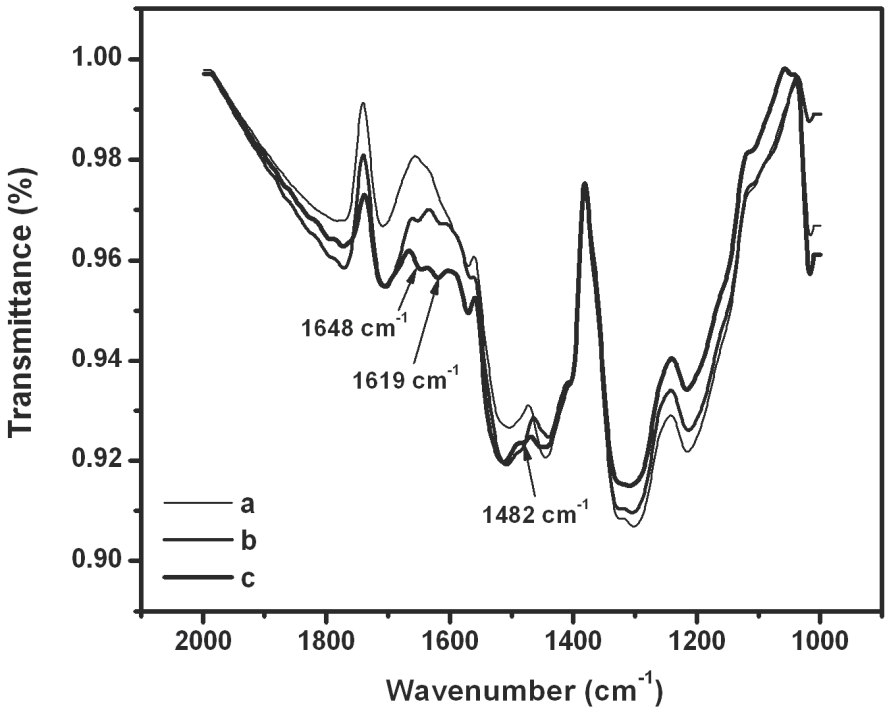

Fig 5.1 FT- IR spectra of (a) unmodified, (b) 1% and (c) 5% of 2-amino-5-chloro-pyridine (acp) modified CDX975 carbon black support

Table 5.1 Elemental analysis results of the unmodified and the aminopyridine (acp) modified CDX975 carbon black support

S.No.	Sample	C %	H %	N %
1	0% acp/ cdx	95.33	0.6	0.15
2	1% acp/ cdx	96.02	0.96	0.23
3	5% acp/ cdx	94.96	0.45	0.84

5.3.4 Thermogravimetric analysis

Fig. 5.2 shows the TGA profile of the unmodified and the aminopyridine modified CDX975 carbon black support. The unmodified CDX975 shows thermal stability till 973 K. But the low temperature weight loss of the modified carbon black sample can be attributed to the loss of the aminopyridine moity.

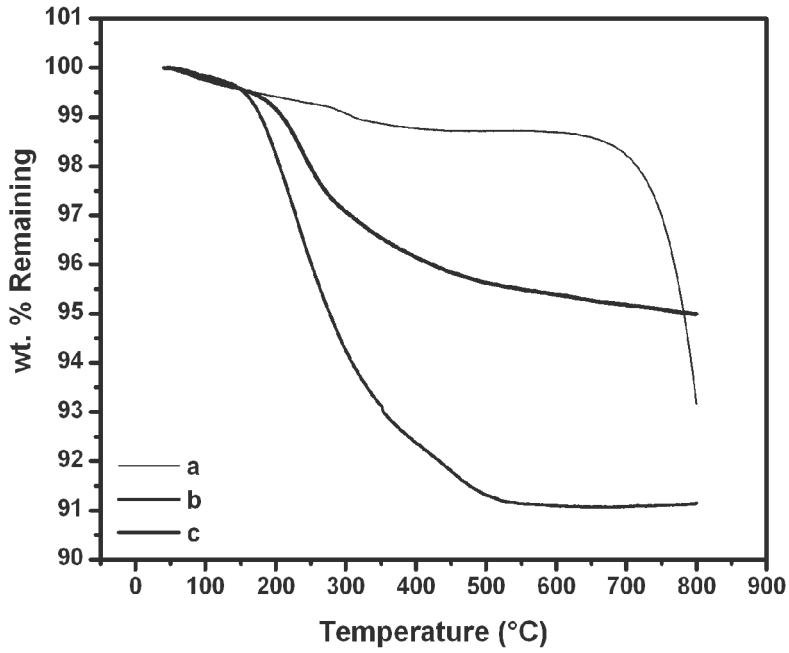

Fig 5.2 TGA profile of (a) unmodified, (b) 1% and (c) 5% 2-amino-5-chloropyridine modified CDX975 carbon black support

5.3.5 X-ray diffraction studies

XRD patterns of the unmodified and aminopyridine modified CDX975 carbon black support is shown in Fig. 5.3. The X-ray diffraction patterns show the peak at the 2θ value around 25°, corresponds to the (002) diffraction peak of the hexagonal structure of the CDX975 carbon black support. It has not shown any significant change in XRD

patterns of the unmodified and the aminopyridine modified samples, indicative of no changes in the carbon structure.

Fig. 5.4 shows the XRD patterns of the 10% Pt loaded on the unmodified and the aminopyridine modified CDX975 samples. The crystallite sizes of Pt has been determined with Debye-Scherrer equation and are given in Table 5.2. It shows that, the aminopyridine modification of the CDX975 support decreases the crystallite size of Pt from 18 to 9 nm. This can be attributed to the better dispersion of Pt particles on the modified carbon black support, because of the better anchoring of Pt on nitrogen functionalities like primary amine or pyridine (Roy *et al*., 1997).

Table 5.2 Average Pt crystallite size and unit cell parameter of the catalyst 10% Pt loaded on unmodified and aminopyridine modified CDX975 carbon black support

S.No.	Sample	XRD crystallite size (nm)	Unit cell parameter a (Å)
1	10% Pt/ 0% acp/ cdx	18.5	3.921
2	10% Pt/ 1% acp/ cdx	13.4	3.917
3	10% Pt/ 5% acp/ cdx	9.4	3.924

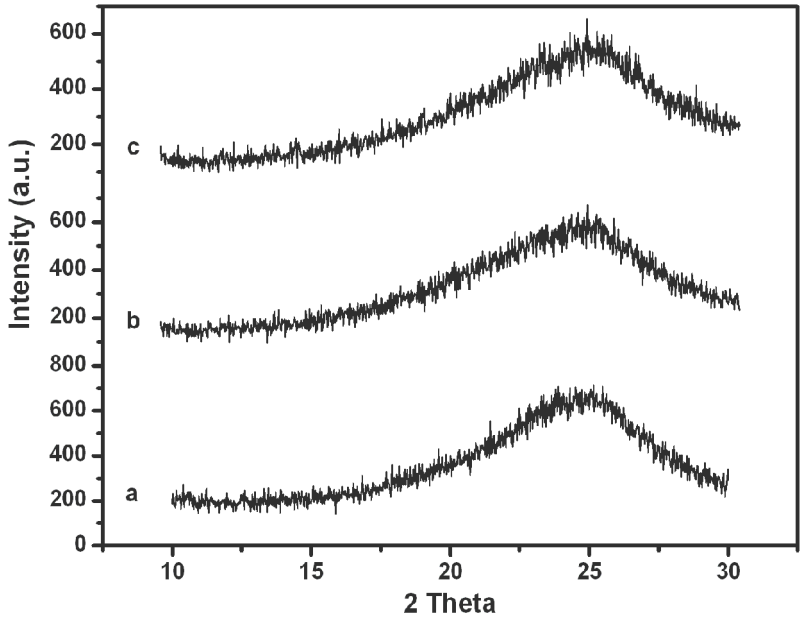

Fig 5.3 **XRD patterns of (a) unmodified (b) 1% and (c) 5% 2-amino-5-chloropyridine modified CDX975 carbon black support**

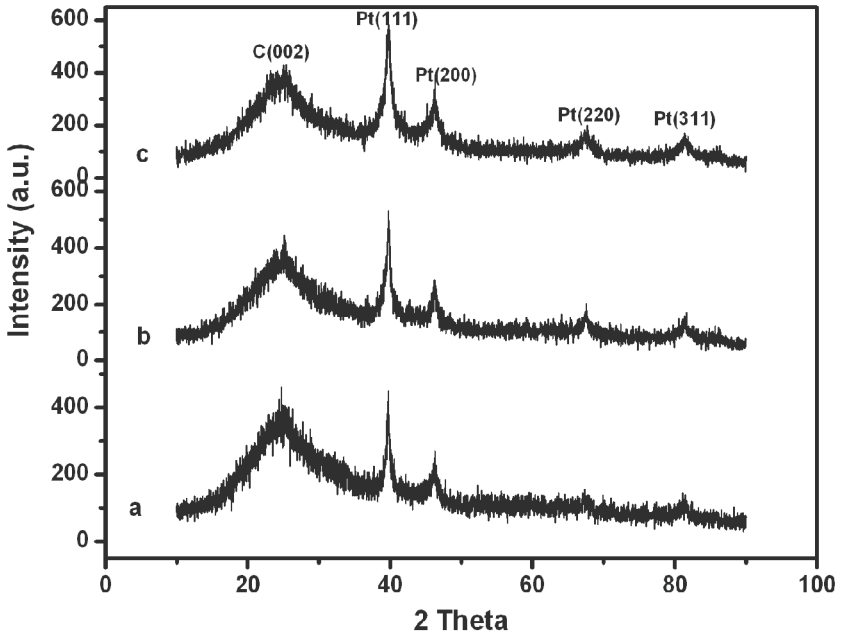

Fig. 5.4 **XRD patterns of 10% Pt loaded on (a) unmodified (b) 1% and (c) 5% 2-amino-5-chloropyridine modified CDX975 carbon black support**

5.3.6 Scanning electron microscopic (SEM) analysis

Fig. 5.5 shows the SEM images of the unmodified and the aminopyridine modified CDX975 samples. The unmodified sample shows an aggregated morphology and the aminopyridine modified sample shows a porous morphology, which may be attributed to the increase of pore volume upon the aminopyridine modification.

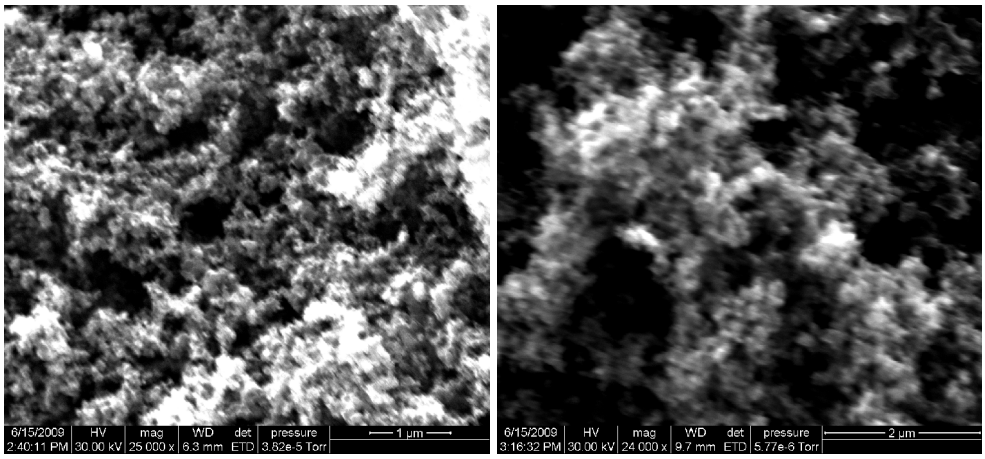

(a) **(b)**

Fig. 5.5 SEM images of (a) the unmodified and (b) 5% 2-amino-5-chloro-pyridine (acp) modified CDX975 carbon black support

5.3.7 Transmission electron microscopic (TEM) analysis

Fig. 5.6 shows the TEM, HRTEM and Electron diffraction images of 10% Pt loaded on the unmodified and the aminopyridine modified CDX975 carbon black catalysts. The TEM images of the unmodified samples show two different particle size distribution. But the TEM images of the aminopyridine modified sample show the uniform dispersion of the Pt nanoparticles. The average Pt particle size measurements show 7.6 nm for the unmodified sample and 3.4 nm for the amino pyridine modified sample.

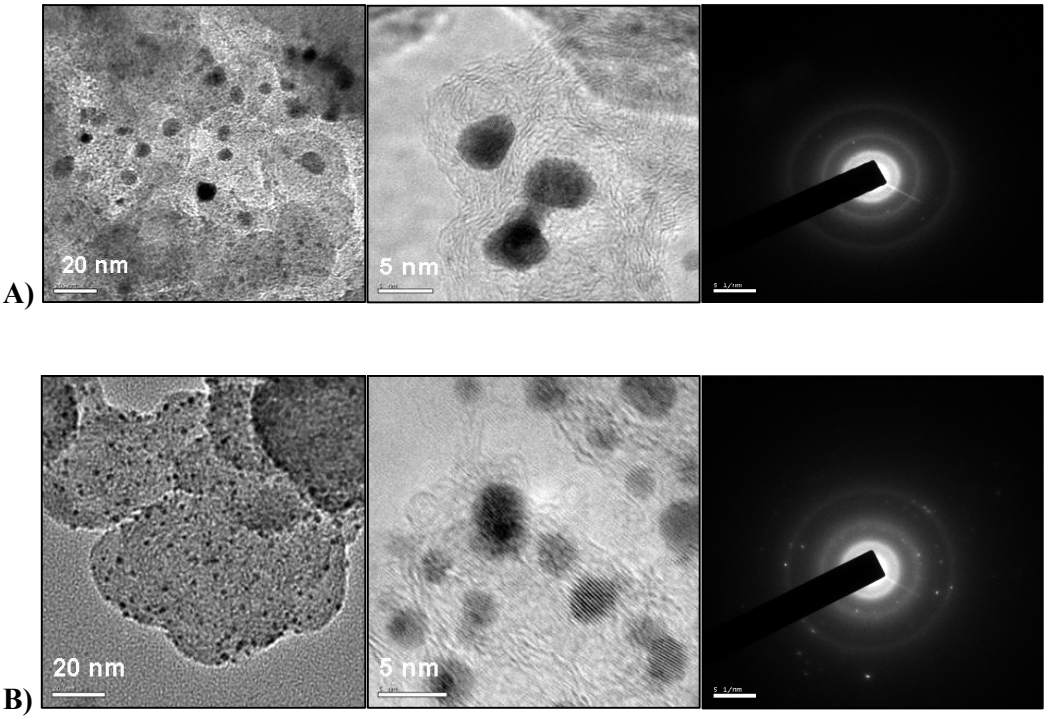

Fig. 5.6 (a) TEM, (b) HRTEM and (c) Electron diffraction images of 10% Pt loaded on (A) unmodified and (B) 5% aminopyridine modified CDX975 carbon black catalysts

5.4 Electrochemical measurements

Cyclic voltammograms of 10% Pt loaded on unmodified and the aminopyridine modified CDX975 catalysts, in 1M sulphuric acid is shown in Fig. 5.7 (A). The catalysts prepared with the modified support shows increased current density for hydrogen adsorption/desorption. This increase in current density can be attributed to the better dispersion of the Pt nanoparticles on the aminopyridine modified carbon black samples. The values of electrochemical active surface area are given in Table 5.3. The modified samples show increased electrochemical active surface area, which can be attributed to the better dispersion of the Pt nanoparticles.

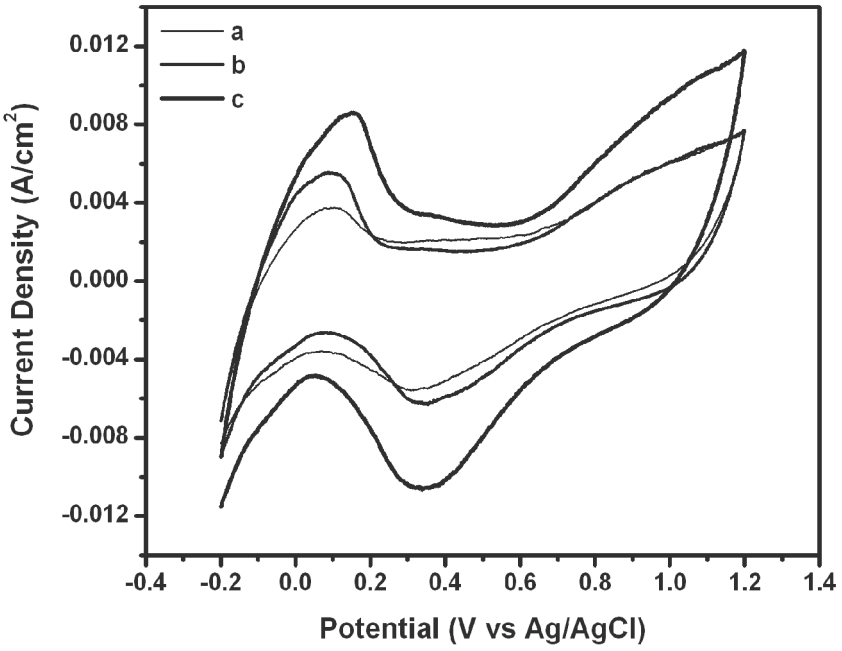

(A)

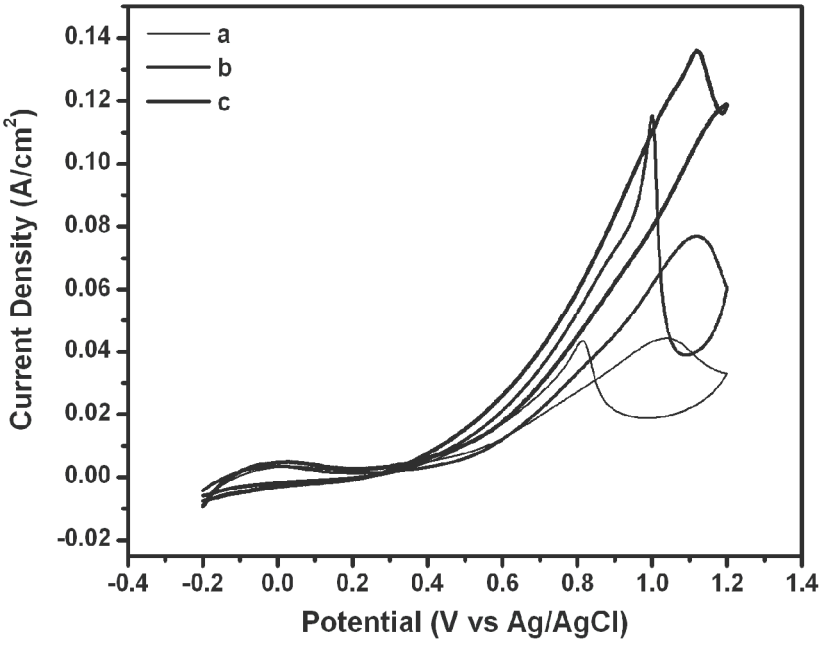

(B)

Fig. 5.7 Cyclic voltammograms in (A) 1M H_2SO_4 and (B) in 1M methanol and 1M H_2SO_4 of 10% Pt loaded on (a) unmodified, (b) 1% and (c) 5% of aminopyridine modified CDX975 carbon black catalysts at the scan rate of 25 mV/s

Table 5.3 Electrochemical active surface area and methanol oxidation activity of 10% Pt loaded on unmodified and aminopyridine modified CDX975 catalysts

Sample	Estimated Pt by ICP %	EAS (m^2/g)	Peak methanol oxidation activity (mA/ cm^2)	Mass specific methanol oxidation activity (A/g)
10% Pt/ 0% acp/ cdx	9.1	19.3	44.3	155
10% Pt/ 1% acp/ cdx	8.6	38.7	77.1	270
10% Pt/ 5% acp/ cdx	8.3	60.0	118.6	415

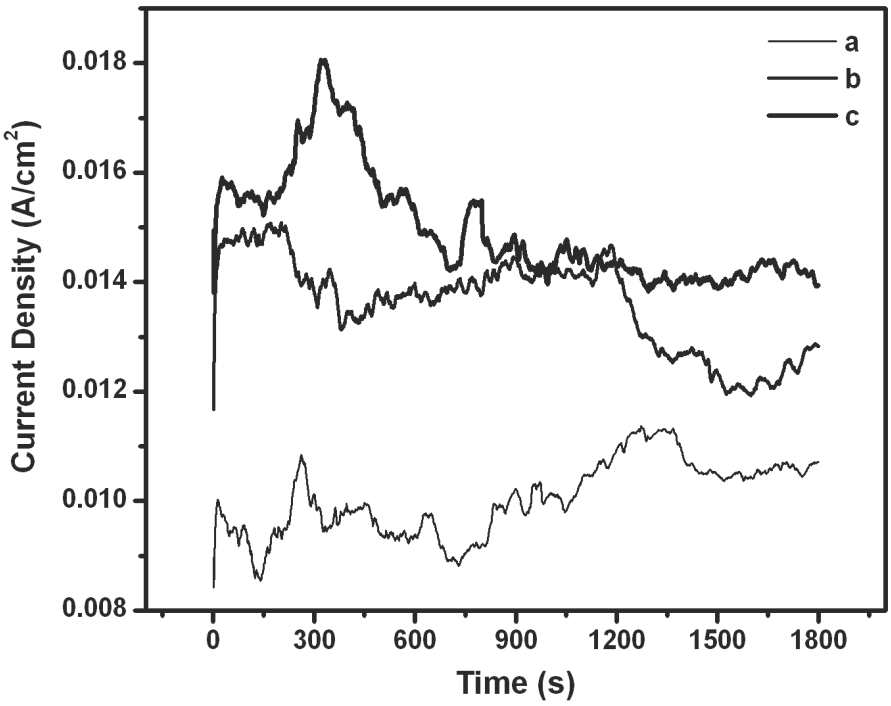

Fig. 5.8 Chronoamperometry of 10% Pt loaded on (a) unmodified (b) 1% and (c) 5% aminopyridine modified CDX975 catalysts at 0.6 V

Fig. 5.7 (B) shows the cyclic voltammograms for methanol oxidation in 1M methanol in 1M sulphuric acid. Table 5.3 shows the methanol oxidation activity measured in terms of the peak current density. The enhanced activity for the aminopyridine

modified samples can be attributed to the increased electrochemical active surface area of the Pt nanoparticles as a result of enhanced dispersion of these Pt nanoparticles on the modified carbon black supports. Similar enhancement in oxygen reduction current density was observed for the nitrogen functionalization of the carbon black support of the Pt loaded catalyst (Roy *et al*., 1997).

Fig. 5.8 shows the chronoamperometry of the unmodified and aminopyridine modified catalysts at 0.6 V. For the aminopyridine modified catalysts, the current density remains to be higher than that of the unmodified one, for the study time of 30 min.

5.5 Summary

- XRD and TEM results have shown a decrease in particle size of Pt nanoparticles as a result of better dispersion on the aminopyridine modified CDX975.

- The electrochemical studies in sulphuric acid have shown an enhancement in electrochemical active surface area of the Pt nanoparticles upon aminopyridine modification of the carbon black support, also confirms the better dispersion of the Pt nanoparticles on the modified support.

- Methanol oxidation studies have shown enhanced activity for the catalyst prepared with aminopyridine modified carbon black support compared to the unmodified one, which can be attributed to the smaller particle size of Pt nanoparticles as a result of enhanced dispersion on the modified carbon black support.

CHAPTER 6

METHANOL OXIDATION STUDIES OF Pt/CDX975 CATALYST PREPARED USING CITRATE AS THE CAPPING AGENT

6.1 Introduction

For the successful implementation of direct methanol fuel cells, the amount of noble metal catalysts used need to be reduced significantly, or, in other words, the performance of the existing catalyst systems need to be increased. On the issue of increasing the electrocatalytic activity, many catalytic materials have been investigated for polymer electrolyte fuel cells (PEFCs) and it has been found that the supported and unsupported Pt and its alloys exhibit better electrocatalytic activity towards H_2 and CH_3OH oxidation as well as O_2 reduction reactions (Guo *et al*., 2005). Pt is often prepared as nanoparticles dispersed on a suitable support to increase the surface to mass ratio (to achieve atomic distribution of Pt) in order to increase the utilization of the expensive and less abundant Pt. Although the carbon support can inhibit the thermally driven Ostwald ripening of small Pt particles to some extent, the control of particle size and size distribution by this factor is rather limited (Chan *et al*., 2004). The higher electrocatalytic activity of Pt and its alloys can be achieved when the metal particles are produced in the nanoscale range. The common approaches adopted for the preparation of supported and unsupported Pt and its alloys include the reduction of metal salts of Pt and the reduction of Pt and its alloy metal salts by using reducing agents such as bisulphate, borohydride, hydrazine, formaldehyde and formic acid (Watanabe *et al*., 1987; Prabhuram and Manoharan, 1998; Castro Luna *et al*., 2000; Goodenough *et al*., 1990; Roth *et al*., 2001; Lizcano-Vulbuena *et al*., 2003). The low temperature methods of preparation designed to

curtail Pt particle growth, such as, microemulsion techniques (Zhang and Chan, 2003; Yadav *et al*., 2003), and the polyol process (Liu *et al*., 2004) are often more complex, entail higher process and environmental costs. A simple aqueous based method of preparation with good size and size distribution control is therefore highly desirable. The control of nucleation and growth of particles during chemical reduction is fundamental to any method of preparation. This is especially so for processes where nanoparticles of the catalytic metal are formed before they are dispersed on the support. Nanoparticles are thermodynamically unstable and their apparent stability comes from an acquired kinetic hindrance to agglomeration. Hence, in order to produce desired sizes of Pt nanoparticles with uniform dispersion on the carbon support, some kind of stabilizing agents, such as surfactants, ligands or polymers, is usually employed during the preparative process (Bonnmann *et al*., 1994; Bonnmann *et al*., 1996; Wang and Hsing, 2002; Paulus *et al*., 2000; Prabhuram *et al*., 2003). Large molecules such as polymers and surfactants, when adsorbed on the metal nanoparticle surface, can prevent nanoparticles in close proximity from being coalesced by the dispersion forces. The presence of these stabilizer molecules on the particle surface, however, could compromise catalytic activity. The removal of stabilizer by thermal treatment may induce particle sintering, thereby undoing the effort in nanoparticle synthesis (Zeng *et al*., 2006). Heat treatment can alter the properties of these catalysts. In the case of PtRu alloys, it is known that heat treatments as low as 220 °C result in Pt and Ru phase separation (Bock *et al*., 2004). The preservation of small particle size and narrow size distribution should not be achieved at the expense of catalytic activity. It was found that even though poly(N-vinyl-2-pyrrolidone) (PVP) stabilized Pt/C catalysts result in Pt particles smaller than 3 nm, but the poor performance is caused by the adsorbed PVP layer, which reduces the number of active Pt sites for catalysis. Electrostatic stabilization is an alternative way to obtain colloidal metal particle dispersions in solution (Zhao *et al*., 2006). Since

Turkevich *et al*. 1986, used citrate for the preparation of Pt nanoparticles, several researches were carried out with the use of citrate as a water soluble stabilizer to obtain Pt nanoparticles. Lin *et al*., 2005 experimentally demonstrated the different roles of citrate as a reductant or a stabilizer and observed that the reducing reaction could not take place below 363 K. The size dependence of the Pt/C catalysts on the concentration of citric acid has been reported by Guo *et al*., 2005, who had proposed a citrate complexation stabilizing mechanism. The citrate anion has been used as a stabilizer to prepare noble metal nanoparticles such as gold (Lin *et al*., 2003), palladium (Turkevich and Kim, 1970), silver (Pillai and Kamat, 2004) and platinum (Henglein and Giersig, 2000; Guo *et al*., 2005). It was reported that the glycolate anion acted as a stabilizer for the size controlled preparation of Pt–Ru colloids (Bock *et al*., 2004). Recently, sodium acetate was also found as a good stabilizer for preparing Pt and Ru nanoparticles in the liquid polyol process (Zhao *et al*., 2006). These carboxylic anions used as stabilizers were possibly preferred to polymer stabilizer for the synthesis of electrocatalysts because the anions were easily removed by washing with deionized water at room temperature. Fig. 6.1 schematically explains the different stabilization methods, such as steric stabilization and electrostatic stabilization (Ozkar and Finke, 2002)**.**

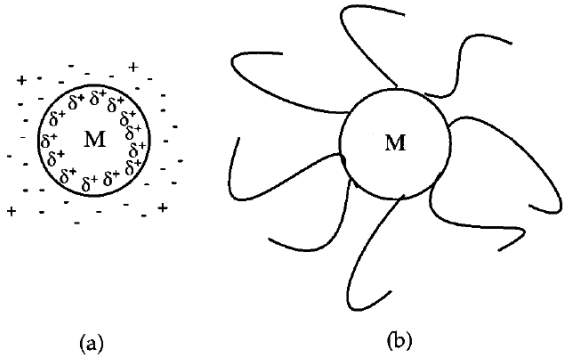

Fig. 6.1 Schematic illustration for (a) an electrostatically stabilized metal (M) particle (i.e., one stabilized by the adsorption of ions and the resultant electrical double layer **(b) a sterically stabilized metal particle** (i.e., one stabilized by the adsorption of polymer chains) (Ozkar and Finke, 2002)

6.2 Preparation of Pt/CDX975 catalyst with the use of citrate as the capping agent

The effect of citrate as the capping agent has been studied on (i) 10% Pt/CDX975 and (ii) 20% Pt/CDX975 catalysts. The need for the study of the 20% Pt/CDX975 also can be explained as follows. Eventhough fuel cell studies are generally aiming to reduce the metal loading, the catalyst layer in the fuel cell needs higher percentage of Pt, in order to get a thinner electrode. The presence of less percentage of Pt and more percentage of carbon, leads to a thicker catalyst layer and this further leads to problems like increased internal resistance. Therefore, preparation of higher loading of Pt is also an important issue. But the increase of metal loading may lead to increase in the size of metal nanoparticles and hence decrease in the catalytic performance.

6.3 Study on 10% Pt/CDX975 catalyst

The 10% Pt/CDX975 catalyst with different mole ratio of (2.4, 6, 12 and 24) citrate/Pt has been prepared by ethylene glycol reduction method. In a typical procedure, the required quantity of citrate is dissolved in 2.5 mL of dist. H_2O and mixed with the required quantity of an aqueous solution of hexachloroplatinic acid (in order to get 10% Pt/C) and ethylene glycol. This suspension is added to the CDX975 carbon black support and stirred at room temperature for 5-10 min. Then it was heat treated at 393 K for 80 min. After cooling to room temperature, it was filtered, washed with copious quantity of distilled water to remove the unreacted citrate and other reaction intermediates. It was also washed with acetone to remove any ethylene glycol and the reaction intermediates. Then it was dried in vacuum oven at 333-343 K for 20 h. The prepared catalysts have been characterized with different techniques.

6.3.1 X-ray diffraction studies

Fig. 6.2 (A) shows the XRD patterns of the 10% Pt/CDX975 catalyst, with and without the capping action of citrate. It shows the characteristic Pt peaks at 2θ values

around 40°, 46°, 68°, 81° and 86° corresponding to the (111), (200), (220), (311) and (222) planes of face centered cubic (*fcc*) structure of Pt (JCPDS card: 4-802). The diffraction peak at the 2θ value around 25° corresponds to the (002) diffraction peak of the hexagonal structure of the CDX975 carbon black support.

It can be observed that the addition of citrate has caused a significant broadening of the Pt peaks. The crystallite size of Pt determined with Debye-Scherrer equation has shown a decrease of crystallite size with the capping action of citrate. In order to study the variation of the particle size of Pt, the 10% Pt/CDX975 catalyst has been prepared with different mole ratios of citrate/Pt of, 2.4, 6, 12 and 24. With the increase in mole ratio, the Pt particle size decreases (Table 6.1). This could be due to the increased dispersion of the Pt nanoparticles on the carbon black support.

Table 6.1 Average Pt crystallite size determined from XRD and Pt particle size from TEM for 10% Pt/CDX975 catalyst with different mole ratios of citrate/Pt

Mole ratio of citrate/Pt	Pt crystallite size XRD (nm)	Pt particle size TEM (nm)
0	9.1	7.5
2.4	4.1	3.0
6.0	3.7	-
12.0	**3.3**	**2.7**
24.0	3.1	-

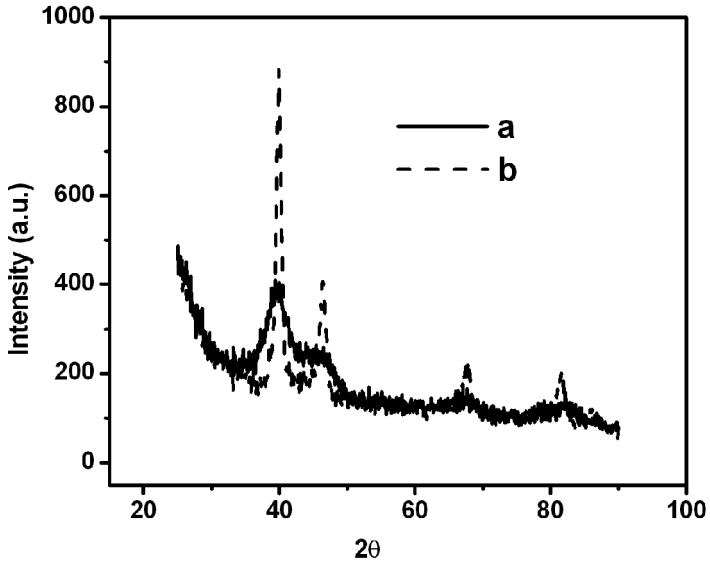

(A)

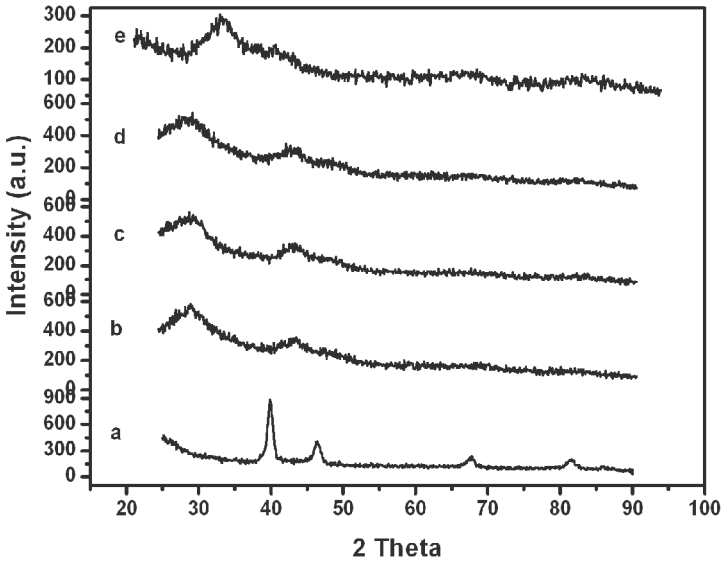

(B)

Fig. 6.2 XRD patterns of 10% Pt/CDX975 catalyst (A) with citrate (a) and without citrate (b) and (B) with different mole ratios of a) 0, b) 2.4, c) 6.0, d) 12.0 and e) 24 of citrate/Pt

6.3.2 TEM analysis

TEM images of the 10% Pt/CDX975 catalysts prepared with and without the addition of citrate are shown in Fig. 6.3. It can be seen that the addition of citrate has affected the Pt particle size from 7.5 nm to 2.7 nm. The particle size for the catalysts prepared with different mole ratio of citrate/Pt is shown in Fig. 6.4. It shows only a marginal decrease of Pt particle size with the increase in citrate/Pt mole ratio (Table 6.1). This could be attributed to the attainment of the optimal dispersion of Pt nanoparticles on the carbon black support and there is a dispersion limitation exerted by the CDX975 carbon black support (Chan *et al*., 2004), which needs to be studied further in detail.

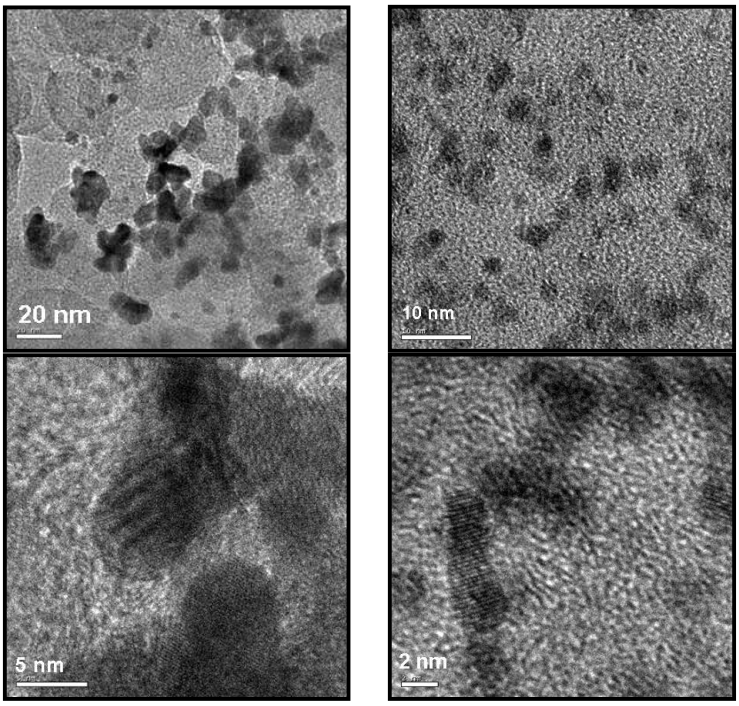

(A) **(B)**

Fig. 6.3 TEM and HRTEM images of 10% Pt/CDX975 catalyst (A) with out citrate (7.5 nm) and (B) with citrate (2.7 nm)

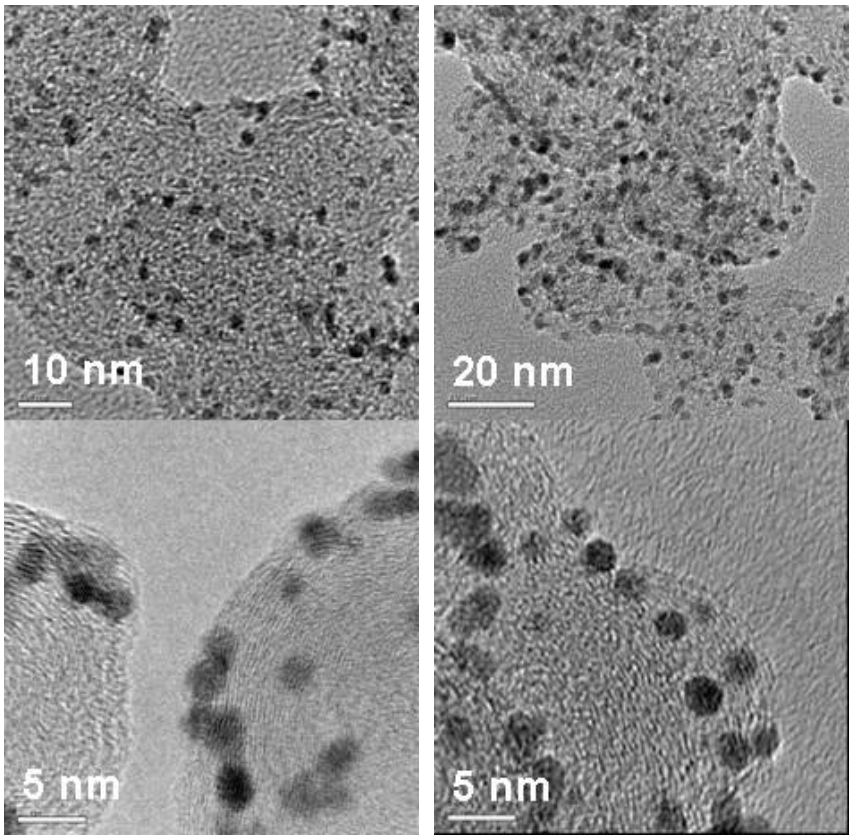

(a) **(b)**

Fig. 6.4 TEM and HRTEM images of 10% Pt/CDX975 catalyst with different mole ratio of citrate/Pt of (a) 2.4 (3.0 nm) and (b) 12 (2.7 nm)

6.3.3 X-ray photoelectron spectroscopic (XPS) studies

XPS spectra of Pt 4f of the 10% Pt/CDX975 catalyst with varying mole ratio of citrate/Pt is shown in Fig. 6.5. The oxidation state of Pt determined from XPS for 10 % Pt/CDX975 catalyst with varying mole ratio of citrate/Pt is given in Table 6.2. It shows the decrease of metallic Pt and increase of Pt in Pt(II) state with the increase of citrate/Pt mole ratio. The existence of more of Pt(II) species in presence of the electrostatic stabilizing agent is already reported by different authors (Bock *et al*., 2004).

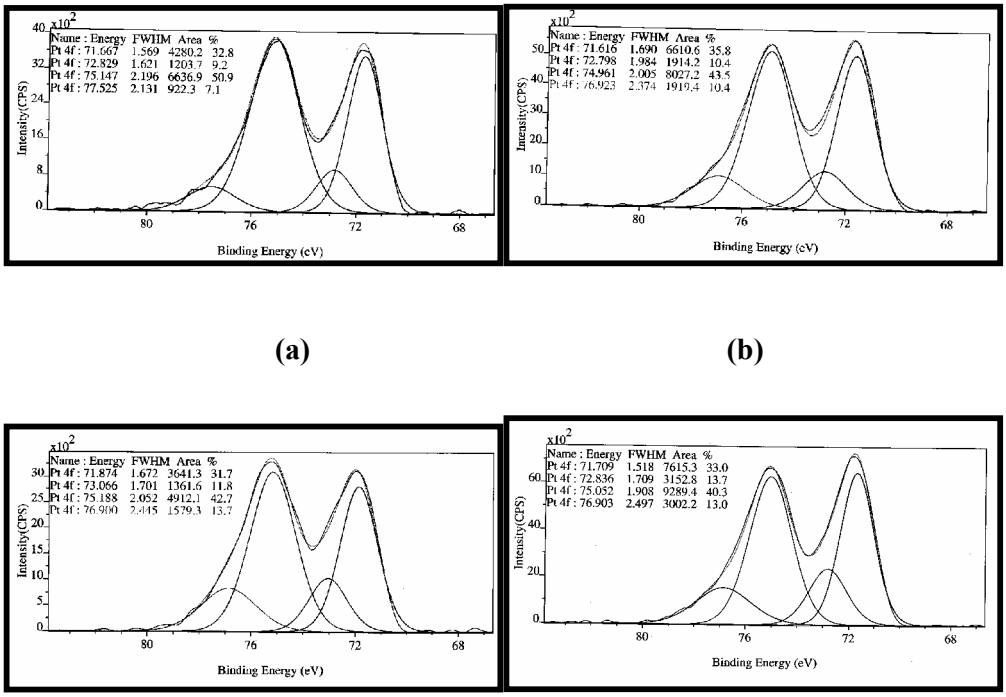

Fig. 6.5 X-ray photoelectron spectra for Pt 4f of 10% Pt/CDX975 prepared with the varying mole ratio of citrate/Pt of (a) 2.4, (b) 6.0, (c) 12.0 and (d) 24.0

Table 6.2 Oxidation states of Pt in 10% Pt/CDX975 catalyst with different mole ratios of citrate/Pt

Mole ratio of citrate/Pt	% Pt(0)	% Pt(II)
0	73.3	26.7
2.4	83.7	16.3
6.0	79.3	20.8
12.0	**74.4**	**24.5**
24.0	73.3	26.7

6.3.4 Electrochemical measurements

Fig. 6.6 (A) shows the current density for hydrogen adsorption/desorption, which is a measure of the electrochemical active surface area of Pt, in other words dispersion of Pt, of 10% Pt/CDX975 catalyst prepared without and with citrate as well as for the commercial E-TEK catalyst of similar metal loading, in 1M sulphuric acid. The catalyst prepared with citrate shows the high current density, measure of the better dispersion of the Pt nanoparticles. Fig. 6.6 (B) shows the hydrogen adsorption/desorption current density for varying mole ratios of citrate/Pt. It shows an increase of the current density with the increase of mole ratio of citrate/Pt at first, with the maximum for the mole ratio of 12. The values of electrochemical active surface areas determined are given in Table 6.3. It also shows the increase at first with increase of citrate/Pt mole ratio and the maximum for the mole ratio of 12.0. This can be attributed to the increasing dispersion of Pt nanoparticles. With further increase of mole ratio of citrate/Pt, the current density decreases, due to the blocking of the active Pt sites by the presence of excess citrate molecules, as reported in similar studies (Guo *et al*., 2005).

Table 6.3 Electrochemical active surface area and methanol oxidation current density of 10% Pt/CDX975 catalyst with different mole ratios of citrate/Pt

Mole ratio of citrate/Pt	EAS (m^2/g)	Peak Methanol Oxidation current density (mA/cm^2)
0	-	148
2.4	7.3	94
6.0	12.4	96
12.0	**17.7**	**202**
24.0	11.8	148

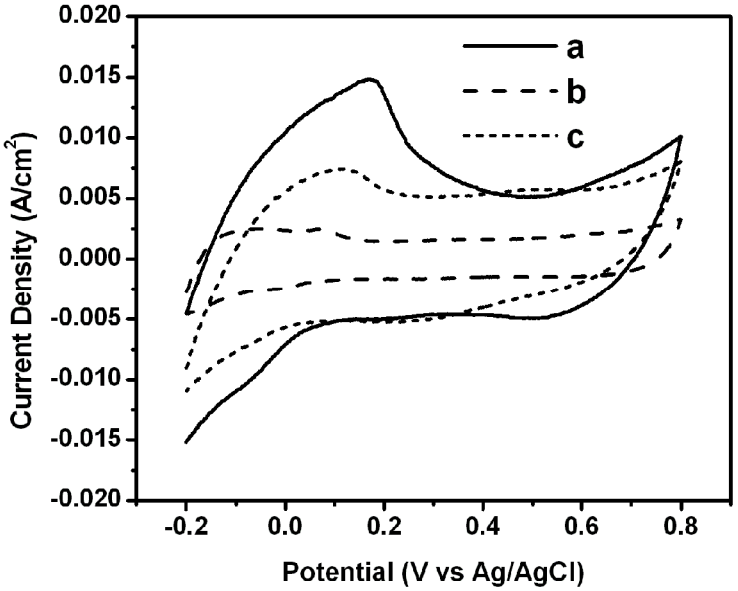

(A)

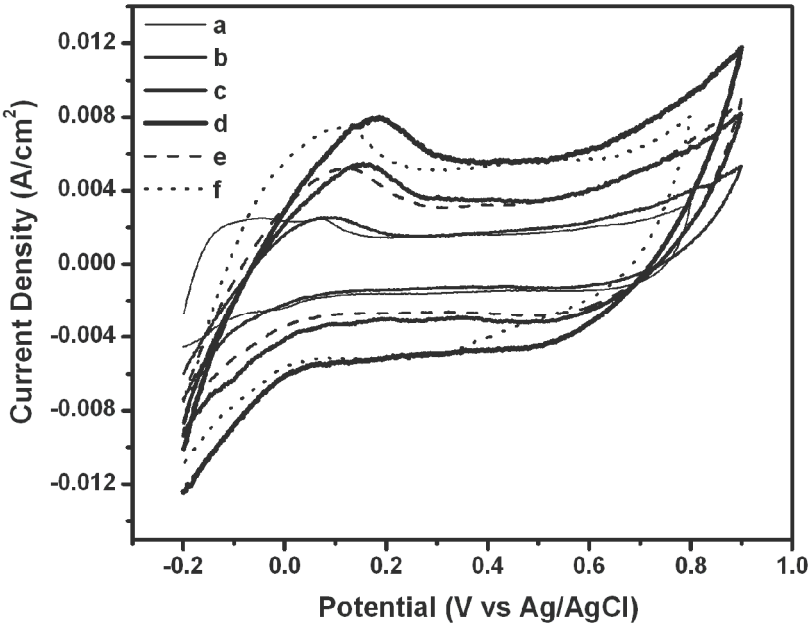

(B)

Fig. 6.6 Cyclic voltammogram of 10% Pt/CDX975 catalyst (A) with citrate(a), without citrate(b) and (c) 10% Pt/C E-TEK catalyst and (B) for different mole ratios of citrate/Pt of (a) 0, (b) 2.4, (c) 6, (d) 12, (e) 24 and (f) 10% Pt/C E-TEK catalyst in 1M H_2SO_4 at a scan rate of 25 mV/s

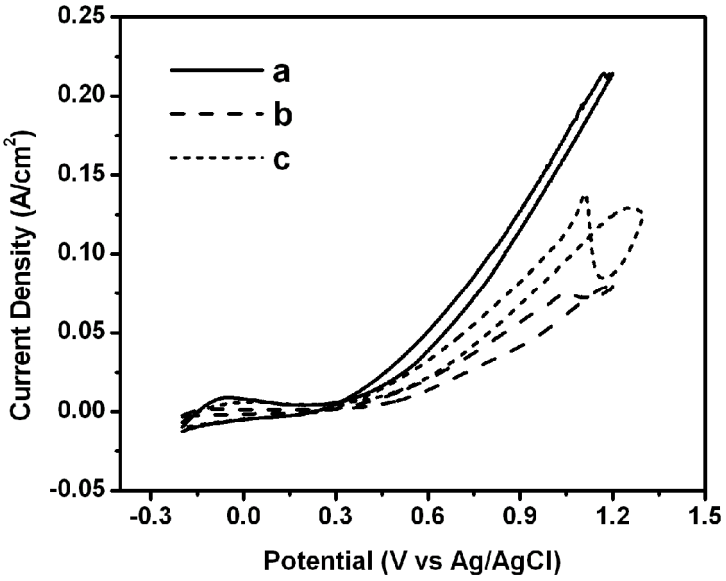

(A)

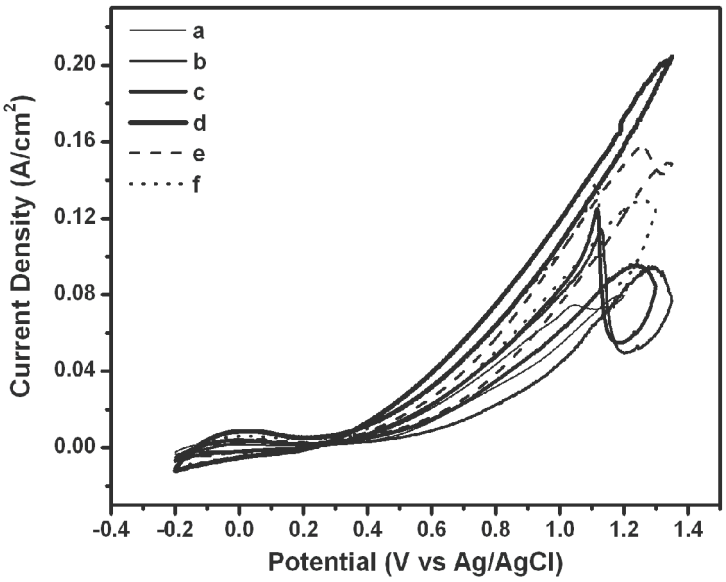

(B)

Fig. 6.7 Cyclic Voltammogram for methanol oxidation of 10% Pt/CDX975 catalyst (A) with (a) without (b) citrate and (c) 10% Pt/C E-TEK catalyst and (B) for different mole ratios of citrate/Pt of (a) 0, (b) 2.4, (c) 6, (d) 12, (e) 24 and (f) 10% Pt/C E-TEK catalyst in 1M methanol and 1M H_2SO_4 at 25 mV/s

Fig. 6.7 shows the cyclic voltammogram for methanol oxidation in 1M methanol and 1M H_2SO_4. Fig. 6.7 (A) shows the methanol oxidation current density for the 10% Pt/CDX975 catalyst prepared with and without citrate along with the one for the commercial E-TEK catalyst of similar metal loading. It shows enhanced methanol oxidation current density for the catalyst prepared with citrate as the capping agent, as compared to the one with out citrate. This can be explained to the enhanced dispersion of the Pt nanoparticles on the carbon black support with the addition of citrate.

Fig. 6.7 (B) shows the methanol oxidation current density for the catalysts prepared with differing mole ratios of citrate/Pt (Table 6.3). It shows an increase in methanol oxidation current density at first with the maximum methanol oxidation activity for the catalyst prepared with the citrate/Pt mole ratio of 12. This can be attributed to the optimum dispersion of the Pt nanoparticles on the carbon black support, as supported by the measurement of electrochemical active surface area. The catalyst which shows the maximum activity also contains the higher percentage of Pt(II) species as observed from XPS results. The onset potential for methanol oxidation also significantly shifts cathodic for the one showing maximum activity. It can be explained in an another way as suggested by few earlier reports (Parsons and VanderNoot, 1988; Goodenough *et al*., 1987), to the presence of higher percentage of Pt(II) species exerts enhanced activity.

The involvement of surface oxides of the electrode materials on the electro-oxidation of small organic molecules has been well argued by Parsons and VanderNoot, 1988. It was argued that, the oxidation of small organic molecules like CO, CH_3OH, HCHO and HCOOH on Pt occurs at the potential of formation of the surface oxide, apart from showing similar oxidation profile. This observation holds for other electrodes

like Au, Ni and Pd also. Goodenough *et al*. have also reported similar observations with the XPS study of the Pt supported on carbon black electrode, before and after methanol oxidation. This study suggested that, an unstable oxide species observed before use of the electrode for methanol oxidation, which could easily donate oxygen during the oxidation, was changed to an inert stable oxide after the electrochemical reaction. The decrease of electrode activity was thus attributed to the change of the unstable oxide to the inert one (Goodenough *et al*., 1987).

Further increase of the mole ratio of citrate/Pt, decreases the methanol oxidation activity. This decrease in activity can be attributed to the blocking of the active Pt sites by the excess citrate molecules, as reported by Guo *et al*., 2005.

Fig. 6.8 shows the chronoamperometry of the 10% Pt/CDX975 catalyst prepared with and without citrate along with that of the commercial E-TEK catalyst of same metal loading at 1.0 V. It shows enhanced current density and stability for the catalyst prepared with citrate as the capping agent, as compared to the one with out citrate and also the commercial catalyst. It supports the advantage of the capping action of citrate.

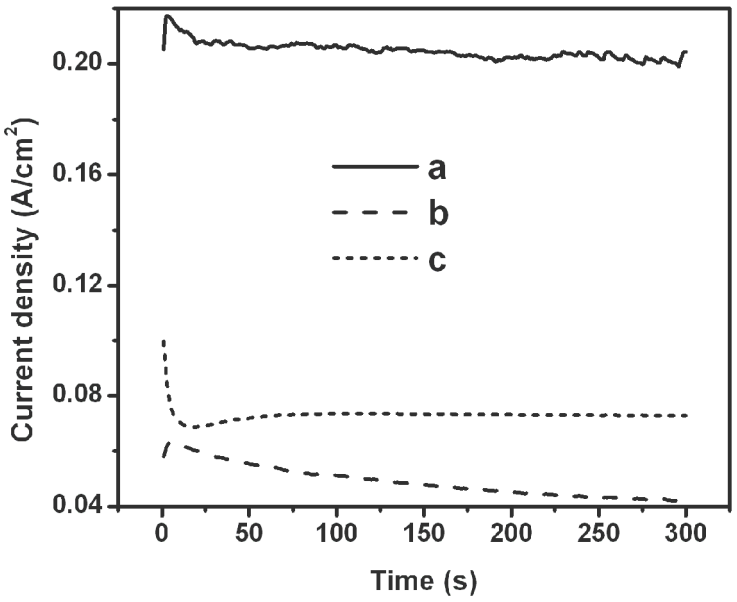

Fig. 6.8 Chronoamperometry of 10% Pt/CDX975 catalyst (a) with b) without citrate and (c) 10% Pt/Vulcan E-TEK catalyst in 1M H_2SO_4 and 1M methanol at 1.0 V

6.4 Study on 20% Pt/CDX975 catalyst

The 20% Pt/CDX975 catalyst with the effect of citrate has been studied with the mole ratios of citrate/Pt of 6, 12, 18 and 24. The preparation of the catalysts has been followed as given in the earlier section (6.3). The prepared catalysts have been characterized by different techniques.

6.4.1 X-ray diffraction studies

Fig. 6.9 (A) shows the XRD patterns of the 20% Pt/CDX975 catalyst, with and without the capping action of citrate. It shows the characteristic Pt peaks at 2θ values around 40°, 46°, 68°, 81° and 86° corresponding to the (111), (200), (220), (311) and (222) planes of face centered cubic (*fcc*) structure of Pt (JCPDS card: 4-802) and the

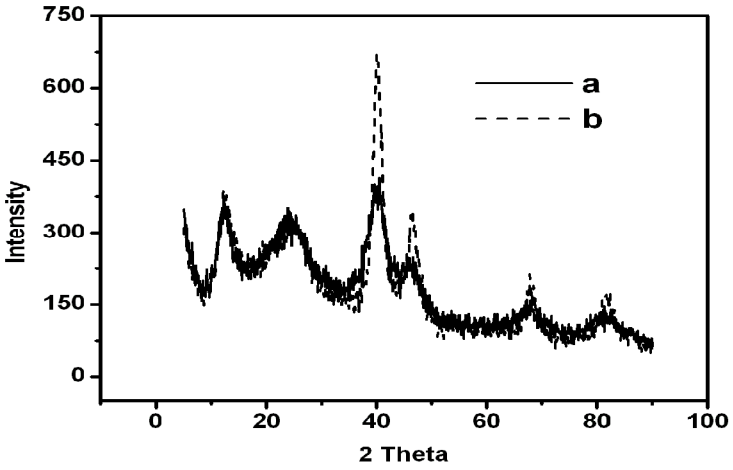

(A)

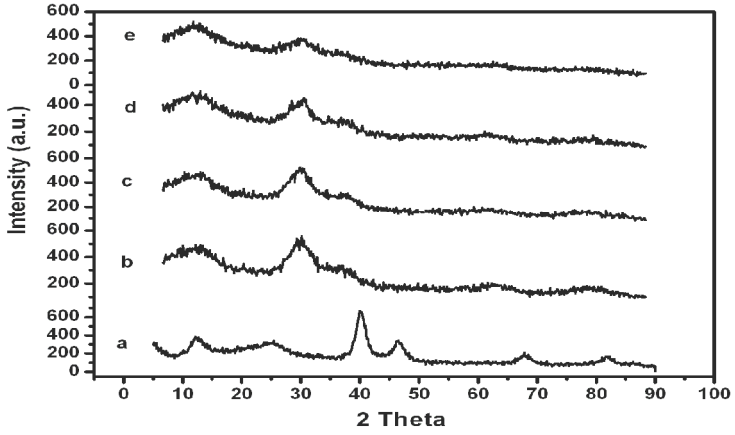

(B)

Fig. 6.9 XRD patterns of 20% Pt/CDX975 catalysts (A) with (a) and without (b) citrate and (B) with different mole ratios of (a) 0, (b) 6, (c) 12.0, (d) 18.0 and (e) 24 of citrate/Pt

diffraction peak at the 2θ value around 25° corresponds to the (002) diffraction peak of the hexagonal structure of the CDX975 carbon black support.

It can be observed that the addition of citrate has caused the significant broadening of the Pt peaks. The crystallite size of Pt determined with Debye-Scherrer equation shows decrease of crystallite size with the capping action of citrate. In order to study the variation of the particle size of Pt, the 20% Pt/CDX975 catalyst has been prepared by varying the mole ratio of citrate/Pt of, 6, 12, 18 and 24. With increase of this mole ratio, the Pt particle size decreases (Table 6.4). This could be explained to the increased dispersion of the Pt nanoparticles on the carbon black support.

Table 6.4 Average Pt crystallite size determined from XRD and Pt particle size from TEM for 20 % Pt/CDX975 catalyst with different mole ratios of citrate/Pt

Mole ratio of citrate/Pt	Crystallite size from XRD (nm)	Particle size from TEM (nm)
0	4.8	5.6
6	3.2	3.7
12	3.0	3.2
18	**2.8**	**3.6**
24	2.3	-

6.4.2 TEM analysis

TEM and HRTEM images of the 20% Pt/CDX975 catalyst prepared with and without citrate are shown in Fig. 6.10. It shows the smaller particle size for the catalyst prepared with citrate as the capping agent. With the effect of citrate, the Pt particle size is seen to be reduced from 5.6 nm to 3.2 nm.

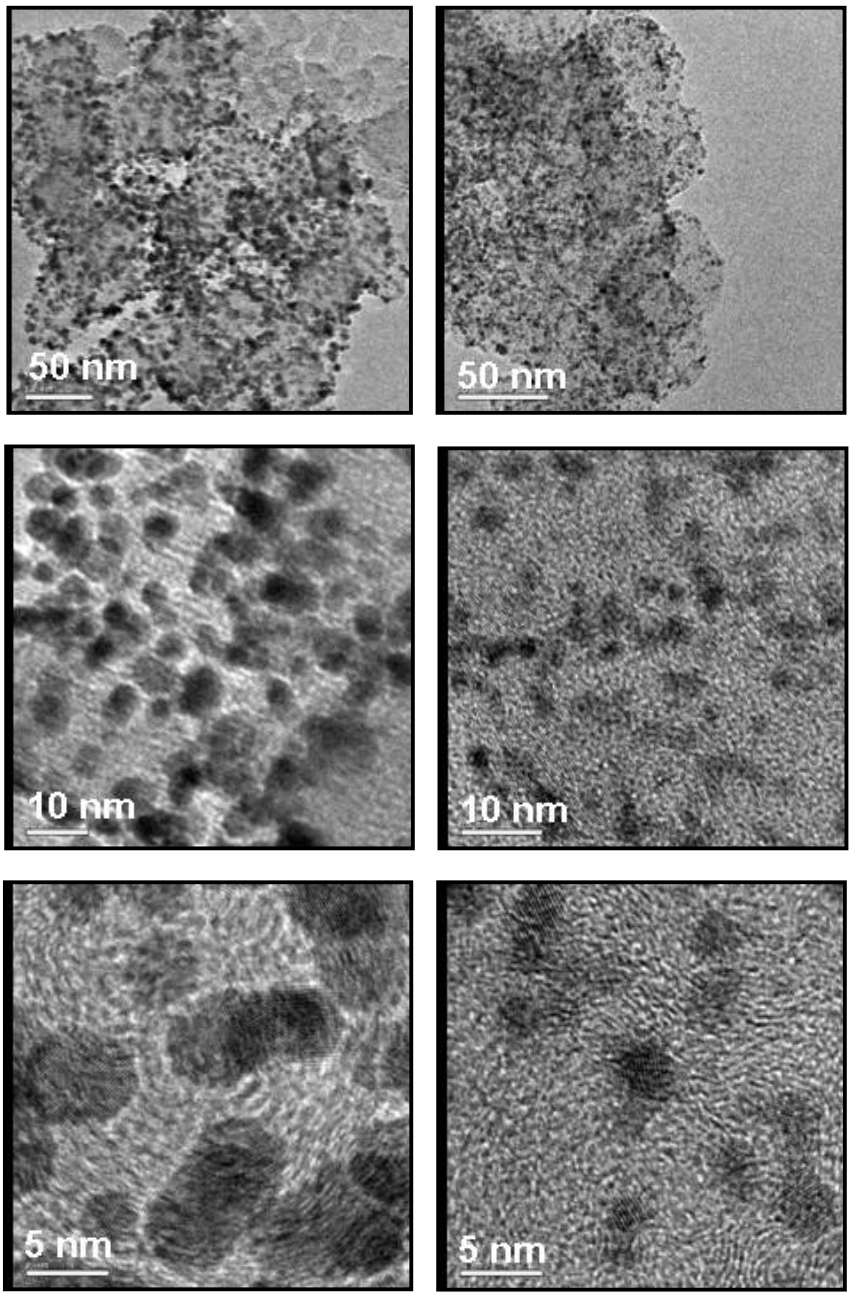

(A) **(B)**

Fig. 6.10 TEM and HRTEM images of 20% Pt/CDX975 catalyst (A) without citrate (5.6 nm) and (B) with citrate (3.2 nm)

Fig. 6.11 shows the TEM and HRTEM for the 20% Pt/CDX975 catalysts prepared with varying mole fractions of citrate/Pt. With the increase of the mole fraction of citrate/Pt from 6 to 18, it can be observed that there is no change in the Pt particle size (3.7 and 3.6 nm for the citrate/Pt mole ratio of 6 and 18 respectively) (Table 6.4). This could be due to the attainment of the optimal dispersion of Pt nanoparticles on the carbon black support and there is a dispersion limitation exerted by the CDX975 carbon black support (Chan *et al*., 2004).

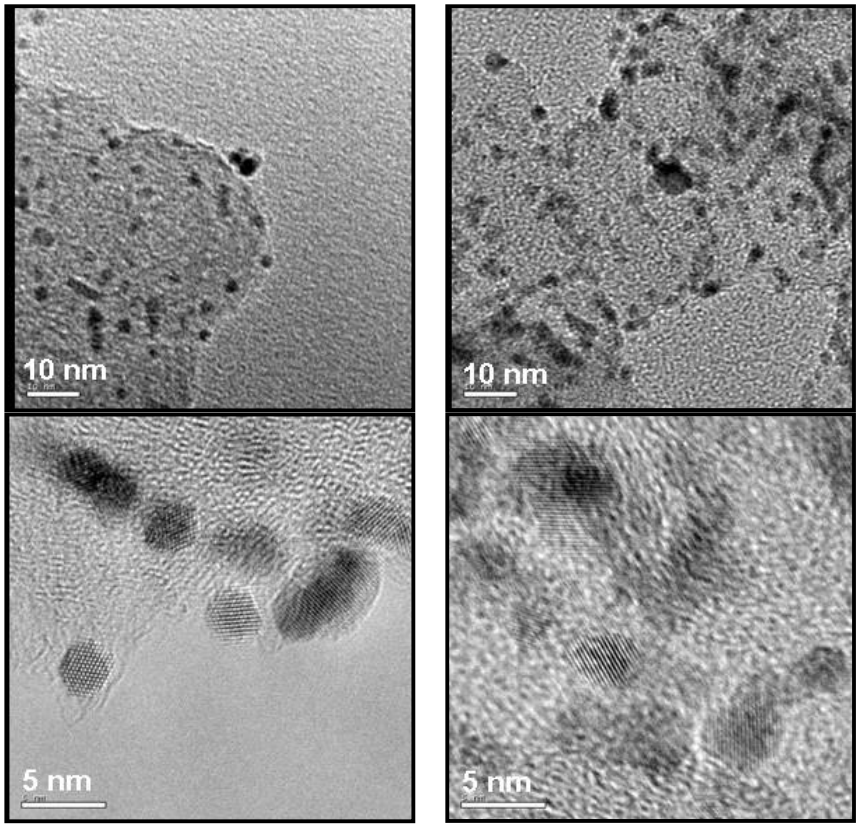

(a) **(b)**

Fig. 6.11 TEM and HRTEM images of 20% Pt/CDX975 catalyst for the citrate/Pt mole ratios of (a) 6.0 and (b) 18

6.4.3 X-ray photoelectron spectroscopic (XPS) studies

Fig. 6.12 shows the XPS spectra for the 20% Pt/CDX975 catalyst with the different mole ratios of citrate/Pt of 6, 18 and 24. The oxidation state of Pt obtained by the deconvolution of Pt 4f peaks is presented in Table 6.5. As observed for the 10% Pt/CDX975 catalyst, with increase of citrate/Pt mole ratio, the percentage of Pt(II) species increases.

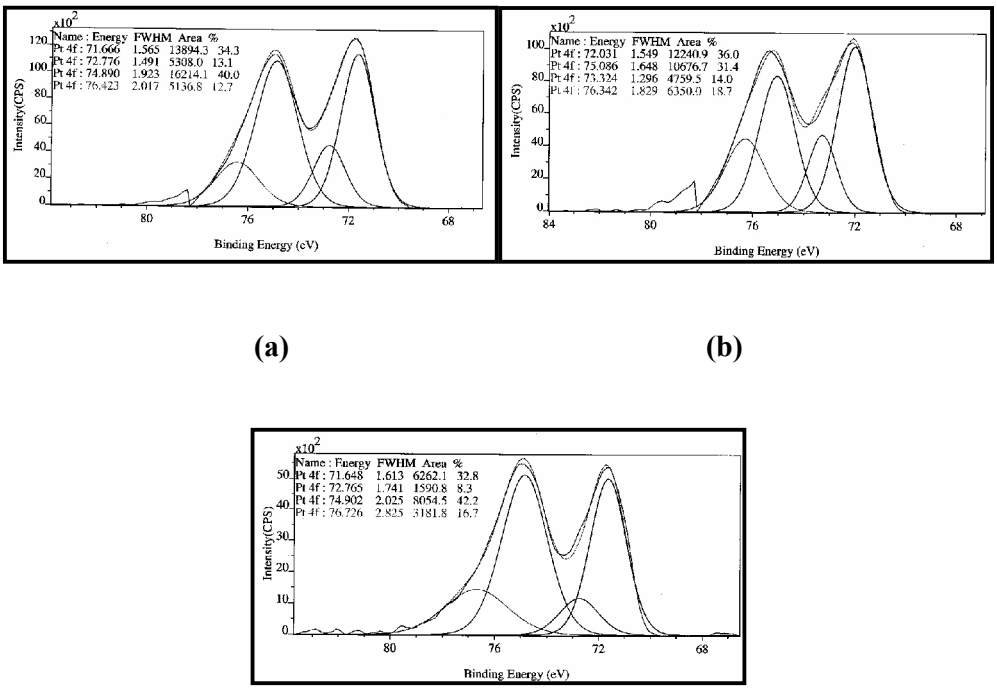

Fig. 6.12 X-ray photoelectron spectra of 20% Pt/CDX975 catalyst prepared with the different mole ratios of citrate/Pt of (a) 6, (b) 18 and (c) 24

Table 6.5 Oxidation state of Pt by XPS of 20% Pt/CDX975 catalyst with different mole ratios of citrate/Pt

Mole ratio of citrate/Pt	% Pt(0)	% Pt(II)
0	-	-
6	74.3	25.8
12	-	-
18	**67.4**	**32.7**
24	75.0	25.0

6.4.4 Electrochemical measurements

Fig. 6.13 (A) shows the current density for hydrogen adsorption/desorption, which is a measure of the electrochemical active surface area of Pt, in other words dispersion of Pt, of 20% Pt/CDX975 catalyst prepared without and with citrate, in 1M sulphuric acid. The catalyst prepared with citrate shows the high current density, which gives the measure of the better dispersion of the Pt nanoparticles. Fig. 6.13 (B) shows the hydrogen adsorption/desorption current density for the 20% Pt/CDX975 catalyst with varying mole ratios of citrate/Pt. It shows an increase of the current density with the increase of mole ratio of citrate/Pt at first, with the maximum for the mole ratio of 18. The electrochemical active surface area values are given in Table 6.6. It also shows an increase at first with the increase of the citrate/Pt mole ratio and the maximum for the mole ratio of 18.0. This can be attributed to the increasing dispersion of Pt nanoparticles. With further increase of the mole ratio of citrate/Pt, the current density decreases, due to the blocking of the active Pt sites by the excess citrate molecules, as reported by similar studies (Guo *et al*., 2005).

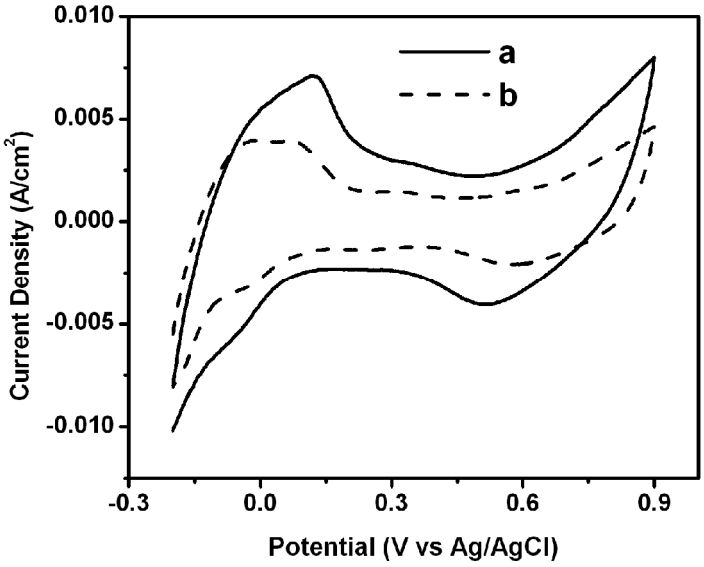

(A)

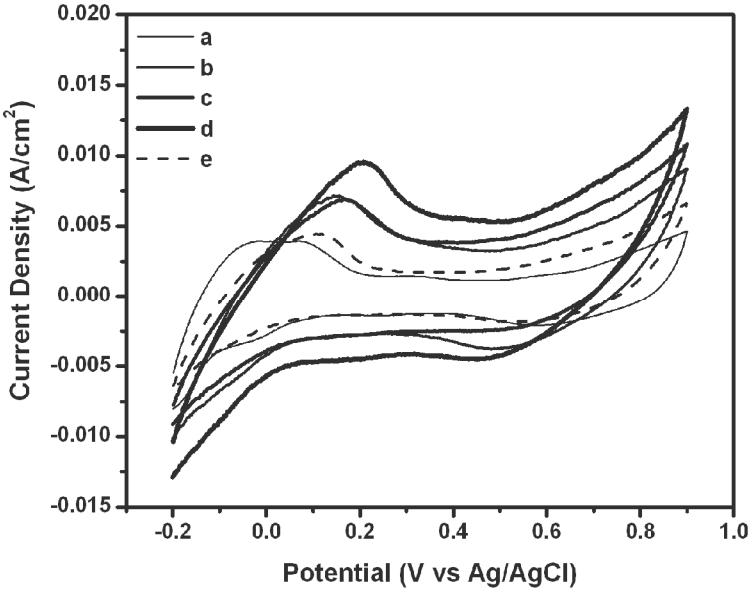

(B)

Fig. 6.13 Cyclic Voltammograms of 20% Pt/CDX975 of (A) with citrate(a) and without citrate(b) and (B) for varying mole ratios of citrate/Pt of (a) 0, (b) 6, (c) 12, (d) 18 and (e) 24, in 1M H_2SO_4at 25 mV/s

Table 6.6 Electrochemical active surface area and methanol oxidation current density of 20 % Pt/CDX975 catalyst with different mole ratios of citrate/Pt

Mole ratio of citrate/Pt	EAS m^2/g	Methanol oxidation peak current density (mA/cm^2)
0	-	66.4
6	10.57	177
12	9.39	176
18	**13.13**	**227**
24	7.08	150

Fig. 6.14 shows the cyclic voltammetry for methanol oxidation in 1M methanol in 1M H_2SO_4 of 20% Pt/CDX975 catalysts. Fig. 6.14 (A) shows the methanol oxidation current density for the catalysts prepared with and without citrate. It shows enhanced methanol oxidation current density for the catalyst prepared with citrate as the capping agent, compared to the one with out citrate. This can be explained to the enhanced dispersion of the Pt nanoparticles on the carbon black support with the addition of citrate. Fig. 6.14 (B) shows the methanol oxidation current density for the catalysts prepared with varying mole ratios of citrate/Pt (Table 6.6). It shows an increase in methanol oxidation current density at first, with the maximum methanol oxidation activity for the catalyst prepared with the citrate/Pt mole ratio of 18. This can be attributed to the optimum dispersion of the Pt nanoparticles on the carbon black support, supported by the measurement of electrochemical active surface area. The catalyst which shows the maximum activity also contains the higher percentage of Pt(II) state, observed from XPS results. The onset potential for methanol oxidation also significantly shift to cathodic for the one showing the maximum activity. As the results are similar to that of the 10% Pt/CDX975 catalyst, the same explanation of the involvement of the Pt(II) species in the oxidation of methanol holds for the 20%

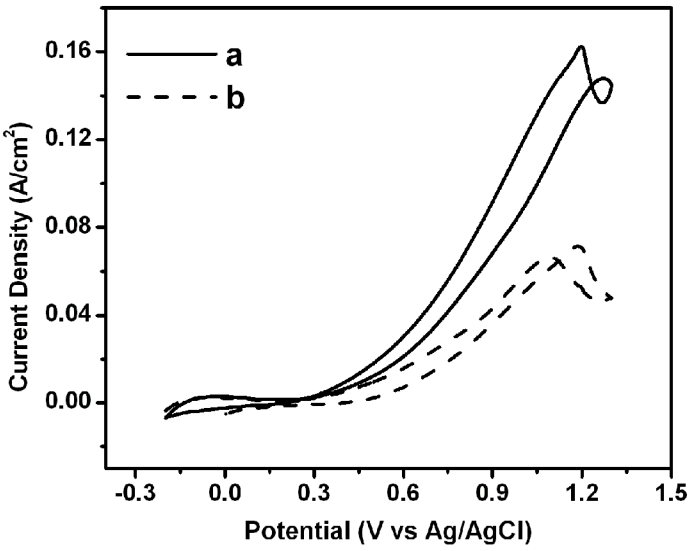

(A)

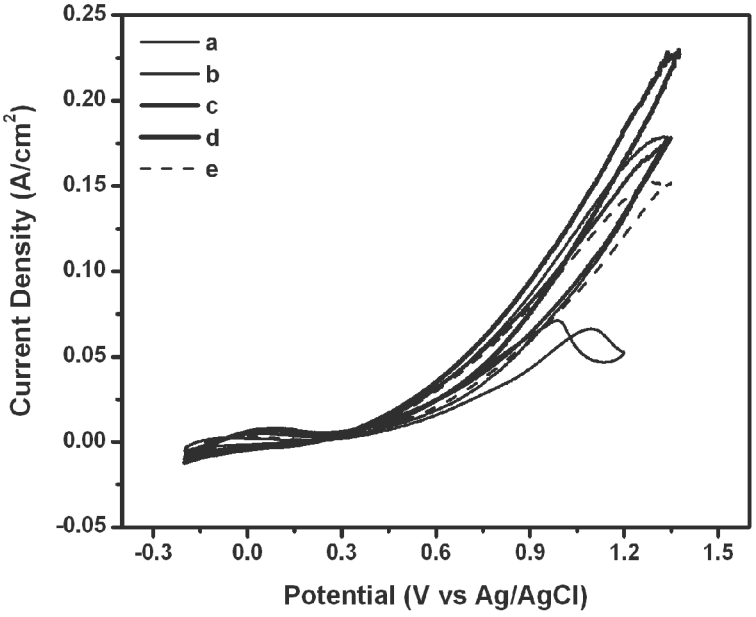

(B)

Fig. 6.14 Cyclic voltammogram of 20% Pt/CDX975 catalyst for methanol oxidation in 1M methanol and 1M H_2SO_4 (A) with citrate(a) and without citrate(b) and (B) for different mole ratios of citrate/Pt of (a) 0, (b) 6, (c) 12, (d) 18 and (e) 24 at 25 mV/s

Pt/CDX975 catalyst also (Parsons and VanderNoot, 1988; Goodenough *et al*., 1987). With the further increase of the mole ratio of citrate/Pt, the methanol oxidation activity decreases. This decrease in activity can be attributed to the blocking of the active Pt sites by the excess citrate molecules, as reported by Guo *et al*., 2005. Fig. 6.15 shows the chronoamperometry at 1.0 V for the 20% Pt/CDX975 catalyst prepared with and without citrate. It shows enhanced current density and stability for the catalyst prepared with citrate as the capping agent, compared to the one with out citrate. It supports the advantage of the capping action of citrate.

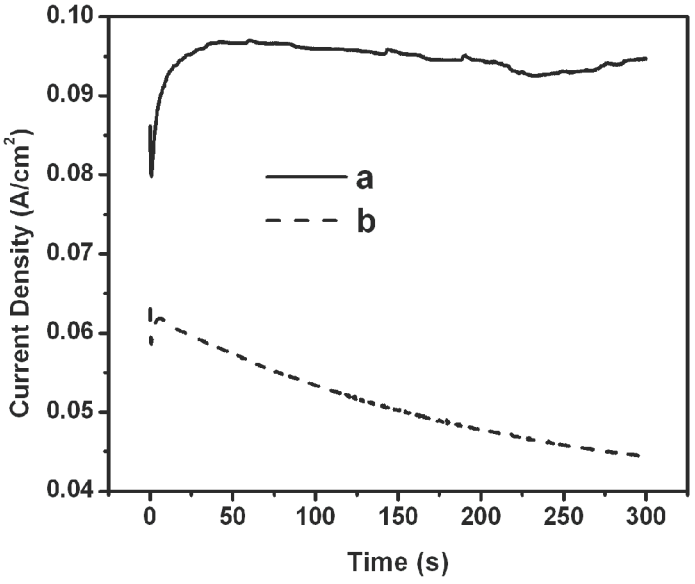

Fig. 6.15 Chronoamperometry of 20% Pt/CDX975 catalyst (a) with citrate and (b) without citrate in 1M H_2SO_4 and 1M Methanol at 1.0 V

6.5 Summary

- XRD results showed the decrease of Pt particle size with the addition of citrate as the stabilizing agent.
- Calculation of Electrochemical Active Surface Area (EAS) has evidenced the better dispersion of the Pt nanoparticles on the carbon black support in presence of citrate.
- The presence of optimum stabilizing agent concentration has resulted in the maximum methanol oxidation activity.
- The existence of Pt in the Pt(II) state through XPS results also supports the existence of the Pt nanoparticles in the presence of the electrostatic stabilizing agent.
- Both the 10% and 20% Pt/CDX975 catalysts show enhanced activity for methanol oxidation for the catalyst having higher percentage of Pt in Pt(II) state. Therefore this study shows the experimental evidence for the enhancement in methanol oxidation by the Pt(II) species as suggested by the earlier reports.

SUMMARY AND CONCLUSIONS

Typical catalyst used in fuel cell electrodes is Pt dispersed on carbon black support, for both anode and cathode. Carbon black has many kinds of functional groups like hydroxyl, carboxyl, lactone, quinone and hydroquinone. Using carbon black support, the catalysts are mostly prepared through the impregnation step, where the metal ions are adsorbed on to the support functional groups especially carboxylic groups through ion exchange methods. Studies on nitrogen functionalization of the carbon black support render the surface basic and expected to anchor the anionic precursor molecules better.

Apart from the surface functional groups, another important aspect of fuel cell catalysts is the three phase boundary (the coexistence of the electron conducting support particles, proton conducting polymer ionomer and the catalyst particle). In fuel cell catalysts, only those catalyst particles, which exist in the three phase boundary are utilized. But the smaller Pt nanoparticles exist with in the inner pores of the carbon black support are not accessible for the bulky proton conducting polymer, and are not utilized for the electrocatalytic reactions. Therefore studies were focused on to increase the proton conduction inside the pore structure of carbon support with the introduction of strong protonic acid groups, which are small enough to reach into the inner pores of the carbon black support (such as alkyl sulfonic acid groups). Another factor which has more influence on the performance of the metal nanoparticles is the particle size. Nanoparticles are thermodynamically unstable and their apparent stability comes from an acquired kinetic hindrance to agglomeration. Hence, in order to produce desired sizes of Pt nanoparticles with uniform dispersion on the carbon support, stabilizing agents, such as surfactants, ligands or polymers, is

usually employed during the preparative process. The presence of these bulky stabilizer molecules on the particle surface, however, could reduce the catalytic activity. The removal of these stabilizer molecules by thermal treatment induces particle sintering, thereby undoing the effort in nanoparticle synthesis. Therefore electrostatic stabilization by carboxylic anions is preferred to the steric stabilization by polymers, as these carboxylic anions can be easily washed off with distilled water.

Early approaches to the preparation of supported catalysts were based on ion exchanging or simple adsorption of the metal precursor onto the supports, but these procedures did not prevent leaching of the active phase. This problem is expected to overcome by the development of several grafting methodologies, which allow the covalent attachment of metal precursor to the different support materials like, organic polymers, silica, zeolites and other mesoporous carbon materials. The present work, therefore is focusing upon the different kinds of functionalization of the carbon black support, which can lead to smaller Pt particle size and hence enhanced dispersion, higher active surface area, better utilization of the expensive, less abundant noble metal catalyst, so that the fuel cell performance could be commercially viable.

The following conclusions are drawn from this study.

- The oxidative treatment conditions with nitric acid of the carbon black support showed an increase in the concentration of carboxylic acid functional groups on the support, as observed from different characterization techniques.

- XRD studies showed smaller particle size of Pt for the catalyst treated with conc. HNO_3 for 60 minutes, which can be attributed to the generation of optimum concentration of the carboxyl functional groups on the surface of the support. Further increase of oxidative condition leads to the aggregation of the

Pt nanoparticles due to the lesser diffusion of these nanoparticles to the inner pores of the support.

- The methanol oxidation studies showed the maximum activity for the catalyst which has been treated with conc. HNO_3 for 60 minutes, which has also been found to have smaller particle size. Hence, the enhanced methanol oxidation activity can be attributed to the increased dispersion of the Pt nanoparticles. The decrease of activity with further increase of oxidative treatment conditions can be attributed to the aggregation of Pt nanoparticles on the surface of the support. This is expected to be caused by the high concentration of carboxyl functional groups generated on the surface which reduces the diffusion of the Pt nanoparticles into the inner pores of the support.

- The grafting of sulfonic acid group on the carbon black support has been carried out with three different sulfonating agents, 2-aminoethanesulfonic acid, ammonium sulfate and sodium sulfite with formaldehyde.

- Studies by FT-IR and pH measurements supported the successful grafting of the sulfonic acid group on the carbon black support.

- XRD studies of the sulfonated catalysts showed redistribution of Pt nanoparticles upon sulfonic acid grafting.

- The studies on the oxidation of methanol has shown an enhanced activity for all the sulfonic acid modified catalysts compared to the unsulfonated ones. The increase in activity can be attributed to two factors: (i) Pt nanoparticle redistribution to smaller particles, thereby increasing the electrochemical

active surface area of Pt and (ii) increased protonic conductivity inside the catalyst support.

- The aminopyridine modification of the carbon black support has shown decrease of particle size of Pt nanoparticles as a result of better dispersion on the modified carbon black support.

- The electrochemical studies in sulphuric acid has shown enhanced electrochemical active surface area upon modification of the carbon black support, evidences the better dispersion of Pt nanoparticles on the aminopyridine modified support.

- Methanol oxidation studies has shown enhanced activity for the catalyst prepared with aminopyridine modified carbon black support compared to the unmodified one, which can be attributed to the smaller particle size of Pt nanoparticles as a result of enhanced dispersion on the modified carbon black support.

- The addition of citrate as the stabilizing agent resulted in the decrease of Pt particle size as observed with XRD and TEM techniques.

- Determination of the values of electrochemical active surface area (EAS) has confirmed the better dispersion of the Pt nanoparticles on the carbon black support in presence of citrate.

- The presence of optimum concentration of stabilizing agent has resulted in the maximum methanol oxidation activity.

- The existence of Pt in the Pt(II) state as deduced from XPS results also supports the existence of the Pt nanoparticles in the presence of the electrostatic stabilizing agent.

- Both the 10% and 20% Pt/CDX975 catalysts show enhanced activity for methanol oxidation for the catalyst having higher percentage of Pt in Pt(II) state. Therefore this study shows the experimental evidence for the enhancement in methanol oxidation by the Pt(II) species.

REFERENCES

1. **Abotsit, G.M.K. and Alan W. Scaroni (1990)** Reaction of carbons with ammonia: effects on the surface charge and molybdenum adsorption. *Carbon,* **2**, 7 9-84.

2. **Anderson, M.L., R.M. Stroud, D.R. Rolison** (2002) Enhancing the Activity of Fuel-cell Reactions by Dispersing Three-dimensional Nanostructured Architectures: Catalyst-modified Carbon-Silica Composite Aerogels. *Nano Lett.*, **2**, 235-240.

3. **Antonucci, P.L., V. Alderucci, N. Giordano, D.L. Cocke and H. Kim** (1994) On the role of surface functional groups in Pt carbon interaction. *J. Appl. Electrochem.,* **24,** 58-65.

4. **Biniak, S., G. Szymanski, J. Siedlewski and A. Swiatkowski** (1997) The characterization of activated carbons with oxygen and nitrogen surface groups. *Carbon*, **35**, 1799-1810.

5. **Bock, C., Chantal Paquet, Martin Couillard, Gianluigi A. Botton and Barry R. MacDougall** (2004) Size-Selected Synthesis of PtRu Nano-Catalysts: Reaction and Size Control Mechanism. *J. Am. Chem. Soc.*, **126**, 8028-8037.

6. **Boehm, H.P**. (1994) Some aspects of the surface chemistry of carbon blacks and other carbons. *Carbon*, **32**, 759-769.

7. **Bonnemann, H., G. Braun, W. Brijoux, R. Brinkmann, S. Tilling, K. Seevogel and K. Siepen** (1996) Nanoscale colloidal metals and alloys stabilized by solvents and surfactants Preparation and use as catalyst precursors. *J. Organomet. Chem.*, **520,** 143-163.

8. **Bonnmann, H., W. Brijoux, R. Brinkmann, E. Dinjus, R. Fretzen, T. Joussen, B. Koppler, B. Korall, P. Neiteler and J. Richter** (1994) Preparation, characterization, and application of fine metal particles and metal colloids using hydrotriorganoborates**.** *J. Mol. Catal.*, **86**, 129-177.

9. **Boutonnet, M., Sara Lögdberg, Erik Elm Svensson** (2008) Recent developments in the application of nanoparticles prepared from w/o microemulsions in heterogeneous catalysis. *Current Opinion in Colloid & Interface Science*, **13**, 270–286.

10. **Boxall, D.L., G.A. Deluga, E.A. Kenik, W.D. King, C.M. Lukehart** (2001) Rapid Synthesis of a Pt1Ru1/Carbon Nanocomposite Using Microwave Irradiation: A DMFC Anode Catalyst of High Relative Performance. *Chem. Mater.,* **13,** 891–900.

11. **Castro Luna, A.M., G.A. Camara, V.A. Paganin, E.A. Ticinelli and E.R.Gonzalez** (2000) Effect of thermal treatment on the performance of CO-tolerant anodes for polymer electrolyte fuel cells. *Electrochem. Commun.,* **2,** 222-225.

12. **Chan, K.Y., J. Ding, J. Ren, S. Cheng and K.Y. Tsang** (2004) Supported mixed metal nanoparticles as electrocatalysts in low temperature fuel cells. *J. Mater. Chem.*, **14,** 505-516.

13. **Chan, K.Y., J. Ding, J. Ren, S. Cheng, K.Y. Tsang** (2004) Supported mixed metal nanoparticles as electrocatalysts in low temperature fuel cells. *J. Mater. Chem*., **14**, 505–516.

14. **Che, G., B.B. Lakshmi, C.R. Martin, E.R. Fisher** (1999) Metal-Nanocluster-Filled Carbon Nanotubes: Catalytic Properties and Possible Applications in Electrochemical Energy Storage and Production. *Langmuir,* **15**, 750–758.

15. **Dickinson, A.J., L.P.L. Carrette, J.A. Collins, K.A. Friedrich, U. Stimming** (2002) Preparation of a Pt_ Ru/C catalyst from carbonyl complexes for fuel cell applications. *Electrochim. Acta,* **47,** 3733–3739.

16. **Du, C.Y., T.S. Zhao and Z.X. Liang** (2008) Grafting of sulfonic acid groups onto the surface of carbon-nanotube supported platinum (Pt/CNT) catalysts by both thermal decomposition of ammonium sulfate and in situ radical polymerization of 4-styrenesulfonate. *J. Power Sources*, **176,** 9–15.

17. **Du, J., Chang Song, Jianghong Zhao and Zhenping Zhu** (2008) Effect of chemical treatment to hollow carbon nanoparticles (HCNP) on catalytic behaviors of the platinum catalysts. Applied Surface Science, **255**, 2989–2993.

18. **Dubau, L., C. Coutanceau, E. Garnier, J. Leger, C. Lamy** (2003) Electrooxidation of methanol at platinum–ruthenium catalysts prepared from colloidal precursors: Atomic composition and temperature effects. *J. Appl. Electrochem.* **33** (2003) 419–429.

19. **Easton, E. B., Z. Qi, A. Kaufman and P. G. Pickup** (2001) Chemical modification of proton exchange membrane fuel cell catalysts with a sulfonated silane. *Electrochem. Solid-State Lett.*, **4**, A59.

20. **Figueiredo, J.L., M.F.R. Pereira, M.M.A. Freitas and J.J.M. Orfao** (1999) Modification of the surface chemistry of activated carbons. Carbon, **37**, 1379–1389.

21. **Fraga, M. A., E. Jordao, M. J. Mendes, M. M. A. Freitas, J. L. Faria, and J. L. Figueiredo** (2002) Properties of Carbon-Supported Platinum Catalysts: Role of Carbon Surface Sites. *J. Catal.*, **209,** 355–364.

22. **Gasteiger, H.A., Shyam S. Kocha, Bhaskar Sompalli, Frederick T. Wagner** (2005) Activity benchmarks and requirements for Pt, Pt-alloy, and non-Pt oxygen reduction catalysts for PEMFCs. *Appl. Catal. B: Environmental,* **56,** 9–35.

23. **Goodenough, J.B., A. Hamnett, B.J. Kennedy and S.A. Weeks** (1987) XPS investigation of platinized carbon electrodes for the direct methanol air fuel cell. *Electrochim. Acta*, **32,** 1233-1238.

24. **Goodenough, J.B., A. Hamnett, B.J. Kennedy, R. Manoharan and S.A. Weeks** (1990) Porous carbon anodes for the direct methanol fuel cell-i the role of the reduction method for carbon supported platinum electrodes. *Electrochim. Acta*, **35**, 199-207.

25. **Guo, J.W., T.S. Zhao, J. Prabhuram and C.W. Wong** (2005) Preparation and the physical/electrochemical properties of a Pt/C nanocatalyst stabilized by citric acid for polymer electrolyte fuel cells. *Electrochim. Acta*, **50,** 1973–1983.

26. **Hamnett, A** (1997) Mechanism and electrocatalysis in the direct methanol fuel cell. *Catal. Today,* **38,** 445-457.

27. **Han, H.I., J.S. Lee, S.O. Park, S.W. Lee, Y.W. Park, H. Kim** (2004) Studies on the anode catalysts of carbon nanotube for DMFC. Electrochim. Acta, **50,** 791–795.

28. **Harada, T., Shigeru Ikeda, Mayu Miyazaki, Takao Sakata, Hirotaro Mori, Michio Matsumura (2007)** A simple method for preparing highly active palladium catalysts loaded on various carbon supports for liquid-phase oxidation and hydrogenation reactions. *J.Mol. Catal. A: Chem.*, **268,** *59-64.*

29. **Henglein, A., and M. Giersig** (2000) Reduction of Pt(II) by H2: Effects of Citrate and NaOH and Reaction Mechanism. *J. Phys. Chem. B*, **104**, 6767-6772.

30. **Jarrais, B., Ana Rosa Silva and Cristina Freire** (2005) Anchoring of Vanadyl Acetylacetonate onto Amine-Functionalised Activated Carbons: Catalytic Activity in the Epoxidation of an Allylic Alcohol. *Eur. J. Inorg. Chem.*, 4582–458.

31. **Jia, N., R. B. Martin, Z. Qi, M. C. Lefebvre, and P. G. Pickup** (2001)**,** Modification of carbon supported catalysts to improve performance in gas diffusion electrodes. *Electrochim. Acta*, **46**, 2863–2869.

32. **Jia, N., R. B. Martin, Z. Qi, M. C. Lefebvre, and P. G. Pickup** (2001)**,** Modification of carbon supported catalysts to improve performance in gas diffusion electrodes. *Electrochim. Acta*, **46**, 2863–2869.

33. **Jia, N., Rex B. Martin, Zhigang Qi, Mark C. Lefebvre and Peter G. Pickup** (2001) Modification of carbon supported catalysts to improve performance in gas diffusion electrodes. Electrochim. Acta, **46**, 2863–2869.

34. **Job, N., Manuel Fernando Ribeiro Pereira, Stéphanie Lambert, Amandine Cabiac, Gérard Delahay, Jean-François Colomer, José Marien, José Luis Figueiredo, Jean-Paul Pirard** (2006) Highly dispersed platinum catalysts prepared by impregnation of texture-tailored carbon xerogels. *J. Catal.* **240**,160–171.

35. **K. Kinoshita** (1988) Carbon: Electrochemical and Physicochemical Properties, Wiley, New York.

36. **Kinoshita**, K., Carbon: Electrochemical and Physicochemical Properties, Wiley, New York, 1988.

37. **Kuroki, H. and Takeo Yamaguchi** (2006) Nanoscale Morphological Control of Anode Electrodes by Grafting of Methylsulfonic Acid Groups onto Platinum–Ruthenium-Supported Carbon Blacks. *J. Electrochem. Soc.,* **153,** A1417-A1423.

38. **Lee, K.C., J.J. Zhang, H.J. Wang, D.P. Wilkinson** (2006) Progress in the synthesis of carbon nanotube- and nanofiber-supported Pt electrocatalysts for PEM fuel cell catalysis. *J. Appl. Electrochem.*, **36**, 507-522.

39. **Li, J., Matthew J.Vergne, Eric D.Mowles, Wei-Hong Zhong, David M.Hercules, Charles M.Lukehart** (2005) Surface functionalization and characterization of graphitic carbon nanofibers (GCNFs). *Carbon* **43,** 2883–2893.

40. **Li, W., C. Liang, J. Qiu, W. Zhou, H. Han, Z. Wei, G. Sun, Q. Xin** (2002) Carbon nanotubes as support for cathode catalyst of a direct methanol fuel cell. *Carbon,* **40**, 791–794.

41. **Li, Z., Wenfu Yan, and Sheng Dai** (2005) Surface Functionalization of Ordered Mesoporous CarbonssA Comparative Study. *Langmuir***, 21**, 11999-12006.

42. **Lima, Weon-Doo Leea, Dong-Hyeok Choia, Dal-Ryung Parkb, Ho-In Leea** (2008) Preparation of platinum nanoparticles on carbon black with mixed binary surfactants: Characterization and evaluation as anode catalyst for low-temperature fuel cell. *J. Power Sources*, **185**, 159–165.

43. **Lin, C.S., M.R. Khan and S.D. Lin** (2005) Platinum states in citrate sols by EXAFS *J. Colloid Interface Sci.* **287,** 366–369.

44. **Lin, Y., G.B. Pan, G.J. Su, X. Hong, L.J.Wan and C.L. Bai** (2003) Study of Citrate Adsorbed on the Au(111) Surface by Scanning Probe Microscopy. *Langmuir,* **19,** 10000-10003.

45. **Liu, H., Chaojie Song, Lei Zhang, Jiujun Zhang,Haijiang Wang, David P. Wilkinson** (2006) A review of anode catalysis in the direct methanol fuel cell. *J. Power Sources,* **155,** 95–110.

46. **Liu, Z.L., X.Y. Liu, X. Su and J.Y. Lee** (2004) Carbon Supported Pt and PtRu Nanoparticles as Catalysts for a Direct Methanol Fuel Cell. *J. Phys. Chem. B,* **108,** 8234-8240.

47. **Lizcano-Vulbuena, W.H., V.A. Paganin, C.A. Leite, F. Galembeck and E.R. Gonzalez** (2003) Catalysts for DMFC: relation between morphology and electrochemical performance. *Electrochim. Acta*, **48**, 3869-3878.

48. **Loh,h., R. E. Cohen, R. F. Baddour** (1987) Modification of carbon surfaces in cold plasmas. *J. Mater. Sci.*, **22**, 2937-2947.

49. **Long, J.W., R.M. Stroud, K.E. Swider-Lyons, D.R. Rolison** (2000) How To Make Electrocatalysts More Active for Direct Methanol Oxidations-Avoid PtRu Bimetallic Alloys!. *J. Phys. Chem. B,* **104**, 9772–9776.

50. **Luna, A.M.C., G.A. Camara, V.A. Paganin, E.A. Ticianelli, E.R. Gonzalez** (2000) Effect of thermal treatment on the performance of CO-tolerant anodes for polymer electrolyte fuel cells. *Electrochem. Commun.*, **2,** 222–225.

51. **Matsumoto, T., T. Komatsu, K. Arai, T. Yamazaki, M. Kijima, H. Shimizu, Y. Takasawa, J. Nakamura** (2004) Reduction of Pt usage in fuel cell electrocatalysts with carbon nanotube electrodes. *Chem. Commun*., 840–841.

52. **McNicol, B,D., D.A.J. Rand, K.R. Williams** (1999) Direct methanol–air fuel cells for road transportation. *J. Power Sources,* **83**, 15–31.

53. **Mizuhata, H., Shin-ichi Nakao and Takeo Yamaguchi** (2004) Morphological control of PEMFC electrode by graft polymerization of polymer electrolyte onto platinum-supported carbon black. *J. Power Sources*, **138,** 25–30.

54. **Molina-Sabio, M., F. Rodrıguez-Reinoso** (2004) Role of chemical activation in the development of carbon porosity. *Colloids Surf. A: Physicochem. Eng. Aspects*, **241**, 15–25.

55. **Moreno-Castilla C, Carrasco-Marın F, Maldonado-Hodar F.J, and Rivera-Utrilla J.** (1998) Effects of non-oxidant and oxidant acid treatments on the surface properties of an activated carbon with very low ash content. *Carbon*, **36**, 145-151.

56. **Moreno-Castilla, C., Ferro-Garcia, M. A., Joly, J. P., Bautista-Toledo, I., Carrasco-Marin, F. and Rivera-Utrilla. J.** (1995) Activated Carbon Surface Modifications by Nitric Acid, Hydrogen Peroxide, and Ammonium Peroxydisulfate treatments. *Langmuir,* **11**, 4386-4392**.**

57. **Nashner, M.S., A.I. Frenkel, D. Somerville, C.W. Hills, J.R. Shapley, R.G. Nuzzo** (1998) Core shell inversion during nucleation and growth of bimetallic Pt/Ru nanoparticles. *J. Am. Chem. Soc.,* **120,** 8093–8101.

58. **Nashner, M.S., A.I. Frenkel, D.L. Adler, J.R. Shapley, R.G. Nuzzo** (1997) Structural Characterization of Carbon-Supported Platinum-Ruthenium Nanoparticles from the Molecular Cluster Precursor $PtRu_5C(CO)_{16}$. *J. Am. Chem. Soc*., **119**, 7760–7771.

59. **Olga Baturin, A., Steven R. Aubuchon and Kenneth J. Wynne** (2006) Thermal stability in air of Pt/C catalysts and PEM fuel cell catalyst layers. *Chem. Mater.*, **18,** 1498–1504.

60. **Ozkar, S. and Richard G. Finke, (2002)** Nanocluster Formation and Stabilization Fundamental Studies: Ranking Commonly Employed Anionic

Stabilizers via the Development, Then Application, of Five Comparative Criteria. *J. AM. CHEM. SOC.* **124,** 5796-5810.

61. **Park, K.W., Jong-Ho Choi, Seol-Ah Lee, Chanho Pak, Hyuck Chang, and Yung-Eun Sung** (2004) PtRuRhNi nanoparticle electrocatalyst for methanol electrooxidation in direct methanol fuel cell. *J. Catal.*, **224,** 236-242.

62. **Parsons, R., and T. VanderNoot** (1988) The oxidation of small organic molecules A survey of recent fuel cell related research. *J. Electroanal. Chem.,* **257,** 9-45.

63. **Patterson, A.L.** (1939) The Scherrer formula for X-ray particle size determination. *Phy. Rev.*, **56**, 978-982.

64. **Paulus, U.A., U. Endruschat, G.J. Feldmeyer, T.J. Schmidt, H. Bonnemann and R.J. Behm** (2000) New PtRu Alloy Colloids as Precursors for Fuel Cell Catalysts. *J. Catal.*, **195,** 383-393.

65. **Peng, H., Lawrence B. Alemany, John L. Margrave and Valery N. Khabashesku** (2003) Sidewall Carboxylic Acid Functionalization of Single-Walled Carbon Nanotubes. *J. AM. CHEM. SOC.*, **125**, 15174-15182.

66. **Pillai, Z.S. and P.V. Kamat** (2004) What Factors Control the Size and Shape of Silver Nanoparticles in the Citrate Ion Reduction Method? *J. Phys. Chem. B*, **108**, 945-951.

67. **Pozio, A., M. De Francesco, A. Cemmi, F. Cardellini and L. Giorgi** (2002) Comparison of high surface Pt/C catalysts by cyclic voltammetry. *J. Power Sources*, **105**, 13–19.

68. **Prabhuram, J., X. Wang, C.L. Hui and I-M. Hsing** (2003) Synthesis and Characterization of Surfactant-Stabilized Pt/C Nanocatalysts for Fuel Cell Applications. *J. Phys. Chem. B*, **107**, 11057-11064.

69. **Prabhuram, J.and R. Manoharan** (1998) Investigation of methanol oxidation on unsupported platinum electrodes in strong alkali and strong acid. *J. Power Sources,* **74**, 54-61.

70. **Puziy, A.M. and O.I. Poddubnaya** (1998) The properties of synthetic carbon derived from nitrogen- and phosphorus-containing polymer. *Carbon,* **36**, 45-50.

71. **Qi, Z. and Peter G. Pickup** (1998) High performance conducting polymer supported oxygen reduction catalysts. *Chem. Commun.*, 2299–2300.

72. **Radmilovic, V., H.A. Gasteiger, P.N. Ross Jr**. (1995) Structure and chemical composition of a supported Pt-Ru electrocatalyst for methanol oxidation. *J. Catal.*, **154,** 98–106.

73. **Raghuveer, V., A. Manthiram** (2004) Mesoporous carbon with larger pore diameter as an electrocatalyst support for methanol oxidation. *Electrochem. Solid-State Lett.* **7,** 336–339.

74. **Raghuveer, V., A. Manthiram** (2005) Mesoporous carbons with controlled porosity as an electrocatalytic support for methanol oxidation. *J. Electrochem. Soc.,* **152,** 1504–1510.

75. **Raghuveer, V., B. Viswanathan** (2002) Can La22xSrxCuO4 be used as anodes for direct methanol fuel cells. *Fuel*, **81,** 2191–2197.

76. **Rajesh, B., K. Ravindranathan Thampi, J. M. Bonard, H. J. Mathieu, N. Xanthopoulos and B. Viswanathan** (2004) Nanostructured Conducting Polyaniline Tubules as Catalyst Support for Pt Particles for Possible Fuel Cell Applications. *Electrochem. Solid-State Lett.*, **7,** A404-A407.

77. **Rajesh, B., K. Ravindranathan Thampi, J.M. Bonard, H.J. Mathieu, N. Xanthopoulos and B. Viswanathan** (2004) Nanostructured Conducting Polyaniline Tubules as Catalyst Support for Pt Particles for Possible Fuel Cell Applications. *Electrochem. Solid-State Lett.*, **7**, A404-A407.

78. **Rajesh, B., K.R. Thampi, J.M. Bonard, N.X. Xanthopoulos, H.J. Mathieu, B. Viswanathan** (2003) Carbon Nanotubes Generated from Template Carbonization of Polyphenyl Acetylene as the Support for Electrooxidation of Methanol. *J. Phys. Chem. B*, **107**, 2701–2708.

79. **Rajesh, B., V. Karthik, S. Karthikeyan, K.R. Thampi, J.M. Bonard, B. Viswanathan** (2002) Pt–WO_3 supported on carbon nanotubes as possible anodes for direct methanol fuel cells. *Fuel,* **81,** 2177-2190.

80. **Ralph, T.R., G.A. Hards, J.E. Keating, S.A. Campbell, D.P. Wilkinson, M. Davis, J. St-Pierre and M.C. Johnson** (1997) Low cost electrodes for proton exchange membrane fuel cells. *J. Electrochem. Soc.*, **144,** 3845–3857.

81. **Roman-Martinez, M. C., D. Cazorla Amor, A. Linares Solano, C. Salinas Martinez De Lecea, H. Yamashita and M. Anpo** (1995) Metal-support interaction in Pt/C catalysts: Influence of the support surface chemistry and the metal precursor. Carbon, **33**, 3-13.

82. **Rosca, I.D., Fumio Watari, Motohiro Uo and Tsukasa Akasaka** (2005) Oxidation of multiwalled carbon nanotubes by nitric acid. *Carbon* **43,** 3124–3131.

83. **Roth, C., N. Martz and H. Fuess** (2001) Characterization of different Pt–Ru catalysts by X-ray diffraction and transmission electron microscopy. *Phys. Chem. Chem. Phys.***, 3,** 315-319.

84. **Roy, S.C., P, A. Christensen, A. Hamnett, K. M. Thomas, and V. Trap** (1996) Direct Methanol Fuel Cell Cathodes with Sulfur and Nitrogen-Based Carbon Functionalily. *J. Electrochem. Soc.*, **143**, 3073-3079.

85. **Roy.S.C., A. W. Harding, A.E. Russell and K.M. Thomas** (1997) Spectroelectrochemical study of the role played by carbon functionality in fuel cell electrodes. *J. Electrochem. Soc.,* **144**, 2323 – 2328.

86. **Schmidt, T.J., M. Noeske, H.A. Gasteiger, R.J. Behm, P. Britz, W. Brijoux, H. Bonnemann** (1997) Electrocatalytic Activity of PtRu Alloy Colloids for CO and CO/H_2 Electrooxidation: Stripping Voltammetry and Rotating Disk Measurements. *Langmuir*, **13**, 2591–2595.

87. **Selvarani, G., A.K. Sahu, N.A. Choudhury, P. Sridhar, S. Pitchumani and A.K. Shukla** (2007) A phenyl-sulfonic acid anchored carbon-supported platinum catalyst for polymer electrolyte fuel cell electrodes. *Electrochim. Acta*, **52,** 4871–4877.

88. **Serp, P., M. Corrias, P. Kalck** (2003) Carbon nanotubes and nanofibers in catalysis. *Appl. Catal. A*, **253**, 337–358.

89. **Shimazaki, Y., Yoshio Kobayashi, Shinji Yamada, Takao Miwa and Mikio Konno** (2005) Preparation and characterization of aqueous colloids of Pt–Ru nanoparticles. *J. Colloid Interface Sci.*, **292**, 122–126.

90. **Shimazu, K., D. Weisshaar and T. Kuwana** (1987) Electrochemical dispersion of Pt microparticles on glassy carbon electrode. *J. Electroanal. Chem.* **223**, 223.

91. **Silva, A.R., Magda Martins, M. Madalena A. Freitas, Jose Luıs Figueiredo, Cristina Freire, and Baltazar de Castro** (2004) Anchoring of Copper(II) Acetylacetonate onto an Activated Carbon Functionalised with a Triamine. *Eur. J. Inorg. Chem,.* 2027-2035.

92. **Suh., D. J., T.J. Park and S. K. Ihm** (1993) Effect of surface oxygen groups of carbon supports on the characteristics of Pd/C catalysts. *Carbon*, **31**, 427-435.

93. **Tang, H., J.H. Chen, Z.P. Huang, D.Z. Wang, Z.F. Ren, L.H. Nie, Y.F. Kuang, S.Z. Yao** (2004) High dispersion and electrocatalytic properties of platinum on well-aligned carbon nanotube arrays. *Carbon*, **42**, 191–197.

94. **Ticianelli, E.A., C.R. Derounin and S. Srinivassan** (1988) Localization of platinum in low catalyst loading electrodes to attain high power densities in SPE fuel cells. *J. Electroanal. Chem.*, **251**, 275.

95. **Titirici, M.M., Arne Thomas and Markus Antonietti (2007)** Aminated hydrophilic ordered mesoporous carbons. *J. Mater. Chem.*, **17**, 3412–3418.

96. **Turkevich, J. and G. Kim** (1970) Palladium: Preparation and Catalytic Properties of Particles of Uniform Size. *Science,* **169,** 873-879.

97. **Turkevich, J., R.S. Miner Jr. and L. Babenkova** (1986) Further Studies on the Synthesis of Finely Divided Platinum. *J. Phys. Chem.*, **90**, 4765–4767.

98. **Uchida, M., Y. Aoyama, N. Eda, A. Ohta** (1995) New preparation method for polymer electrolyte fuel cells. *J. Electrochem. Soc.*, **142**, 463.

99. **Uchida, M., Y. Fukuoka, Y. Sugawara, N. Eda and A. Ohta** (1996) Effects of microstructure of carbon support in the catalyst layer on the performance of Polymer-Electrolyte fuel cell. *J. Electrochem. Soc.*, **143,** 2245.

100. **Viswanathan, B** and **M. Aulice Scibioh** (2008) Fuel Cells: Principles and Applications, CRC Press.

101. **Wang, X., and I.-M. Hsing** (2002) Surfactant stabilized Pt and Pt alloy electrocatalyst for polymer electrolyte fuel cells. *Electrochim. Acta*, **47**, 2981-2987.

102. **Watanabe, M., M. Tomikawa and S. Motoo** (1985) Preparation of a high performance gas diffusion electrode. *J. Electroanal. Chem.* **182,** 193-196.

103. **Watanabe, M., M. Uchida and S. Motoo** (1987) Preparation of highly dispersed pt + ru *alloy* clusters and the activity for the elecirooxidation of methanol. *J. Electroanal. Chem.,* **229**, 395-406.

104. **Watanabe, M., M. Uchida, S. Motoo** (1987) Preparation of highly dispersed pt + ru *alloy* clusters and the activity for the elecirooxidation of methanol. *J. Electroanal. Chem.,* **229,** 395–406.

105. **Willson, M.S. and S. Gottesfeld** (1992) High Performance Catalyzed Membranes of Ultra-low Pt Loadings for Polymer Electrolyte Fuel Cells. *J. Electrochem. Soc.*, **139,** 28.

106. **Willson, M.S., and S. Gottesfeld** (1992) Thin- film catalyst layers for polymer electrolyte fuel cell electrodes. *J. Appl. Electrochem.*, **22,** 1.

107. **Xu, Z., Zhigang Qi and Arthur Kaufman** (2003) Advanced Fuel Cell Catalysts Sulfonation of Carbon-Supported Catalysts Using 2-Aminoethanesulfonic Acid. *Electrochem. Solid State Lett.*, **6,** A171-A173.

108. **Xu, Z., Zhigang Qi and Arthur Kaufman (**2005) Superior Catalysts for Proton Exchange Membrane Fuel Cells Sulfonation of Carbon-Supported Catalysts Using Sulfate Salts. *Electrochem. Solid State Lett.*, **8,** A313-A315.

109. **Xua, Y., Xiaofeng Xie, Jianwei Guo, Shubo Wang, Yaowu Wang, V.K. Mathur** (2006) Effects of annealing treatment and pH on preparation of citrate-stabilized PtRu/C catalyst. *J. of Power Sources,* **162,** 132–140.

110. **Yadav, O.P., A. Palmqvist, N. Cruise and K. Holmberg** (2003) Synthesis of platinum nanoparticles in microemulsions and their catalytic activity for the oxidation of carbon monoxide. *Colloids Surf. A: Physicochem. Eng. Aspects,* **221**, 131-134.

111. **Yeung, K.L. and E.E. Wolf** (1992) Scanning Tunneling Microscopy Studies of Size and Morphology of Pt/Graphite catalysts. *J. Catal.*, **135,** 13-26.

112. **Yu, J.S., S. Kang, S.B. Yoon, G. Chai** (2002) Fabrication of Ordered Uniform Porous Carbon Networks and Their Application to a Catalyst Supporter. *J. Am. Chem. Soc.,* **124,** 9382–9383.

113. **Yu, R., Luwei Chen, Qiping Liu, Jianyi Lin, Kuang-Lee Tan, Siu Choon Ng, Hardy S. O. Chan, Guo-Qin Xu, and T. S. Andy Hor** (1998) Platinum Deposition on Carbon nanotubes via Chemical Modification. *Chem. Mater.***, 10**, 718-722.

114. **Zeng, J., Jim Yang Lee and Weijiang Zhou** (2006) Activities of Pt/C catalysts prepared by low temperature chemical reduction methods. *Applied Catalysis A: General.*, **308,** 99–104.

115. **Zhang, L., J.J. Zhang, D.P. Wilkinson, H.J. Wang** (2006) Progress in preparation of non-noble electrocatalysts for PEM fuel cell reactions. *J. Power Sources*, **156**, 171–182.

116. **Zhang, X. and K.Y. Chan** (2003) Water-in-Oil Microemulsion Synthesis of Platinum Ruthenium Nanoparticles; Their Characterization and Electrocatalytic Properties. *Chem. Mater.,* **15**, 451-459.

117. **Zhao, J., Peng Wang, Weixiang Chen, Run Liu, Xiang Li and Qiulin Nie** (2006) Microwave synthesis and characterization of acetate-stabilized Pt nanoparticles supported on carbon for methanol electro-oxidatio. *J. of Power Sources,* **160,** 563–569.

LIST OF PUBLICATIONS

Refereed Journals

1. **Viswanathan, B., Chidambaram, V., Chandravathanam, S.**, (2004) On the nature of noble metal electrodes prepared using formaldehyde as reducing agent, *Indian Journal of Chemistry*, 43A, 706-709.
2. **Chandravathanam, S., Viswanathan, B. and Varadarajan, T.K.**, (2009) Effect of aminopyridine functionalization of Carbon Black, *Bulletin of the Catalysis Society of India*, 8(4), 143-148.

Participation in Internationational / National Conferences

1. **Chandravathanam, S., Raghuveer., V, Viswanathan, B.,** (2005) Functionalization of carbon support for noble metal anode catalysts for DMFC applications, presented in Ninth Grove Fuel Cell Symposium, 4-6 October, London, UK.
2. **Chandravathanam, S., Viswanathan, B., Varadarajan, T.K.**, (2010) Effect of grafting of methylsulfonic acid group on Pt supported carbon black catalyst for methanol electrooxidation, presented in Indo-Hungarian workshop on 'Future Frontiers in Catalysis' held in Indian Institute of Technology Madras, Chennai, during 16-18 February.
3. **Chandravathanam, S., Viswanathan, B., (2006)** Application of Nano materials in Safety, Security and Defense, presented in National Seminar on 'Recent Trends in Chemistry' conducted at Jayaraj Annapackiam College for Women, Periakulam, during 27-28, Sep.
4. **Chandravathanam, S., Viswanathan, B., Varadarajan, T.K., (2007)** Preparation of Pt/C catalyst for methanol electrooxidation, presented in National Seminar on 'Recent Trends in Chemistry' conducted at Jayaraj Annapackiam College for Women, Periakulam, during 9-10 Aug.
5. **Chandravathanam, S., Viswanathan, B., Varadarajan, T.K., (2009)** Enhanced utilization of Pt/C catalyst for methanol electrooxidation, presented in National Seminar on 'Recent Trends in Chemistry, RTC-3' conducted at Jayaraj Annapackiam College for Women, Periakulam, during 26-27 Feb.
6. **Chandravathanam, S., Viswanathan, B., Varadarajan, T.K., (2010)** Effect of aminopyridine functionalization of carbon black support for direct methanol fuel cell application, presented in National Conference on 'Recent Trends in Chemistry, RTC-4' held at Jayaraj Annapackiam College for Women, Periakulam, during 18-19 Feb.